NANYANG TECHNOLOGICAL UNIVERSITY

DEGRADATION OF IODINATED DISINFECTION BY-PRODUCTS IN WATER BY UV, UV/H_2O_2 AND UV/PERSULFATE TREATMENT

XIAO YONGJUN

SCHOOL OF CIVIL AND ENVIRONMENTAL ENGINEERING

2017

DEGRADATION OF IODINATED DISINFECTION BY-PRODUCTS IN WATER BY UV, UV/H_2O_2 AND UV/PERSULFATE TREATMENT

XIAO YONGJUN

School of Civil and Environmental Engineering

A thesis submitted to
the Nanyang Technological University
in partial fulfilment of the requirement for the degree of
Doctor of Philosophy

2017

ACKNOWLEDGEMENT

During the last four and a half years of this study, I have gone through an enriching experience not only academically but also of life. It is really not an easy road. The main reason that I can persistently pursue my study is the generous help, guidance, and understanding from the helpful persons who have kindly contributed their knowledge, experience and talents.

First of all, I would like to take this opportunity to express my sincere gratitude to my supervisor, A/P Lim Teik Thye, for his invaluable suggestions and guidance. As a part-time graduate student, I am deeply impressed by his patience, encouragement, and understanding. I also want to express my gratitude to my co-supervisor, A/P Richard D. Webster at School of Physical and Mathematical Sciences for his support and encouragement during my study in NTU.

I would also like to express my special thanks to my colleagues in Water Quality Office, Public Utilities Board. Without their guidance and help, I could not perform my research project smoothly.

Finally, I would like to thank my family members especial my wife, Rongli. With their understanding and support, I have time to think and conduct my project.

ABSTRACT

It is well known that iodinated trihalomethanes (I-THMs) and iodoacids could be formed as iodinated disinfection by-products (I-DBPs) during water treatment and water reclamation processes when iodide is present in the source waters. The formation of I-DBPs such as CHI_3 can lead to odor and taste problem and meanwhile pose a potential health effect because I-DBPs have been reported to be more toxic than their brominated and chlorinated analogues. However, to the best knowledge of the author, there is still no well-documented study on the post-formation mitigation of I-DBPs during water and wastewater treatment processes.

In this context, in the first part of this study, photolysis with germicidal UV254 nm was applied to remove I-THMs, as photon energy of UV254 (472 kJ mol^{-1}) is sufficiently high to photo-cleave carbon-halogen bonds (209, 280, and 397 kJ mol^{-1} for C-I, C-Br, and C-Cl, respectively) and there are evident UV254 absorption of I-THMs (i.e., molar absorption coefficients of 6 I-THMs including $CHCl_2I$, CHClBrI, $CHBr_2I$, $CHClI_2$, $CHBrI_2$, and CHI_3 at UV254 range from 167 to 1131 M^{-1} cm^{-1}). Experimental results showed that I-THMs underwent a fast photodegradation process through cleavage of carbon-halogen bonds with first-order rate constants in the range of 0.1-0.6 min^{-1}. The influence of matrix species such as humic acid (HA), HCO_3^-, SO_4^{2-}, Cl^-, and NO_3^- on the direct photolysis rates of I-THMs was evaluated. Direct photolysis of I-THMs in different types of water including DI water, treated water, surface water, and secondary effluent was also examined. A quantitative structure-activity relationship (QSAR) model for direct photolysis of I-THMs and brominated THMs (B-THMs) was established to analyze the correlation between the chemical reactivity and molecular structure of I-THMs and B-THMs. However, at a UV dose of 140 mJ cm^{-2} which is the upper-bound value for water disinfection, the removal percentages of the 6 I-THMs investigated in this study were only between 6% and 30%.

In the second part of this study, photodegradation of I-THMs was investigated with UV/H_2O_2. $CHCl_2I$ and CHI_3 were selected as model compounds, because $CHCl_2I$ is most resistant to UV254 direct photolysis and CHI_3 is the most cytotoxic among 6

I-THMs. To holistically evaluate the efficiency of I-THMs photodegradation under different conditions, the effects of pH, H_2O_2 dose as well as matrix species including HA, HCO_3^-, SO_4^{2-}, Cl^-, and NO_3^- on the photodegradation kinetics were investigated. A steady-state kinetic model was established to successfully predict the destruction of I-THMs in different types of water including laboratory synthetic water, and surface water. On this basis, electrical energy per order (EE/O) concept was applied to evaluate the efficiency of the photodegradation process and to optimize the H_2O_2 dose for different scenarios.

In the final part of this study, degradation of iodoacids by UV, UV/H_2O_2, and UV/PS (persulfate, $S_2O_8^{2-}$) was extensively investigated. UV direct photolysis of 4 iodoacids including ICH_2CO_2H, $IClCHCO_2H$, $IBrCHCO_2H$, and I_2CHCO_2H followed first-order kinetics with rate constants in the range of 0.057-0.71 min^{-1}. A QSAR model was subsequently established and applied to correlate the chemical reactivity with chemical structure as well as to predict the direct photolysis rates of 6 other structurally similar iodoacids which are commercially unavailable for study. However, at a UV dose of 140 mJ cm^{-2}, the removal percentages of 4 iodoacids were in the range of 3.35% to 34.7%. Subsequently, degradation of iodoacetic acid (IAA, ICH_2CO_2H), the most photo-recalcitrant and toxic species among all iodoacids, by the UV/H_2O_2 and UV/PS processes were compared in terms of the effects of pH, oxidant dose, and matrix species such as HA and HCO_3^- on its photodegradation rate as well as the end-products formed and operating cost. Different types of water including DI water, treated water, surface water, and secondary effluent were used as water matrix to further evaluate the effectiveness of these AOPs for IAA removal. Since $SO_4^{\bullet-}$ can be transformed to $HO^{\bullet}$ to some extent, the respective contributions of UV, $HO^{\bullet}$, and $SO_4^{\bullet-}$ for IAA removal in the UV/PS process were also determined. Economic comparison of these two AOPs for IAA removal was also conducted based on total cost of electrical energy and oxidant.

LIST OF PUBLICATIONS

The content of thesis has been published in the following journal papers.

A. Journal articles

1. Xiao, Y.; Fan, R.; Zhang, L.; Yue, J.; Webster, R.D.; Lim, T.T. **2014**. Photodegradation of iodinated trihalomethanes in aqueous solution by UV 254 irradiation. ***Water Research***, 49, 275-285.

2. Xiao, Y.; Zhang, L.; Yue, J.; Webster, R.D.; Lim, T.T. **2015**. Kinetic modeling and energy efficiency of UV/H_2O_2 treatment of iodinated trihalomethanes. ***Water Research***, 75, 259-269.

3. Xiao, Y.; Zhang, L.; Zhang, W.; Lim, K.Y.; Webster, R.D.; Lim, T.T. **2016**. Comparative evaluation of iodoacids removal by UV/persulfate and UV/H_2O_2 processes. ***Water Research***, 102, 629-639.

B. Conference contributions

1. Xiao, Y.; Zhang, L.; Yue, J.; Lim, T.T. **2014**. Photodegradation of iodinated trihalomethanes by UV and UV/H_2O_2 treatment, oral presentation, IUVA (International Ultraviolet Association) 2014 Americas Regional Conference, 26-28 October, New York, U.S.

2. Xiao, Y.; Zhang, L.; Yue, J.; Lim, T.T. **2015**. Degradation of iodinated trihalomethanes and iodoacids by UV and UV/H_2O_2: kinetics, effect of operational parameters and energy efficiency, oral presentation, IWA Micropol & Ecohazard Conference 2015, 22-26 November, Singapore.

TABLE OF CONTENTS

LIST OF TABLES

LIST OF FIGURES

LIST OF ABBREVIATIONS AND SYMBOLS

Abbreviations

AOP	Advanced oxidation process
BS	Bond strength
B-THM	Brominated trihalomethane
DBP	Disinfection by-product
DI	Deionized water
HA	Humic acid
HAA	Haloacetic acid
HOI	Hypoiodous acid
IAA	Iodoacetic acid
I-DBP	Iodinated disinfection by-product
I-THM	Iodinated trihalomethane
mTA	m-toluic acid
NB	Nitrobenzene
OTC	Odor threshold concentration
pCBA	p-chlorobenzoic acid
pNBA	p-nitrobenzoic acid
QSAR	Quantitative structure-activity relationship
RO	Reverse osmosis
ROS	Reactive oxygen species
NOM	Natural organic matter
THM	Brominated/chlorinated trihalomethane
TOC	Total organic carbon
UV	Ultraviolet
U.S. EPA	U.S. Environmental protection agency
Vis	Visible electromagnetic radiation

Symbols

σ	Electronic effect constant
ε	Molar absorption coefficient
λ	Wavelength
Φ	Quantum yield
q_p	Photon flux emitted by a UV lamp
C	Concentration of organic pollutant
c_0	Speed of light
E_s	Steric effect constant
h	Planck's constant
I_o	Average photonic intensity per volume
b	Optical path length
k	Time-based first-order rate constant
k_f	Fluence-based first-order rate constant
N_A	Avogadro's constant

CHAPTER 1 Introduction

1.1 Background

It is well known that disinfection provides two main functions in water treatment processes. The primary function of disinfection is to inactivate or kill pathogens. Another function is to provide the residual of disinfectant in product water and preclude re-growth of micro-organism in water distribution system. However, besides pathogen inactivation or kill, chemical disinfectants such as chlorine are also strong oxidants, which can react with natural organic matters (NOM) and bromide/iodide present in the source waters (river, lake, and groundwater) to produce various organic and inorganic disinfection by-products (DBPs) (Xie, 2004).

The discovery of disinfection by-products (DBPs), including chloroform ($CHCl_3$) and other trihalomethanes (THMs) in chlorinated drinking water, were first reported by Bellar (1974) and Rook (1974). Since then, there has been increasing concern about the potential health effects caused by DBPs. On this basis, in 1979, the U.S. Environmental Protection Agency (U.S. EPA) issued a regulation to control total 4 brominated/chlorinated THMs including $CHCl_3$, $CHBr_2Cl$, $CHBrCl_2$, and $CHBr_3$ (U.S. EPA, 1979). Subsequently, U.S. EPA enforced the enhanced surface water treatment rule (1989) and the two stage (1998, 2006) D/DBP rule (U.S. EPA, 1998;2006). Now, 4 THMs and 5 haloacetic acids (HAAs) are the organic DBPs regulated by U.S. EPA. And the maximum contaminant levels (MCLs) of 4 THMs and 5 HAAs are 80 and 60 $\mu g\ L^{-1}$, respectively.

With the stricter regulations for THMs and HAAs, many water treatment plants have made some changes of the disinfection processes to comply with the new regulations. In practice, the primary disinfectant is switched from chlorine to other disinfectants including ozone, chlorine dioxide and chloramines, etc. However, new problems have arisen with the changes of disinfectants. For example, while the use of chloramines can greatly diminish or eliminate the

formation of THMs and HAAs, it can lead to the generation of very toxic emerging DBPs, such as iodinated disinfection by-products (I-DBPs), when iodide is present in the source waters (i.e., from natural source, sea water or brine) (Bichsel and von Gunten, 2000). Iodinated trihalomethanes (I-THMs) and iodoacids represent two major groups of I-DBPs.

1.2 Motivation and knowledge gap

Early concerns about I-DBPs are attributed to the characteristic medicinal odors and taste of I-THMs (Hansson et al., 1987; Cancho et al., 2001). For instance, it was reported that the odor threshold concentration of iodoform (CHI_3) was 0.1 µg L^{-1}, which is significantly lower than those of $CHCl_3$ and $CHBr_3$ (100 and 300 µg L^{-1}, respectively) (Cancho et al., 2000; Cancho et al., 2001). The taste threshold concentration of CHI_3 was reported as 5 µg L^{-1} (Hansson et al., 1987). This could explain the reported nuisance arising from low concentrations of I-THMs that are able to cause strong offensive odors and taste in drinking water.

In the most recent decade, I-DBPs have been found to be more genotoxic and cytotoxic than the regulated brominated and chlorinated analogues (Richardson et al., 2008). For example, CHI_3 was reported as 60 times and 146 times more cytotoxic in Chinese hamster ovary (CHO) cells than $CHBr_3$ and $CHCl_3$, respectively (Richardson et al., 2008). The cytotoxicity of iodoacetic acid (IAA) in CHO cells was 3.2 times and 288 times higher than bromoacetic acid (BAA) and chloroacetic acid (CAA), respectively. The genotoxicity of IAA in CHO cells was 2.0 times and 47 times higher than BAA and CAA, respectively (Plewa et al., 2004). I-DBPs have been identified in drinking water worldwide. For example, dichloroiodomethane ($CHCl_2I$) had been found in 85 of 111 water plants in U.S. and was detected more frequently than $CHBr_3$ (Brass et al., 1977). In an occurrence study, iodoacids including IAA, bromoiodoacetic acid, (*Z*)-3-bromo-3-iodo-propenoic acid, (*E*)-3-bromo-3-iodo-propenoic acid, and (*E*)-2-iodo-3-methylbutenedioic as well as I-THMs ($CHClI_2$, CHClBrI, $CHBr_2I$, $CHClI_2$, $CHBrI_2$, and CHI_3) were found at sub-µg L^{-1} to µg L^{-1} levels in drinking waters from 23 cities in U.S. and Canada (Richardson et al., 2008). In

another occurrence study, both CHI_3 and IAA were detected at sub-μg L^{-1} to μg L^{-1} levels in the drinking waters from 13 water plants in Shanghai, China (Wei et al., 2013). It can be said that I-DBPs should be considered when evaluating the drinking water exposure.

With the recent introduction of the standards of I-THMs and iodoacids to the market, significant research efforts have been directed to understand I-DBPs occurrence (Cancho et al., 2000; Krasner et al., 2006; Richardson et al., 2008; Farré et al., 2012; Wei et al., 2013), formation (Gallard et al., 2009; Pressman et al., 2010; Smith et al., 2010; Jones et al., 2011; Jones et al., 2012a; Jones et al., 2012b; Allard et al., 2013; Ye et al., 2013; Wang et al., 2014; Zhang et al., 2015b), analysis (Cancho et al., 1999; Cancho et al., 2000; Allard et al., 2012; Li et al., 2012b; Liu et al., 2013; Cardador et al., 2015), and health effects (Plewa et al., 2004; Richardson et al., 2008; Pressman et al., 2010). However, to date, only a few studies have been reported on the transformation of I-THMs at different process stages during water and advanced water treatment processes (Cancho et al., 2000; Farré et al., 2012) and there is still no study about the post-formation mitigation of iodoacids. In the previous studies, conventional water treatment process (sedimentation, sand filtration, and ozonation) and advanced membrane technologies such as reverse osmosis (RO) could not remove I-THMs effectively (Cancho et al., 2000; Farré et al., 2012).

To the best knowledge of the author, there is no experimental kinetic study on I-DBPs degradation and only a few of predicted degradation kinetics of I-DBPs by quantitative structure-activity relationship (QSAR) models have been reported. QSAR model is a useful tool to correlate the chemical activities with molecular structures as well as to predict the chemical activity of any compound which has a similar molecular structure as the ones used to establish the QSAR model. Generally, based on the experimental results of degradation of brominated/chlorinated DBP species, the QSAR models were established thereof and then used to predict the degradation rate of the corresponding I-DBPs analogues (Zhang and Minear, 2002; Chen et al., 2010; Chen, 2011). There has been no experimental result to validate the predicted degradation

kinetics of I-DBPs. In this context, it is necessary to perform systematic experiments to directly investigate the degradation kinetics of I-DBPs.

Besides post-chlorination, pre-chlorination and intermediate-chlorination are also applied in some water treatment plants. Pre-chlorination removes the odor and taste compounds and also enhances the following coagulation. The intermediate-chlorination is applied at settled water to prevent fouling of sand filter or ultrafiltration/microfiltration membrane. DBPs including I-DBPs could be generated during pre-chlorination, intermediate-chlorination and post-chlorination processes. Compared to that at the stage of post-chlorination process, I-DBPs are more easily generated during pre-chlorination and intermediate-chlorination processes, as the concentrations of DBPs precursor and iodide at these two stages are higher than those at the stage of post-chlorination. Thus, one of the possible strategies to mitigate the presence of I-DBPs in treated water or reclaimed water is to install an effective I-DBPs removal system after sand filter or membrane filtration system.

To date, UV facilities have been installed for disinfection in many water and advanced water treatment plants worldwide. Besides the main function of UV disinfection, many studies have been conducted to investigate the degradation of organic pollutants by UV irradiation. For example, N-Nitrosodimethylamine (NDMA) and I-DBPs analogues including brominated THMs (B-THMs) and brominated haloacetic acids (B-HAAs) could be degraded by UV254 direct photolysis (Nicole et al., 1991; Sharpless and Linden, 2003; Kwok et al., 2004; Jo et al., 2011). Compared to C-Br bond (280 kJ mol^{-1} of bond energy), C-I bond (209 kJ mol^{-1} of bond energy) can be photo-cleaved more easily after absorbing UV254 (472 kJ mol^{-1} of photon energy). In the past decades, the UV/H_2O_2 process, one of the most common advanced oxidation processes (AOPs), has been extensively studied and applied to remove recalcitrant organic pollutants in the advanced treatment of drinking water and wastewater. In the UV/H_2O_2 process, the degradation of organic pollutants involves both UV direct photolysis and hydroxyl radical ($HO^{\bullet}$)-assisted indirect photolysis. Another type of AOP, the UV/PS (persulfate, $S_2O_8^{2-}$) process, has recently

attracted significant scientific interest for the removal of recalcitrant organic pollutants via the generation of sulfate radical ($SO_4^{\bullet-}$) (Tsitonaki et al., 2010; He et al., 2014a; He et al., 2014b). Since $SO_4^{\bullet-}$ can be transformed to $HO^{\bullet}$ to some extent, the degradation of the organic pollutant in the UV/PS process is attributed to UV direct photolysis, as well as $SO_4^{\bullet-}$- and $HO^{\bullet}$-assisted indirect photolysis (He et al., 2014b; Yuan et al., 2014). It is worth mentioning that the UV/PS process has been demonstrated to remove some carboxylic acids effectively through decarboxylation by $SO_4^{\bullet-}$ (Madhavan et al., 1978; Davies et al., 1985; Criquet and Leitner, 2009). Therefore, it is believed that UV, UV/H_2O_2, and UV/PS have the potential to be effective technologies to degrade I-DBPs including I-THMs and iodoacids.

1.3 Objective and scope of works

The aim of the present study is to investigate the degradation of I-DBPs in aqueous solution by UV254, UV/H_2O_2, and UV/PS processes in order to develop a cost-effective strategy for post-formation mitigation of I-DBPs. To address the aforementioned knowledge gap, the scopes of works in the present study are as follows.

i. To investigate the UV254 direct photolysis of I-THMs:
   - Conduct and compare the degradation kinetics of I-THMs and THMs by UV254 irradiation;
   - Evaluate the influences of matrix species such as humic acid (HA), HCO_3^-, SO_4^{2-}, Cl^-, and NO_3^- on the direct photolysis kinetics;
   - Examine UV direct photolysis of I-THMs in the different types of water including DI water, treated water, surface water, and secondary effluent;
   - Identify the photodegradation end-products;
   - Establish QSAR model based on the experimental results of direct photolysis of I-THMs and B-THMs.

ii. To investigate the degradation of I-THMs in the UV/H_2O_2 process:

- Evaluate the effects of operational parameters such as pH; H_2O_2 dose, and matrix species on the photodegradation kinetics;
- Establish a steady-state kinetic model to predict the degradation rate of I-THMs by UV/H_2O_2 in the different types of water;
- Identify the photodegradation end-products;
- Apply electrical energy per order (EE/O) concept to evaluate the cost- and energetic-efficiencies of the photodegradation process and to optimize the H_2O_2 dose for different scenarios.

iii. To compare the degradation of iodoacids in the UV/H_2O_2 and UV/PS processes:

- Conduct UV254 direct photolysis of iodoacids;
- Establish a QSAR model to predict the direct photolysis rate of other commercially unavailable iodoaicds;
- Compare the effects of pH, oxidant dose, and matrix species on the photodegradation kinetics in the UV/PS and UV/H_2O_2 processes;
- Compare the photodegradation kinetics of iodoacids by the UV/PS and UV/H_2O_2 processes in different types of water;
- Determine the respective contributions of UV, $HO^{\cdot}$, and $SO_4^{\cdot-}$ for iodoacid removal in the UV/PS process;
- Identify and compare the photodegradation end-products in the UV/PS and UV/H_2O_2 processes;
- Conduct economic comparison of these two UV-based AOPs based on total cost of electrical energy and oxidant.

1.4 Organization of thesis

Chapter 1 includes the introduction to the background, motivation and knowledge gap, objectives and scopes of this research, as well as the organization of this thesis. Chapter 2 provides a literature review on the formation, occurrence, and toxicity of I-DBPs. It also presents the fundamentals of UV direct photolysis such as quantum yield and the formation, oxidation mechanism, and oxidation rate of $HO^{\cdot}$ and $SO_4^{\cdot-}$ as well as the recent

development of UV/H_2O_2 and UV/PS AOPs. Chapter 3 details the experimental setup, chemicals used, analytical methods, and the characteristics of the photoreactor used in this study. Chapter 4 presents the major findings on UV254 direct photolysis of 6 I-THMs. Chapter 5 discusses about the degradation of I-THMs by UV/H_2O_2 treatment. Chapter 6 evaluates the degradation of iodoacid by UV/PS in comparison with UV/H_2O_2 treatment. Chapter 7 outlines the major conclusions from this study and recommendations for the future work.

CHAPTER 2 Literature review

2.1 I-DBPs

2.1.1 Formation pathways of I-DBPs

The transformation of iodine during water treatment processes is illustrated in Figure 2.1. Iodide present in the source water can be rapidly oxidized to hypoiodous acid (HOI) by ozone, chlorine, and chloramines. It was found that HOI is very stable in the presence of chloramines (Bichsel and von Gunten, 1999). In contrast, HOI will be further oxidized to iodate (IO_3^-) by ozone and chlorine. IO_3^- is regarded as a non-toxic sink of iodine in drinking water, because only HOI can react with natural organic matters (NOM) to generate I-DBPs such as I-THMs and iodoacids. On the other hand, the disproportionation of HOI proceeds slowly to produce I^- and IO_3^- (Bichsel and von Gunten, 1999).

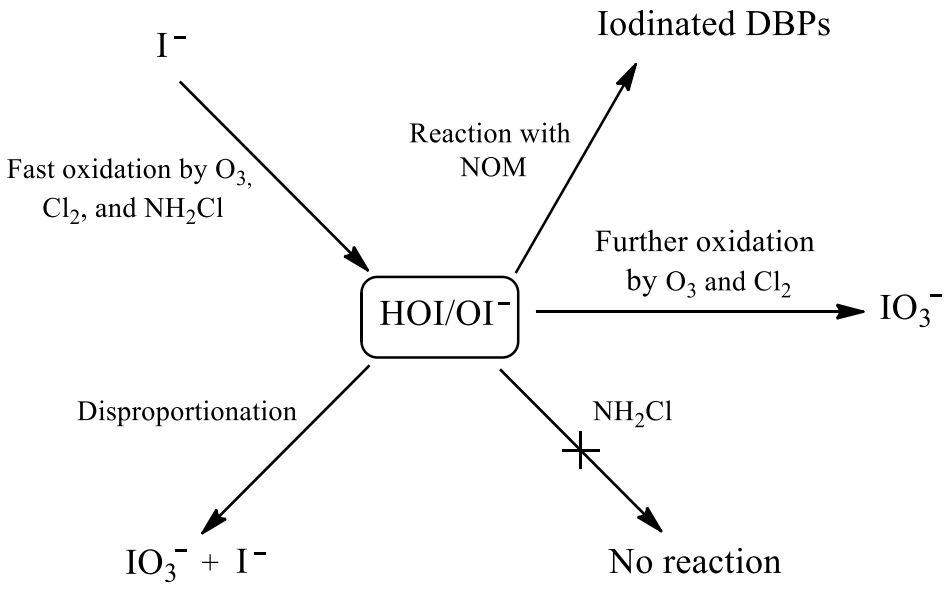

Figure 2.1 Transformation of iodine during water treatment processes (Bichsel and von Gunten, 1999).

An illustration of CHI_3 formation is as shown in Figure 2.2. There are a total of 3 reaction steps including enolization, iodination, and hydrolysis during CHI_3 formation processes. In the first step, α-methyl carbonyl compound is enolized

to its corresponding enol in the presence of some species such as hydroxide (HO^-). In the second step, electrophilic substitution reaction between HOI and the formed enol occurs to produce iodocarbonyl compound whereby HOI acts as an electrophile. The iodination of the α-methyl carbonyl compound occur 3 times and the methyl group has been converted to the corresponding triiodomethyl group. In the final step, hydrolysis of triiodocarbonyl compound proceeds to produce CHI_3 and the corresponding acid (RCO_2H) (Bichsel and von Gunten, 2000).

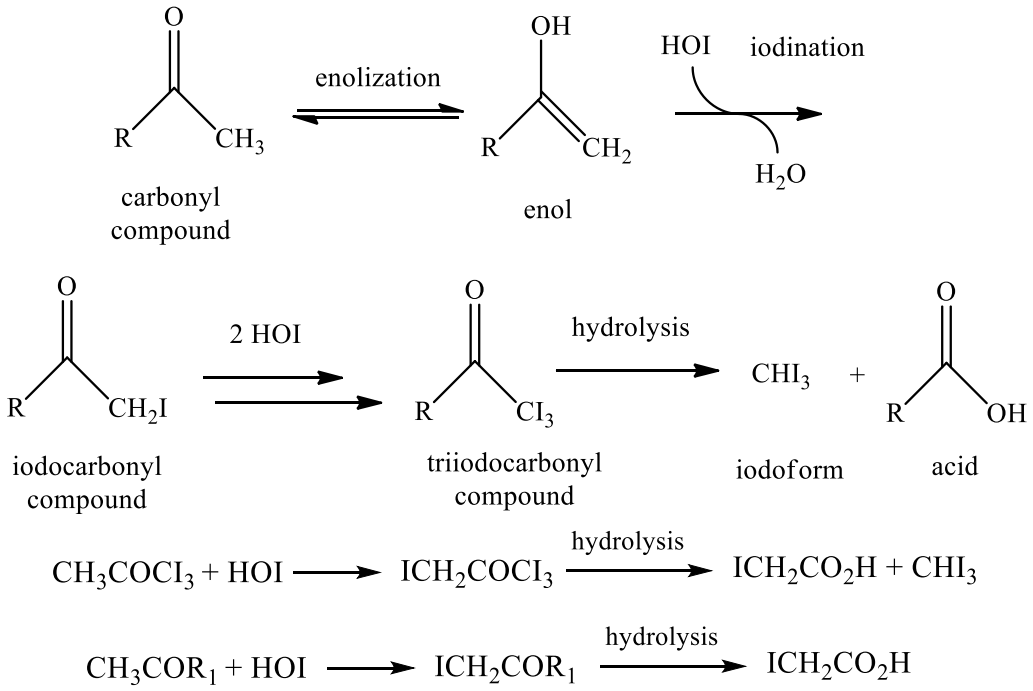

Figure 2.2 The formation pathway of CHI_3 and ICH_2CO_2H from HOI and α-methyl carbonyl compound (Bichsel and von Gunten, 2000; Xie, 2004).

The formation of iodinated acetic acids can also be demonstrated with the reaction between α-methyl carbonyl compound and HOI (Figure 2.2). For example, when R is methyl group, the triiodocarbonyl compound (CH_3COCI_3) can be further oxidized to tetraiodopropanone (ICH_2COCI_3), pentaiodopropanone ($I_2CHCOCI_3$), and hexaiodopropanone (CI_3COCI_3), which can be hydrolyzed to mono-, di-, and tri-iodoacetic acids. Iodinated acetic acids can also be formed by the reaction between CH_3COR_1 and HOI, where R_1 is an oxidizable group. If HOCl and/or HOBr are also present in the reaction solution, haloacetic acids containing I, Br and Cl atom can be formed.

As shown in Figure 2.3, the half-life of HOI in the presence of chlorine is in the range of minutes to hours, which indicates that I-DBPs formation during chlorination process is possible. In contrast, the formation of I-DBPs is suppressed when ozone is used as a disinfectant, because HOI can be oxidized by ozone to IO_3^- in seconds. On the other hand, the half-life of HOI in the presence of chloramines is in years, indicating the I-DBPs are readily formed during chloraminaton process (Bichsel and von Gunten, 1999). Therefore, I-DBPs are attracting more attention from water utilities, especially for those using chloramines as primary disinfectant.

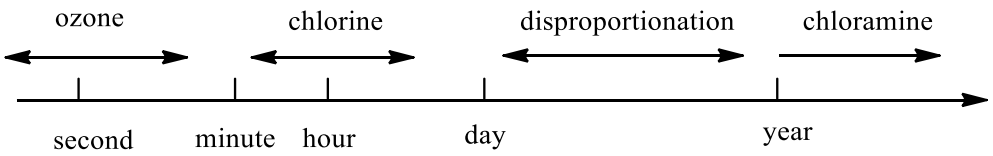

Figure 2.3 The half-lives of HOI in the presence of different disinfectants (Bichsel and von Gunten, 1999).

2.1.2 Taste and odor problems related to I-DBPs

Early concerns about I-DBPs are due to the characteristic pharmaceutical or medicinal odors and tastes of I-THMs in drinking water (Hansson et al., 1987; Cancho et al., 2001). As shown in Table 2.1, the odor threshold concentrations (OTCs) of I-THMs decreases with the increase of iodine atoms in the molecule and follows the trend of $CHI_3 < CHXI_2 < CHX_2I$. The OTCs of I-THMs are in the range of 0.1 to 8.9 μg L^{-1}, which are 1 to 2 orders of magnitudes lower than those of $CHBr_3$ and $CHCl_3$ (100 and 300 μg L^{-1}, respectively) (Cancho et al., 2001). Additionally, the taste threshold concentration of CHI_3 was established as 5 μg L^{-1} in a previous study (Hansson et al., 1987), because it was reported that the water containing CHI_3 at this concentration tasted as plastic or medicine. It means that I-THMs, especially CHI_3, at a very low concentration are able to cause odor and taste problems in drinking water.

Table 2.1 Odor descriptor and threshold concentration for I-THMs (Cancho et al., 2001)

Species	Odor descriptor	OTC (μg L^{-1})
$CHCl_2I$	sweet, syrup	8.9
CHClBrI	sweet, fresh grass, perfumed, alcoholic	8.4
$CHBr_2I$	medicinal, sweet, perfumed, bitumen	6.4
$CHClI_2$	medicinal, sweet, solvent candy	0.2
$CHBrI_2$	medicinal, sweet, solvent, perfumed	0.2
CHI_3	medicinal, sweet, perfumed, gum	0.1

2.1.3 Toxicity of I-DBPs

In the most recent decade, new concerns about I-DBPs are attributed to their higher cytotoxicities and genotoxicities. I-DBPs have been predicted to be more toxic than their brominated and chlorinated analogues (Plewa et al., 2004; Richardson et al., 2007; Richardson et al., 2008). The prediction is based on the evidences that brominated DBPs have been reported to be more toxic than the corresponding chlorinated analogues. Furthermore, iodine is anticipated to be more biologically reactive than bromine and chlorine (Richardson et al., 2007). Some mammalian cell toxicity results supported this hypothesis, as shown in Figure 2.4. For example, one previous study demonstrated that CHI_3 was 60 times and 146 times more cytotoxic in Chinese hamster ovary (CHO) cells than $CHBr_3$ and $CHCl_3$, respectively; $CHBrI_2$ was 8 times more cytotoxic than $CHBrCl_2$; $CHBr_2I$ was 3 times more cytotoxic than $CHBr_2Cl$ (Richardson et al., 2008). In addition, comparing the cytotoxicities and genotoxicities among 6 I-THMs, CHI_3 was found to be the most cytotoxic species, while $CHClI_2$ was the most genotoxic species. It was also observed that the cytotoxicity of IAA in CHO cells was 3 times and 287 times higher than BAA and CAA, respectively (Richardson et al., 2008). Plewa et al. (2004) also observed that IAA was 2 times and 47 times more genotoxic in CHO cells than BAA and CAA, respectively . Generally, among the haloacetic acids, IAA is the most cytotoxic and genotoxic DBP in mammalian cells. These toxicity results suggested that I-DBPs including I-THMs and iodoacids are worth investigating due to their higher toxicities, although the concentrations of I-DBPs may be much lower than those of their brominated and chlorinated analogues.

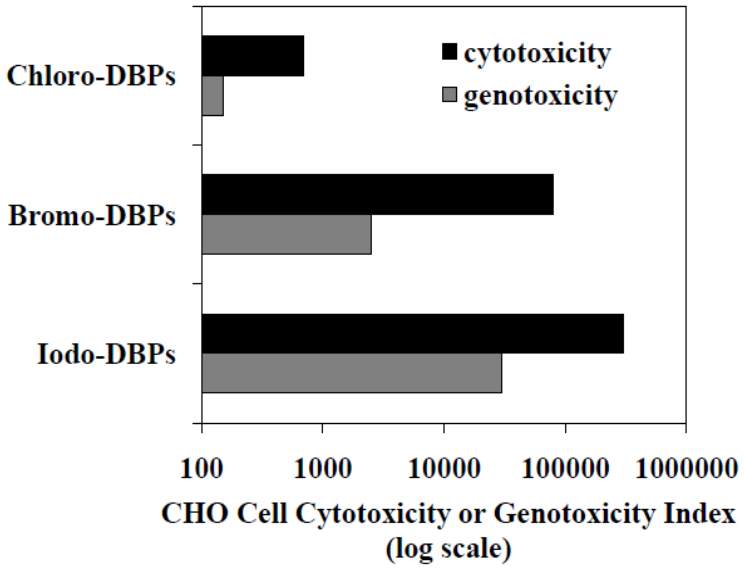

Figure 2.4 Toxicity of halogenated-DBPs (Jones, 2009).

2.1.4 Occurrence studies of I-DBPs

A DBPs occurrence study was conducted at 12 drinking water treatment plants in U.S. (Krasner et al., 2006). A number of disinfectants including chlorine, ozone, chlorine dioxide, and chloramines were used in these 12 plants. It was found that THMs and HAAs were the two major groups of halogenated DBPs in the finished water. The total concentration of I-THMs was typically much lower than the sum of THMs. However, high concentration of I-THMs was observed in one plant where chloramines were used as primary disinfectant and the source water contained high concentration of bromide and iodide. The total concentration of I-THMs was 81% of the sum of THMs. And the concentration of $CHCl_2I$ was the highest among I-THMs and THMs (Figure 2.5). Additionally, another significant finding was that IAA, bromoiodoacetic acid (BIAA), (*Z*)-3-bromo-3-iodo-propenoic acid, (*E*)-3-bromo-3-iodo-propenoic acid, and (*E*)-2-iodo-3-methylbutenedioic were observed for the first time at this chloramination plant.

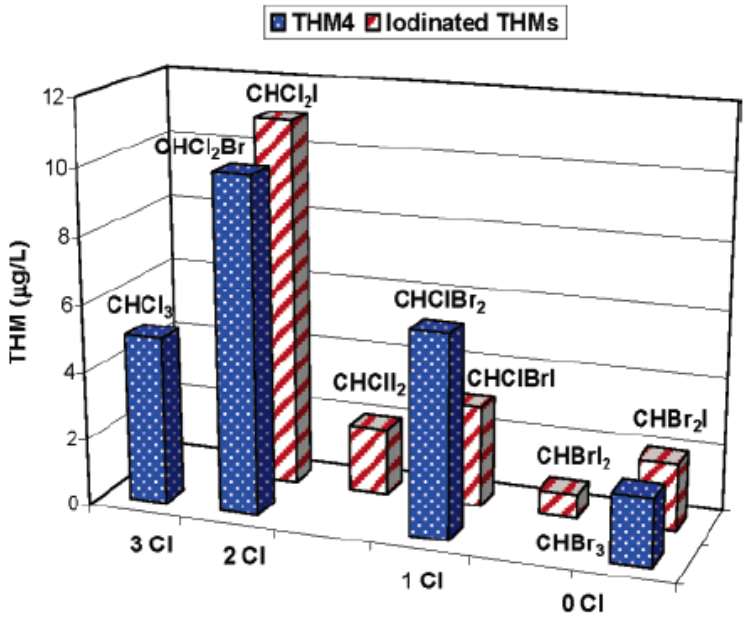

Figure 2.5 THMs and I-THMs formation when chloramine was used as disinfectant in one plant (Krasner et al., 2006).

As high concentrations of I-THMs and iodoacids were detected in the chloramination plant, Richardson et al. (2008) conducted a further occurrence study focusing on 5 iodoacids and 2 I-THMs in chloraminated and chlorinated drinking waters from 23 cities in the U.S. and Canada. Only $CHCl_2I$ and CHBrClI among 6 I-THMs were monitored in that study, because these 2 species were commonly detected in the previous occurrence study. Most of the selected plants used chloramines as disinfectant, while 2 chlorination plants were also selected for comparison.

In general, iodoacids and I-THMs were detected at ng L^{-1} to low µg L^{-1} level in the finished drinking water from most of the plants (Table 2.2). The maximum concentration of IAA, BIAA, (*Z*)-3-bromo-3-iodo-propenoic acid, (*E*)-3-bromo-3-iodo-propenoic acid, (*E*)-2-iodo-3-methylbutenedioic, $CHCl_2I$, and CHBrClI in the all finished drinking water were 1.7, 1.4, 0.5, 0.28, 0.58, 10.2, and 7.9 µg L^{-1}, respectively. The concentrations of I-THMs were higher than those of the corresponding iodoacids. In addition, the concentrations of I-THMs were higher than most previously reported values. This is because this occurrence study focused on the plants with chloramination, whereby observation of high concentration of I-DBPs is rational.

The effect of iodide concentration and free chlorine contact time on I-DBPs formation was also evaluated in that occurrence study. Generally, the increase of iodide concentration in source waters led to increase of I-DBPs formation. A longer prechlorination contact time resulted in the decrease of I-DBPs formation, because iodide can be rapidly oxidized by chlorine to iodate that serves as a sink for iodide. In contrast, a shorter prechlorination contact time led to increase of I-DBPs formation, because the dominant species in the presence of chloramines was HOI which could react with NOM to produce I-DBPs. Results from that occurrence study support the proposed formation mechanism of I-DBPs. For example, the total concentrations of iodoacids and I-THMs in plant 10 (chlorine used as disinfectant) were the lowest among all of the selected plants, although the iodide (7.3 μg L^{-1}) and TOC (3.5 mg L^{-1}) were at the moderate level in the source water. In addition, the concentrations of I-DBP were also low in the chloramination plant 18 with long prechlorination contact time (e.g., > 45 min), despite moderate concentration of iodide (10.4 μg L^{-1}) in its source water. On the other hand, higher levels of I-DBPs were observed in the chloramination plants such as plant 1, 2, 12, 13, 17, and 19, where the prechlorination contact time was very short (e.g., < 1 min) and the source water contained high concentration of bromide and iodide (Table 2.2).

Table 2.2 Concentrations of some selected iodoacids and I-THMs in an occurrence study (Richardson et al., 2008)

Plant	Sampling time	Disinfectant	TOC[a]	Bromide	Iodide	IAA[d]	BIAA	*Z*	*E*	diacid	CHBrClI	$CHCl_2I$	Sum iodoacids	Sum I-THMs
1	2005	NH_2Cl	5.8	NR[b]	NR	**1.7**	0.52	0.077	0.061	0.36	NR	NR	2.72	NR
1	2006	NH_2Cl	5.1	699	65	0.093	0.29	0.085	**0.28**	0.064	5.4	1.5	0.81	6.9
2	2006	NH_2Cl	5.6	133	1.0	0.015	0.091	0.050	0.13	0.027	1.4	3.5	0.37	4.9
6	2006	NH_2Cl	3.3	96	0.4	0.007	0.026	0.032	0.013	0.027	0.2	1.1	0.11	1.3
7	2006	NH_2Cl	3.4	105	ND	0.014	0.005	0.010	0.003	0.004	0.13	0.30	0.04	0.43
10	2006	Cl_2	3.5	214	7.3	0.033	0.005	0.010	0.003	0.004	0.25	0.22	0.05	0.47
12	2005	NH_2Cl	5.2	316	NR	0.006	0.030	ND	ND	0.077	1.5	**7.9**	0.11	9.4
12	2006	NH_2Cl	5.2	204	10.3	0.078	0.048	0.003	0.032	0.031	0.98	5.1	0.19	6.1
13	2006	NH_2Cl	5.1	186	22.3	0.070	0.044	0.010	0.037	0.028	2.1	5.7	0.19	7.8
15	2006	NH_2Cl	NR	107	ND	0.050	0.056	0.038	0.013	0.012	0.2	2.2	0.17	2.4
17	2005	NH_2Cl	7.4	1087	NR	0.021	0.49	**0.50**	0.086	0.31	**10.2**	2.1	1.41	12.3
17	2006	NH_2Cl	3.9	NR	22.4	0.018	0.038	0.064	0.11	0.048	3.5	0.6	0.28	4.1
18	2006	NH_2Cl	3.2	35	10.4	0.033	0.035	0.009	0.005	0.009	ND	0.46	0.09	0.46
19	2005		4.5	545	NR	0.062	**1.4**	ND[c]	ND	**0.58**	0.16	0.61	2.04	0.76
19	2006	Cl_2(but natural ammonia present to form NH_2Cl)	5.0	300	104.2	0.67	0.29	0.082	ND	0.017	0.72	1.1	1.1	1.8

a. Unit for TOC: mg L^{-1}; unit for other parameters: µg L^{-1}; b. NR: not reported; c. ND: not detected; d. IAA: iodoacetic acid; BIAA: bromoiodoacetic acid; *Z*: (*Z*)-3-bromo-3-iodo-propenoic acid; *E*: (*E*)-3-bromo-3-iodo-propenoic acid; diacid: (*E*)-2-iodo-3-methylbutenedioic.

Besides the above findings, the observations of I-DBPs in drinking water were also reported in other studies. For example, a total amount of 37 water samples were collected from Barcelona drinking water distribution system for I-THMs monitoring. Of which, 33 water samples analyzed contained $CHCl_2I$, while 27 water samples contained CHClBrI. Additionally, CHI_3 was observed in only 3 samples (Khiahi et al., 1999). In another occurrence study, both IAA and CHI_3 were also detected at ng L^{-1} to low µg L^{-1} levels in drinking waters from 13 water plants in Shanghai, China, with maximum levels of 1.66 µg L^{-1} and 1.25 µg L^{-1} for IAA and CHI_3, respectively (Wei et al., 2013). In a national organic monitoring survey, $CHCl_2I$ had been observed in 85 out of 111 water plants in U.S. and was detected more frequently than $CHBr_3$ (Brass et al., 1977). Another example is that high level of CHI_3 was observed in the finished drinking water in Australia, when one big water plant used chloramines to replace chlorine in order to maintain the residual of disinfectant in its big distribution system. As a result, complaints were immediately received from the customers. This problem was solved by addition of chlorine for a few minutes before adding ammonia instead of the reverse order (Hansson et al., 1987).

2.1.5 Transformation of I-DBPs at different process stages during water and advanced water treatment processes

To date, only a few studies have been reported on the transformation of I-THMs at different process stages during water and advanced water treatment processes (Cancho et al., 2000; Farré et al., 2012) and there is still no well-documented study on the post-formation mitigation of iodoacids.

In one study, water samples were collected from different process stages at Barcelona water treatment plant for I-THMs monitoring (Cancho et al., 2000). Conventional treatment processes in this water treatment plant included pre-chlorination, flocculation, sand filtration, ozonation, granular activated carbon (GAC) filtration, and post-chlorination. The average levels of TOC, bromide, and iodide in source water were 5.0 mg L^{-1}, 700 µg L^{-1}, and 3.2 µg L^{-1}, respectively. As shown in Table 2.3, 4 species including $CHCl_2I$, CHClBrI, $CHBr_2I$, and $CHClI_2$ were identified during water treatment processes, and the concentration of each

species was less than 1 μg L^{-1}. $CHCl_2I$ was found in the prechlorinated and sand filtered water. $CHClI_2$ was detected in the sand filtered water. Both CHClBrI and $CHBr_2I$ were detected in the prechlorinated, sand filtered, and ozonated water. It was worth mentioning that the concentrations of these identified species were insignificantly different in the prechlorinated, sand filtered, or ozonated water. It suggested that conventional treatment processes including sedimentation, sand filtration, and ozonation could not remove I-THMs effectively. In contrast, GAC filtration technology appeared promising to remove I-THMs effectively, because all of 6 I-THMs could not be detected after GAC filtration.

Table 2.3 Concentration of I-THMs at different process stages at Barcelona water treatment plant (Cancho et al., 2000)

Species	Raw water	Prechlorination	Sand filtration	Ozonation	GAC	Distribution system
$CHCl_3$	0.2	8.7[a]	15	14	10	9.5
$CHCl_2Br$	–[b]	14	24.5	23	19	21
$CHClBr_2$	0.1	21	39	37	29	34
$CHBr_3$	0.2	13	29	27	17	26
$CHCl_2I$	–	0.1	0.2	–	–	–
CHClBrI	–	0.2	0.6	0.2	–	–
$CHBr_2I$	–	0.1	0.2	0.1	–	–
$CHClI_2$	–	–	0.1	–	–	–
$CHBrI_2$	–	–	–	–	–	–
CHI_3	–	–	–	–	–	–
TTHMs	0.5	57.1	108.6	101.3	75	90.5

a. Unit: μg L^{-1}; b. It represents the result is below detection limit.

In another study, the transformation of I-THMs during advanced water treatment processes was also investigated (Farré et al., 2012). The advanced water treatment plant consisted of the following processes in sequence: coagulation, disinfection with chloramines, ultrafiltration (UF), RO, UV-based AOP, and final disinfection with chlorine. Secondary effluent from a wastewater treatment plant was used as source water. Water samples were collected from different process stages for monitoring of DBPs including I-THMs. The relative proportions (on a molar basis) of several groups of DBPs at each stage were displayed in Figure 2.6. I-THMs were firstly detected in UF feed after disinfection and remained persistent in RO feed and permeate. It was also important to highlight that the relative proportions of I-THMs

among the DBPs monitored were insignificantly different in UF feed, RO feed and RO permeate. It suggested that advanced membrane technologies including UF and RO could not remove I-THMs effectively. In contrast, I-THMs seemed to be effectively eliminated by UV-based AOP.

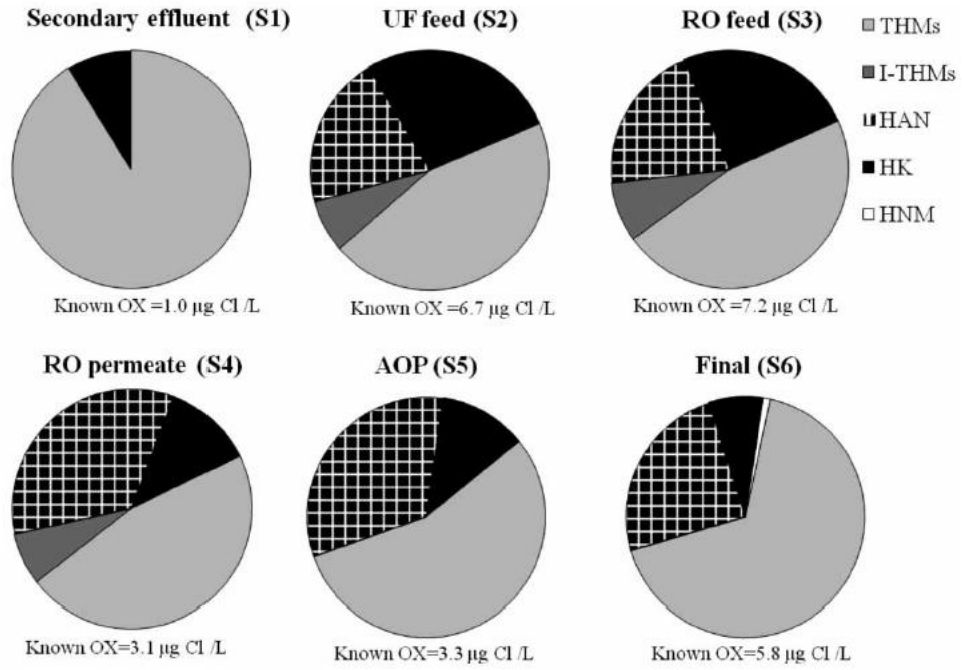

Figure 2.6 The relative proportions (on a molar basis) of several groups of DBPs at each stage during the advanced water treatment processes. HAN: haloacetonitriles; HK: haloketones; HNM: halonitromethanes (Farré et al., 2012).

2.2 UV direct and indirect photolysis

2.2.1 UV direct photolysis

2.2.1.1 Reaction pathways during direct photolysis

A ground state molecule (RX) under the UV irradiation can be promoted to its electronically excited state (RX^*). When the molecules contain a chromophore group with carbon-halogen (C-X) bond, homolysis of the C-X bond proceeds to form a carbon centered radical and halogen atom (Equation 2.1). Subsequently, the carbon centered radical formed can be efficiently trapped by molecular oxygen

present in the reaction medium to generate peroxyl radical that will be further transformed to its photoproducts (Equation 2.2). Other mechanisms for direct photolysis of the organic pollutant in water include the electron transfer from the electronically excited state (RX^*) to the molecular oxygen present in the reaction medium, which leads to the formation of substrate radical cation and superoxide radical. A series of subsequent reactions such as recombination of the radical ions or hydrolysis of the radical cation occurs to produce the corresponding photoproducts (Equation 2.3). Additionally, the RX^* formed can be deactivated by a quencher via energy transfer, electron transfer, or chemical reaction etc. For example, RX^* may be quenched by molecular oxygen to generate singlet molecular oxygen (Equation 2.4) (Oppenlander, 2003).

$$RX + hv \rightarrow RX^* \rightarrow R^{\bullet} + X^{\bullet} \quad (2.1)$$

$$R^{\bullet} + O_2 \rightarrow RO_2^{\bullet} \rightarrow \text{photoproduct} \quad (2.2)$$

$$RX^* + O_2 \rightarrow O_2^{\bullet -} + RX^{\bullet +} \rightarrow \text{photoproduct} \quad (2.3)$$

$$RX^* + O_2 \rightarrow RX + {}^1O_2 \quad (2.4)$$

The direct photolysis rate of the organic pollutant depends on the UV absorbance of the organic pollutant at the wavelength in question, quantum yield of the whole photochemical processes, and the photon flux emitted by UV lamp at that wavelength (Wols and Hofman-Caris, 2012).

2.2.1.2 UV absorbance

To evaluate the photochemical potential of the organic pollutant under UV/Vis direct irradiation, it is necessary to measure its UV/Vis absorbance (Oppenlander, 2003). Subsequently, it is essential to compare the homolytic bond dissociation energy (D) of the bond that is photo-cleaved in the photochemical reaction and photon energy at the wavelength in question. In the photochemistry and photochemical engineering, there are 2 commonly used terms related to photon energy at the specific wavelength. The first term is threshold wavelength (λ_{THW}) that is regarded as the maximum wavelength at which the photon energy is equal to

the energy of the bond that is photo-cleaved in the photochemical reaction (Bolton and Cater, 1994). It can be determined according to Equation 2.5.

$$\lambda_{THW}(\text{nm}) = \frac{N_A hc_o}{D} = \frac{1.1963 \cdot 10^5 (\text{kJ nm mol}^{-1})}{D(\text{kJ mol}^{-1})} \quad (2.5)$$

where N_A is Avogadro's constant in mol^{-1}; h is Planck constant in J s; c_o is the speed of light in m s^{-1}. The second term is the absorption onset (λ_{onset}) that is defined as the specific wavelength at which absorption of UV/Vis irradiation by a molecule starts and its corresponding molar absorption coefficient (ε) reaches 1.0 M^{-1} cm^{-1} (Bolton and Cater, 1994). The bond dissociation energy (D), the corresponding threshold wavelength (λ_{THW}), and absorption onset (λ_{onset}) of some environmentally important molecules are presented in Table 2.4. For most species, the absorption onsets (λ_{onset}) are much lower than their calculated threshold wavelengths (λ_{THW}). One possible explanation is that excess energies are needed for the formed primary radicals to escape the solvent (water) cage. Otherwise, recombination of the formed primary radical occurs rapidly, as the rate of diffusion of the primary radicals out of the solvent cage is often much smaller than the rate of recombination (Bolton and Cater, 1994). As shown in Table 2.4, the absorption onset (λ_{onset}) of H_2O_2 is 310 nm, which is much lower than its calculated threshold wavelength (λ_{THW} = 562 nm). It suggests that $HO^{\cdot}$ could not be generated when H_2O_2 is exposed to the irradiation at 562 nm, as H_2O_2 is optically transparent at this wavelength (i.e., H_2O_2 has no light absorption at 562 nm). In contrast, with exposure to the UV irradiation below 310 nm, homolysis of peroxy bond (-O-O-) in the molecule of H_2O_2 proceeds to form $HO^{\cdot}$. For ozone, the absorption onset was measured as 330 nm. It means that UV irradiation below 330 nm is absorbed by O_3 and promotes the bond dissociation with generation of the reactive oxygen species such as singlet molecular oxygen (^1A_g) and singlet oxygen atoms (^1D). The latter (^1D) can be further transformed to $HO^{\cdot}$ through a series of subsequent reactions. Additionally, photodissociation of H_2O under the vacuum-UV (VUV) irradiation below 190 nm leads to the generation of hydrogen atom and $HO^{\cdot}$, as the absorption onset of H_2O was measured as 190 nm. Due to efficient production of $HO^{\cdot}$, these 3

reaction systems described above are classified as AOPs and commonly used for mineralization and oxidation of the organic pollutants during water and wastewater treatment processes.

Table 2.4 Primary photochemical processes of some environmentally important molecules in the gas phase (Oppenlander, 2003)

Molecule	Primary products	D (kJ mol^{-1})	Threshold wavelength (λ_{THW}) in nm	Absorption onset (λ_{onset}) in nm
H_2O_2	2 $HO^{\cdot}$	213	562	310
N_2	$NO^{\cdot}$ + $^{\cdot}O^{\cdot}$ (^3P)	945	127	126
O_2	2 $^{\cdot}O^{\cdot}$ (^3P)	498	240	190
O_3	$O_2(^1A_g)$ + $O^{\cdot}$ (^1D)	292	410	330
H_2O	$H^{\cdot}$ + $HO^{\cdot}$	498	240	190

Like H_2O_2, some organic pollutants are able to dissociate in the presence of UV irradiation alone. For example, *S*-nitrosotoluene-α-thiol ($C_6H_5{\cdot}CH_2{\cdot}SNO$) strongly absorbs UV irradiation at the wavelength from 200 to 400 nm. Its UV absorption spectrum exhibits a strong band with a maximum at 220 nm ($\varepsilon = 10^4\ M^{-1}\,cm^{-1}$) and a median band with a maximum at 340 nm ($\varepsilon = 1030\ M^{-1}\,cm^{-1}$). Additionally, there is a weak band with a maximum at 560 nm ($\varepsilon = 26\ M^{-1}\,cm^{-1}$). A previous study demonstrated that UV irradiation at 365 nm was able to photolyze *S*-nitrosotoluene-α-thiol, as this compound has an evident UV absorbance at 365 nm and the photon energy (330 kJ mol^{-1}) at this wavelength is sufficient to photo-cleave the weak -S-N- bond (217 kJ mol^{-1}) in the molecule (Barrett et al., 1965).

2.2.1.3 Quantum yield, photon flux, and photoreaction kinetics

The quantum yield (Φ) is an indicator of the overall efficiency of a photochemical reaction (Braun et al., 1991). The quantum yield is defined as the number of the target molecules decomposed divided by the number of photon absorbed by the target molecules per unit time (Equation 2.6).

$$\Phi = -\frac{dM/dt}{\Phi_{p,abs}} \tag{2.6}$$

$$M = CV \tag{2.7}$$

$$\Phi_{p,abs} = q_{p,abs} A \tag{2.8}$$

where M is the total number of molecules decomposed per unit time in mol and can be calculated according to Equation 2.7; $\Phi_{p,abs}$ is the total number of photon absorbed by the target molecules per unit time in E s^{-1} and is equal to absorbed photon flux ($q_{p,abs}$, E m^{-2} s^{-1}) times irradiation area (A, m^2); C is the concentration of target compound in mol L^{-1}; V is the volume of the reaction solution in L.

Substitution of Equations 2.7 and 2.8 into Equation 2.6 leads to Equation 2.9.

$$\Phi = -\frac{dC/dt \cdot V}{q_{p,abs} A} \tag{2.9}$$

Additionally, Equation 2.9 can be rearranged to Equation 2.10 that is the rate expression of a photochemical reaction.

$$-\frac{dC}{dt} = \Phi q_{p,abs} \frac{A}{V} \tag{2.10}$$

According to Beer-Lambert Law, $q_{p,abs}$ can be expressed as follows.

$$q_{p,abs} = q_P - q_{p,trans} = q_P (1 - 10^{-\varepsilon Cb}) \tag{2.11}$$

where q_p is the photon flux emitted by a UV lamp in E m^{-2} s^{-1}; $q_{p,trans}$ is the transmitted photon flux in E m^{-2} s^{-1}; b is the optical path length in cm and is equal to $\frac{V}{A}$; ε is the molar absorption coefficient of the organic pollutant at the wavelength in question in M^{-1} cm^{-1}.

Substitution of Equation 2.11 into Equation 2.10 leads to Equation 2.12.

$$-\frac{dC}{dt} = \Phi q_p (1 - 10^{-\varepsilon Cb}) \frac{A}{V} \tag{2.12}$$

In a diluted solution of the organic pollutant, if UV absorbance of the solution is very low (i.e., $2.303\varepsilon Cb < 0.02$), $10^{-\varepsilon Cb}$ in Equation 2.12 can be simplified to $1 - 2.303\varepsilon Cb$ through Taylor expansion. Then, Equation 2.12 can be written as Equation 2.13.

$$-\frac{dC}{dt} = 2.303\Phi\varepsilon q_p C \quad (2.13)$$

When the total number of photon absorbed by the target molecules is expressed by the product of the average photonic intensity per volume (I_o, E L^{-1} s^{-1}) and the volume of the reaction solution (V, L), similar formulas for direct photolysis rate can also be derived as shown in Equations 2.14 and 2.15.

$$-\frac{dC}{dt} = \Phi I_O(1-10^{-\varepsilon Cb}) \quad (2.14)$$

$$-\frac{dC}{dt} = 2.303\Phi\varepsilon I_O bC \quad (2.15)$$

It is obvious from Equations 2.13 and 2.15 that the photodegradation rate of the organic pollutant is proportional to the quantum yield (Φ) and the molar absorption coefficient of the organic pollutant (ε) at the wavelength in question. The photodegradation rate is also related to the photon flux (q_p) or the average photonic intensity per volume (I_o) emitted by the UV lamp and optical path length which depend on the geometry of photoreactor.

Quantum yield may vary with the change of the wavelength of the absorbed UV irradiation, but some photochemical systems exhibit constant quantum yields over a specific range of wavelength. Such photochemical systems with well-known quantum yields, termed as actinometer are commonly used to measure the photon flux (q_p) emitted by a UV lamp (Oppenlander, 2003). For example, iodide/iodate has been used as an actinometer to measure the photon flux emitted by UV254 lamp (Rahn, 1997). And this method is commonly used to determine the disinfection efficiency. Additionally, some other actinometric methods have been developed to measure the radiation efficiencies of the novel UV lamps, e.g. using 3,4-dimethoxynitrobenezne as an actinometer at 308 nm (Zhang et al., 1999), uridine at 222 nm (Zhang et al., 1997), and methanol at 172 nm (Heit et al., 1998).

As mentioned above, the photon flux (q_p) or the average photonic intensity per volume (I_o) of the photoreactor system can be measured from chemical actinometry. Subsequently, quantum yield of the organic pollutant investigated can be

determined according to Equation 2.13 or 2.15, based on molar absorption coefficient and experimentally observed first-order rate constant of the organic pollutant by direct photolysis.

2.2.2 UV indirect photolysis

2.2.2.1 Formation of hydroxyl and sulfate radical

UV-based AOPs have been intensively investigated for oxidation and mineralization of the organic pollutants. There are a variety of UV-based AOPs technologies including UV/H_2O_2, UV/H_2O_2/Fe^{3+}, UV/O_3, UV/TiO_2, vacuum UV (VUV), UV/$S_2O_8^{2-}$(UV/PS), and UV/HSO_5^- etc. These technologies have a common feature with efficient production of reactive radical species such as $HO^{\bullet}$ and $SO_4^{\bullet-}$. The focuses of this study are UV/H_2O_2 and UV/PS AOP and their application for removal of I-DBPs including I-THMs and iodoacids. Thus, in this section, the formation of $HO^{\bullet}$ in the UV/H_2O_2 process and $SO_4^{\bullet-}$ in the UV/PS process were discussed as follows.

H_2O_2 and $S_2O_8^{2-}$ have a similar structure with a peroxy bond (-O-O-). Two hydrogen atoms in the molecule of H_2O_2 are replaced by SO_3 to form $S_2O_8^{2-}$. It was reported that the bond distances of -O-O- in H_2O_2 and $S_2O_8^{2-}$ are 1.460 and 1.497 Å, respectively, while the bond energy of -O-O- in H_2O_2 and $S_2O_8^{2-}$ are 213.3 and 140 kJ mol^{-1}, respectively (Yang et al., 2010). The photon energy of UV254 is 472 kJ mol^{-1}, which is sufficient to cleave the -O-O- bond in H_2O_2 and $S_2O_8^{2-}$. The molar absorption coefficients of H_2O_2 and $S_2O_8^{2-}$ at UV254 are 19.6 and 20 M^{-1} cm^{-1}, respectively (Kwon et al., 2015). Under UV254 direct irradiation, the ground state of H_2O_2 and $S_2O_8^{2-}$ can be promoted to its electronically excited state. Subsequently, homolytic cleavage of -O-O- bond in the electronically excited molecule leads to the formation of the primary radical species, $HO^{\bullet}$ and $SO_4^{\bullet-}$, respectively. The formation quantum yields of $HO^{\bullet}$ and $SO_4^{\bullet-}$ at this wavelength are 1.0 and 1.4, respectively (Baxendale and Wilson, 1957; Mark et al., 1990). In comparison with the selective radical species such as $CO_3^{\bullet-}$ and $Cl^{\bullet}$, both $HO^{\bullet}$ and $SO_4^{\bullet-}$ react with a wide range of organic pollutants at a near diffusion-controlled rate, due to their

higher redox potential (1.8 to 2.7 V/NHE and 2.6 to 3.1V/NHE for $HO^{\bullet}$ and $SO_4^{\bullet-}$, respectively) (Zhang et al., 2015a). Compared to $HO^{\bullet}$, $SO_4^{\bullet-}$ has a longer lifetime ($t_{1/2}$ =< 1 and $t_{1/2}$ =< 30-40 μs for $HO^{\bullet}$ and $SO_4^{\bullet-}$, respectively), higher redox potential at neutral pH, and reacts faster with pollutants through electron transfer mechanism (Dogliotti, 1967; Madhavan et al., 1978; Oppenlander, 2003; Chan and Chu, 2009; Oh et al., 2016). For example, $SO_4^{\bullet-}$ promotes the decarboxylation of carboxylic acid through electron transfer oxidation (Madhavan et al., 1978). Additionally, both H_2O_2 and $S_2O_8^{2-}$ present limited ability to oxidize organic compounds directly (Table 2.5).

$$H_2O_2 + hv \rightarrow 2HO^{\bullet} \quad (2.16)$$

$$S_2O_8^{2-} + hv \rightarrow 2SO_4^{\bullet-} \quad (2.17)$$

Table 2.5 Redox potential of selected radicals and oxidants

Couple	E/V	Remark	Reference
$HO^{\bullet} / H_2O$	2.62 2.39 2.15	pH 3 pH 7 pH 11	(Zhang et al., 2016)
$SO_4^{\bullet-} / SO_4^{2-}$	2.6-3.1	–	(Eberson, 1982)
$CO_3^{\bullet-} / CO_3^{2-}$	1.50	–	(Oppenlander, 2003)
$CO_3^{\bullet-} / HCO_3^-$	1.78	pH 7	(Medinas et al., 2007)
$Cl^{\bullet} / Cl^-$	2.41	–	(Huie et al., 1991)
H_2O_2	1.78	–	(Brillas et al., 2009)
$S_2O_8^{2-}$	2.01	–	(Brillas et al., 2009)

In the UV/H_2O_2 process, the overall organic pollutant photodegradation involves UV direct photolysis and $HO^{\bullet}$-assisted indirect photolysis, as described by Equation 2.18.

$$-\frac{dC}{dt} = \Phi I_o f (1-10^{-\varepsilon Cb}) + k_{HO^{\bullet},M} C_{HO^{\bullet}} . C \quad (2.18)$$

where $k_{HO\cdot,M}$ is the second-order rate constant of $HO^{\cdot}$ reacting with the organic pollutant in $M^{-1}\ s^{-1}$; $C_{HO\cdot}$ is the steady-state concentration of $HO^{\cdot}$ in the UV/H_2O_2 process in mol L^{-1}; other terms are as defined previously.

In the UV/ $S_2O_8^{2-}$ process, $SO_4^{\cdot-}$ can be converted to $HO^{\cdot}$ to some extent (Equations 2.19 and 2.20). Therefore, the overall degradation is attributed to direct photolysis as well as $SO_4^{\cdot-}$- and $HO^{\cdot}$-assisted indirect photolysis, as described by Equation 2.21.

$$SO_4^{\cdot-} + H_2O \rightarrow HO^{\cdot} + SO_4^{2-} (k < 60 s^{-1}) \quad (2.19)$$

$$SO_4^{\cdot-} + OH^{-} \rightarrow HO^{\cdot} + SO_4^{2-} (k = 6.5x10^{7} M^{-1}s^{-1}) \quad (2.20)$$

$$-\frac{dC}{dt} = \Phi_{\lambda} I_o f (1-10^{-\varepsilon Cb}) + k_{SO_4^{\cdot-},M} C_{SO_4^{\cdot-}} C + k_{HO^{\cdot},M} C_{HO^{\cdot}} C \quad (2.21)$$

where $k_{SO_4\cdot-,M}$ is the second-order rate constant of $SO_4^{\cdot-}$ reacting with the organic pollutant in $M^{-1}\ s^{-1}$; $C_{SO_4\cdot-}$ and $C_{HO\cdot}$ are the steady-state concentrations of $SO_4^{\cdot-}$ and $HO^{\cdot}$ in the UV/PS process in mol L^{-1}, respectively; other terms are as defined previously.

2.2.2.2 Oxidation mechanism of hydroxyl and sulfate radical

$HO^{\cdot}$ can primarily react with the organic pollutant through 2 oxidation mechanisms: (i) by electrophilic addition to a double bond (a) or an aromatic ring (b); (ii) by hydrogen abstraction from a carbon atom (Schwarzenbach et al., 2003). Generalized examples of each mechanism are shown in Figure 2.7.

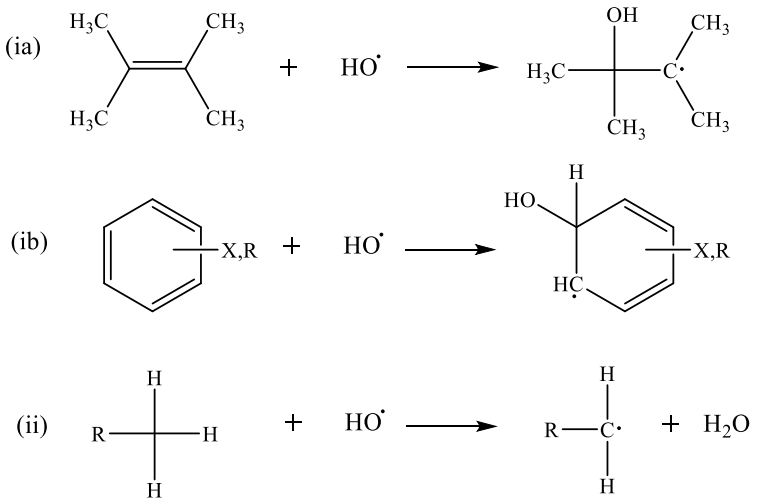

Figure 2.7 Generalized examples for oxidation mechanism of $HO^{\cdot}$

$SO_4^{\cdot-}$ oxidation of the organic pollutant occurs primarily through 3 oxidation mechanisms: (i) by electrophilic addition to a double bond; (ii) by abstracting a hydrogen atom from a saturated carbon; (iii) by electron transfer from a carboxyl group and from certain neutral molecules (Norman et al., 1970; Criquet and Leitner, 2009). Generalized examples of each mechanism for $SO_4^{\cdot-}$ oxidation of the organic pollutant are shown in Figure 2.8.

Compared to $HO^{\cdot}$, $SO_4^{\cdot-}$ reacts more slowly with organic pollutants through hydrogen abstraction and addition. On the other hand, $SO_4^{\cdot-}$ oxidizes some organic pollutants with higher rate constants through electron transfer oxidation. For example, most aliphatic acids can be degraded effectively by $SO_4^{\cdot-}$ through electron transfer oxidation of carboxyl group, while their reactions with $HO^{\cdot}$ led to little decarboxylation (Madhavan et al., 1978).

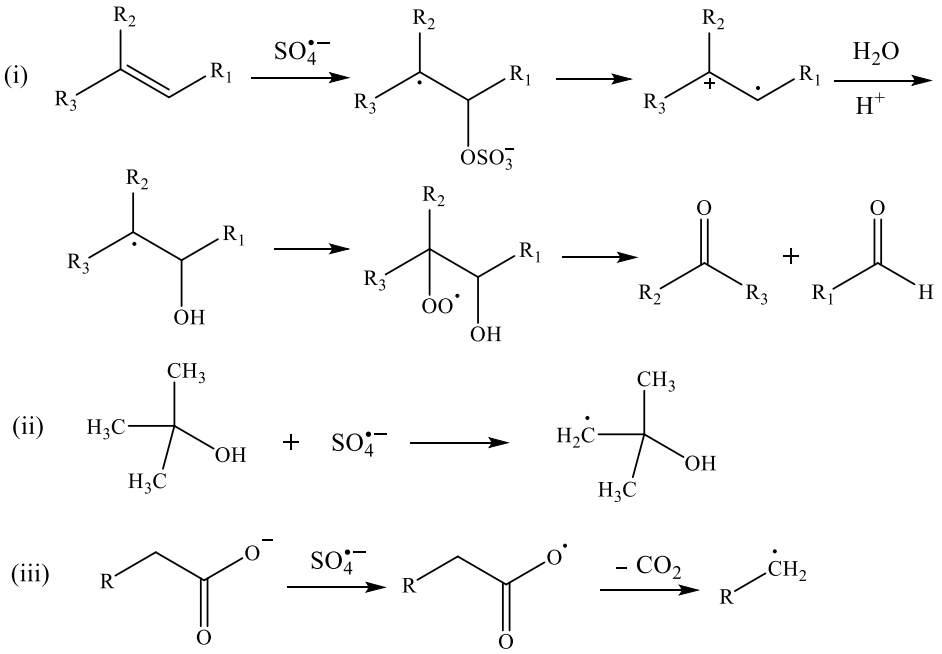

Figure 2.8 Generalized examples for oxidation mechanism of $SO_4^{\bullet -}$.

2.2.2.3 Oxidation rates of hydroxyl and sulfate radical with organic compounds

It was reported that the decay of $HO^{\bullet}$ could not be monitored due to its weak ultraviolet absorption and short lifetime. Therefore, the second-order rate constants of organic compounds reacting with $HO^{\bullet}$ could not be determined through monitoring the decay of $HO^{\bullet}$ (Buxton et al., 1988). Instead, some chemicals are employed as molecular probe for trapping $HO^{\bullet}$ to form the stable and quantifiable products (Jankowski et al., 2000; Yang et al., 2004; Wu et al., 2007b). For example, the diamagnetic spin trap, 5,5'-dimethyl-1-pyrrplin N-oxide (DMPO) can react with $HO^{\bullet}$ to produce a stable paramagnetic spin-adduct, which can be monitored by electron paramagnetic resonance (EPR) spectroscopy. The method has been used to quantify the concentration of $HO^{\bullet}$ and to determine the formation efficiency of $HO^{\bullet}$ in the UV-based AOPs (Wolfrum et al., 1994). Subsequently, the second-order rate constants of many organic compounds reacting with $HO^{\bullet}$ have been quantitatively measured (Kochany and Bolton, 1991).

In contrast, $SO_4^{\bullet-}$ was identified from its optical absorption spectrum with a maximum at 450 nm (ε = 1100 M^{-1} cm^{-1}) (Neta et al., 1988). The pseudo-first-order decay rate of $SO_4^{\bullet-}$ absorption at 450 nm was measured with the increase of the concentration of the organic compound studied. Subsequently, the second-order rate constant of the organic compound reacting with $SO_4^{\bullet-}$ was determined through a linear plot of the decay rate of $SO_4^{\bullet-}$ versus the concentration of the organic compound. For example, by pulse radiolysis of persulfate, the second-order rate constants of $SO_4^{\bullet-}$ reacting with anisole and nitrobenzene were determined as 5 x 10^9 M^{-1} cm^{-1} and < 10^6 M^{-1} cm^{-1}, respectively (Neta et al., 1977).

On this basis, a competition kinetics approach has been commonly applied to determine the second-order rate constants of $HO^{\bullet}$/ $SO_4^{\bullet-}$ reacting with the organic pollutant studied. According to this method, a chemical such as nitrobenzene, para-chlorobenzoic acid, and m-toluic acid can be selected as reference compounds, because this kind of compounds are readily oxidized by $HO^{\bullet}$ or $SO_4^{\bullet-}$ with known second-order rate constants. Simultaneous photodegradation of the target compound and the reference compound in the UV-based AOPs was conducted to determine the second-order rate constants of the target compound reacting with $HO^{\bullet}$ or $SO_4^{\bullet-}$. It is assumed that the reaction of $HO^{\bullet}$ or $SO_4^{\bullet-}$ with target compound and reference compound proceed in parallel independently. Therefore, the second-order rate constants of the target compound can be determined according to Equation 2.22.

$$k_{radical,M} = \frac{k_{obs,M} - k_{UV,M}}{k_{obs,R} - k_{UV,R}} k_{radical,R} \qquad (2.22)$$

where $k_{radical,M}$ and $k_{radical,R}$ are the second-order rate constants of the target compound and reference compound reacting with $HO^{\bullet}$ or $SO_4^{\bullet-}$, respectively; $k_{obs,M}$ and $k_{obs,R}$ are the observed pseudo-first-order rate constants of target compound and reference compound in the UV-based AOP, respectively; $k_{UV,M}$ and $k_{UV,R}$ are the direct photolysis rate constants of the target compound and reference compound in the UV-based AOP, respectively. The experiments could be conducted repeatedly with different initial concentrations of the reference compound and the obtained

average values will be used to calculate the second-order rate constant of the organic pollutant reacting with $HO^{\cdot}$ or $SO_4^{\cdot -}$.

Using the methods mentioned above, the second-order rate constants of $HO^{\cdot}$ and $SO_4^{\cdot -}$ reacting with many inorganic and organic species were determined (Table 2.6).

Table 2.6 The second-order rate constants of $HO^{\cdot}$ and $SO_4^{\cdot -}$ reacting with some inorganic and organic species

Species	2^{nd}-order rate constant with $HO^{\cdot}$ ($M^{-1} s^{-1}$)	2^{nd}-order rate constant with $SO_4^{\cdot -}$ ($M^{-1} s^{1}$)	Reference
HCO_3^-	8.5×10^6	9.1×10^6	(Buxton et al., 1988; Neta et al., 1988)
CO_3^{2-}	3.9×10^8	6.1×10^6	(Buxton et al., 1988; Zuo et al., 1999)
$H_2PO_4^-$	$\sim 2 \times 10^4$	$< 7 \times 10^4$	(Buxton et al., 1988; Neta et al., 1988)
HPO_4^{2-}	1.5×10^5	1.2×10^6	(Buxton et al., 1988; Neta et al., 1988)
nitrobenzene	3.9×10^9	$< 10^6$	(Neta et al., 1977; Buxton et al., 1988)
p-nitrobenzoic acid	2.6×10^9	$< 10^6$	(Neta et al., 1977; Buxton et al., 1988)
p-chlorobenzoic acid	4.5×10^9	3.6×10^8	(Neta et al., 1977; Buxton et al., 1988)
m-toluic acid	7.6×10^9	2.0×10^9	(Neta et al., 1977; Buxton et al., 1988)
benzoic acid	4.3×10^9	1.2×10^9	(Neta et al., 1977; Buxton et al., 1988)
methanol	9.8×10^7	1.1×10^7	(Buxton et al., 1988; Neta et al., 1988)
t-butanol	6.0×10^8	8.4×10^5	(Buxton et al., 1988; Clifton and Huie, 1989)

2.2.3 Recent development of UV/H_2O_2 and UV/PS AOP

2.2.3.1 UV/H_2O_2 AOP

In recent years, a number of studies have been performed to investigate the degradation of organic pollutants by UV/H_2O_2 processes. A summary of some studies is listed in Table 2.7.

Table 2.7 Summary of some studies about the degradation of organic pollutants by UV/H_2O_2 AOP

Target pollutant	Treatment	Experimental conditions	Observation	Reference
Estrone (E1), b-Estradiol (E2), and 17a-Ethinyl Estradiol (EE2)	UV, UV/H_2O_2, pilot-scale	LP-Hg lamp, C_0 = 5 µm, estrogenic activity with YES bioassay, type of water: drinking water and treated wastewater	UV (1000 mJ cm^{-2}): E1 (70% removal) > EE2 (13%) >E2 (7%). UV/H_2O_2 (1000 mJ cm^{-2} and 40 mg L^{-1}): E1 = EE2 = E2 > 99% removal. 80% removal of the initial estrogenic activity (520 mJ cm^{-2} + 30 mg L^{-1} H_2O_2). 0.15 €m^{-3} (10 m^3 h^{-1}, 520 mJ cm^{-2} + 30 mg L^{-1} H_2O_2).	(Cédat et al., 2016)
Ofloxacin	UV254 UV365	C_0 = 10 mg L^{-1}, H_2O_2 doses from 0.03 to 0.47 g L^{-1}, pH 3, 7, and 11	97% removal of ofloxacin (UV254 + 0.27 g L^{-1} H_2O_2, 30 min, pH 7). The degradation rate: UV254 > UV365, acidic conditions > alkaline conditions. EE/O: 2.2 (UV254) < 22.5 $kWhm^{-3}order^{-1}$(UV365)	(Lin et al., 2016)
Venlafaxine (VFX), o-desmethylvenlafaxine (OVFX)	UV/H_2O_2	LP-Hg lamp (0.11 W cm^{-2}), C_0 = 20 mg L^{-1}, 700 mg L^{-1} H_2O_2, toxicity assay with *vibrio fischeri* bacteria.	99.9% removal of VFX and DVFX after 5 and 30 min, respectively. 11 transformation products identified for VFX and 6 for DVFX. The toxicity increased during the UV/H_2O_2 process.	(García-Galán et al., 2016)
Atrazine (ATZ), Carbamazepine (CBZ), Diclofenac (DCL), Triclosan (TCS)	UV/H_2O_2	LP-Hg lamp (4 x 15 W), 10 mg L^{-1} H_2O_2, toxicity with Daphnia magna, type of water: river water.	The degradation rate: DCL > TCL > ATZ > CBZ. Toxicity increased at a UV dose of 300 mJ cm^{-2}, then decreased at 1200 mJ cm^{-2}.	(Rozas et al., 2016)
Acetaminnophen (ACE)	UV/H_2O_2	LP-Hg lamp (1.28 x 10^{-8} E L^{-1} s^{-1}), C_0 = 10 µM, 1 mM H_2O_2, effect of halides and NOM	The degradation increased due to generation of $ClBr^{\bullet-}$, which is very reactive to electron-rich moieties of ACE. Transformation products identified.	(Li et al., 2015)
Oxytetracycline	UV UV/H_2O_2	LP-Hg lamp (0.1 W cm^{-2}), C_0 =10 µM, 1 mM H_2O_2, effect of pH and bicarbonate	Over pH 3 to 11, the high degradation rate was observed at pH 5.5. A slight increase of degradation rate in the presence of high concentration of carbonate or bicarbonate.	(Liu et al., 2015)
Azo dye reactive orange 16	UV/H_2O_2	LP-Hg lamp (1.95 mW cm^{-2}), C_0 = 50 mg L^{-1}, 25 mM H_2O_2, toxicity assay with *vibrio fischeri* bacteria.	Transformation products identified. Toxicity increased first, and then decreased.	(Mitrović et al., 2014)
Cylindrospermopsin (CYN)	UV/H_2O_2	LP-Hg lamp (0.1 mW cm^{-2}), C_0 = 5 µM, 0.5 mM H_2O_2, type of water: natural water.	Transformation by-products identified.	(He et al., 2014c)
Chlorpyrifos	UV/H_2O_2	LP-Hg lamp (20 W), C_0 = 15 mg L^{-1}, 450 mg L^{-1} H_2O_2, toxicity assay with *vibrio fischeri* bacteria.	> 99% removal at 60 min. Toxicity increased slightly first, then decreased.	(Femia et al., 2013)
Atrazine and other pollutants (from pesticides to pharmaceuticals, solvents)	UV/H_2O_2 full-scale	MP-Hg lamp, installed between dual media filtration and GAC filtration	> 80% removal of atrazine at an electrical energy of 0.56 $kWhm^{-3}$ and 6 mg L^{-1} H_2O_2. Most target pollutants were removed to below their detection limits of 0.02 µg L^{-1}after the UV/H_2O_2 process.	(Kruithof and Martijn, 2013)

Among these studies, more research works have been conducted to evaluate the effect of pH, matrix species etc. on the performance of the UV/H_2O_2 processes. The optimum pHs for degradation of organic pollutants in the UV/H_2O_2 processes were different in many studies (Liu et al., 2015; Lin et al., 2016; Zhang et al., 2016). The degradation rates of ofloxacin in the UV/H_2O_2 processes followed the order of pH 3 > pH 7 > pH 11 (Lin et al., 2016). Liu et al (2015) investigated the oxidation of oxytetracycline (OXT) by UV/H_2O_2 process at different pHs (3 to 11). A higher degradation rate was observed at pH 5.5. Generally, both HCO_3^- and CO_3^{2-} which are commonly present in natural water had negative effect on the process efficiencies in most studies (Kwon et al., 2015; Devi et al., 2016; Zhang et al., 2016). However, the degradation of oxytetracycline (OXT) in the UV/H_2O_2 process was not inhibited in the presence of HCO_3^- or CO_3^{2-} (Liu et al., 2015). Instead, the degradation rate increased slightly at high concentration of HCO_3^- or CO_3^{2-}. On this basis, the authors designed the experiments to determine the second-order rate constant of $CO_3^{\bullet-}$ reacting with OTC as 2.9 x 10^8 M^{-1} s^{-1} (pH 10.4). It means that $CO_3^{\bullet-}$ is also reactive to OTC. These results suggest that HCO_3^- and CO_3^{2-} might have both negative and positive effect on the performance of UV/H_2O_2 AOP.

Cl^- is another matrix species commonly found in the natural water. There are some reports available about the effect of Cl^- on the degradation efficiency of UV/H_2O_2 AOP (Yang et al., 2014; Li et al., 2015; Zhang et al., 2016). Yang et al (2014) reported that Cl^- adversely effected the degradation of benzoic acid (BA) and cyclohexanecarboxylic acid (CCA) in the UV/H_2O_2 process. But, it had no effect on the degradation of 3-cyclohexene-1-carboxylic acid (3CCA), due to the generation of chloride species such as $Cl^{\bullet}$ and $Cl_2^{\bullet-}$, which is also very reactive to olefin. In another study, Cl^- had a minimal effect on the degradation of acetaminophen in the UV/H_2O_2 process, while the degradation rate decreased with the increase of Br^- (Li et al., 2015). Interestingly, the degradation rate increased obviously in the presence of both Cl^- and Br^-. This was due to generation of $ClBr^{\bullet-}$, which was also reactive to electron-rich moieties of acetaminophen (Li et al., 2015). From the above discussion, it can be concluded that pH and matrix species exhibit different

influences on the degradation of organic pollutants depending on their structures and chemical properties. Thus, it is essential to evaluate the individual effects of these factors when a new organic pollutant is treated by UV/H_2O_2 process.

Furthermore, there is a concern of the application of UV/H_2O_2 for organic pollutants removal, i.e., the formation of unknown transformation by-products/intermediates. To address this issue, toxicity tests have been carried out in many studies (Femia et al., 2013; Cédat et al., 2016; Rozas et al., 2016). For example, Rozas et al (2016) conducted toxicity test with Daphnia magna during the UV/H_2O_2 treatment of organic pollutants including atrazine and carbazepine (Rozas et al., 2016). Higher toxicity was observed at a low UV dose of 300 mJ cm^{-2}. It suggested that the higher toxic intermediates were generated during the treatment process. At a higher UV dose of 1200 mJ cm^{-2}, toxicity declined obviously. Besides the toxicity test, more research efforts have been made to identify the transformation by-products (He et al., 2014c; Li et al., 2015; García-Galán et al., 2016). He et al (2014c) investigated the degradation mechanism of cylindrospermopsin (CYN) by the UV/H_2O_2 process. Various degradation by-products were identified by LC-QTOF-MS. The authors proposed that $HO^{\cdot}$ attacked CYN at 3 sites: hydroxymethyl uracil, tricylic alkanoid, and sulfate group (Figure 2.9). There was a common difference of 2 Da (two hydrogen) among the number of transformation by-products within each group, which indicated the formation of C=C bond or oxidation of secondary alcohol. The differences of 16 Da (one oxygen atom) and 80 Da ($-SO_3$) among the identified by-products in each group represented the hydroxylation pathway and elimination pathway of sulfate group, respectively. Generally, there were 3 reaction mechanisms in the course of reaction: hydroxyl addition, alcoholic oxidation or dehydrogenation, and elimination of sulfate. For each site of CYN attacked by $HO^{\cdot}$, the degradation pathways were proposed correspondingly based on the identified by-products in their study.

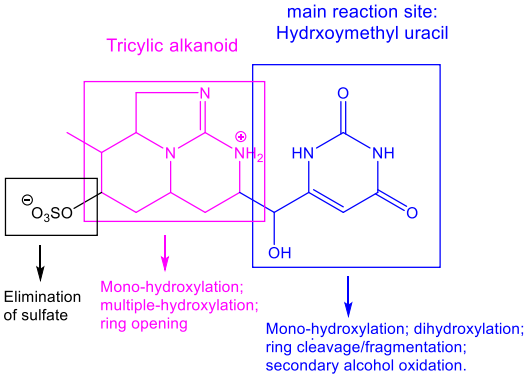

Figure 2.9 Degradation mechanism of cylindrospermopsin (CYN) by $HO^{\cdot}$ (He et al., 2014c).

UV/H_2O_2 AOP has been applied in field-scale drinking water and advanced water treatment plants. For example, in North Holland, UV/H_2O_2 system was integrated in an existing conventional surface water treatment plant, which consisted of coagulation, sedimentation, dual media filtration, and granular activated carbon (GAC) filtration (Kruithof and Martijn, 2013). UV/H_2O_2 system was installed between dual media filtration and GAC filtration (Figure 2.10(a)). GAC filter could remove the residual H_2O_2 and the oxidation by-products generated during the oxidation process. 25 priority pollutants were identified in the source water. Before installing the UV/H_2O_2 system, the concentrations of most pollutants were removed to below 0.1 µg L^{-1} after GAC filtration. However, ethylenediaminetetraacetic acid (EDTA), one of the 25 priority pollutants, could not be removed by GAC effectively. After installation of UV/H_2O_2 system, EDTA was not detected in the finished water, even the concentration of EDTA in the source water was up to 6 µg L^{-1}. The concentrations of other pollutants found in the source water were also removed to below their detection limits of 0.02 µg L^{-1} in the finished water. To further reduce the operating cost, the plant operator is planning to increase the UV transmissions (UVT) of the filtered water, which has a strong impact on the electrical energy demand (EED). The UVT of the water is determined by NOM and nitrate, which could be removed by pre-treatment processes to some extent. The UVT of dual media filtered water was 85% by the current pre-treatment processes. Under these conditions, the EED for 80% atrazine removal by UV/H_2O_2 treatment was 0.56 $kWhm^{-3}$. The plant operator is deciding to replace the current pre-

treatment processes by the combination of ion exchange and ceramic membrane micro-filtration (Figure 2.10(b)). The UVT of the membrane filtered water can increase to 93%, which can lower the EED for 80% atrazine removal to 0.34 $kWhm^{-3}$. As a result, the plant can increase the treatment capability from 3000 to 4200 m^3 h^{-1}. It can be said that UV/H_2O_2 process is a robust barrier to control organic pollutants with attractive energetic efficiency.

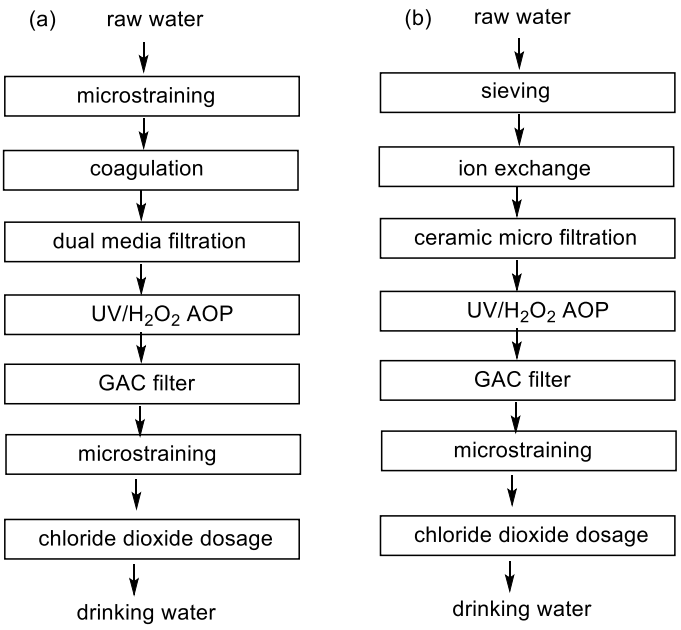

Figure 2.10 (a) Treatment scheme with UV/H_2O_2 AOP for surface water treatment in North Holland; (b) retrofit treatment scheme with ion exchange and ceramic microfiltration pre-treatment (Kruithof and Martijn, 2013).

2.2.3.2 UV/PS AOP

Compared to UV/H_2O_2 AOP which has been investigated for more than 20 years, UV/PS AOP has only attracted more attention in the recent years. Thus, most studies of US/PS AOP were conducted in bench-scale only. A summary of the recent development of UV/PS AOP is presented in Table 2.8.

Table 2.8 Summary of some studies about the degradation of organic pollutants by UV/PS AOP

Target pollutant	Treatment	Experimental conditions	Observation	Reference
2,4-Di-tert-butylphenol	UV/PS	LP-Hg lamp (75 W), C_0 = 24.2 µM, PS = 1 mM, effect of pH, anion, and NOM	The degradation rates remained constant at pH 3-7 and slightly decreased from 7-10. Chloride enhanced the degradation, while NOM inhibited the degradation. Transformation by-products identified.	(Wang et al., 2016)
Oxytetracycline	UV/PS	LP-Hg lamp (15 W), effect of pH, background water matrix,	The highest degradation rate at pH 5.5-8.5. Chloride inhibited the degradation, while bicarbonate enhanced the degradation. Qualitative determination of the contribution of sulfate and hydroxyl radical. Transformation by-products identified.	(Liu et al., 2016)
2,4,6-trichloroanisole	UV/PS	LP-Hg lamp (0.16 mW cm^{-2}), effect of pH, PS dose, and background water matrix	The degradation rate decreased with increasing pH from 4 to 9. Chloride slightly inhibited the degradation, while bicarbonate had a negative effect on the degradation. The respective contribution of sulfate and hydroxyl radicals predicted by the kinetic model. Transformation by-products identified.	(Luo et al., 2016)
Azathioprine	UV/PS UV/H_2O_2	LP-Hg lamp (5.57 x 10^{-9} E s^{-1} cm^{-2}), effect of pH, chloride, and bicarbonate	UV/PS was more effective than UV/PS for azathioprine removal. Chloride slightly inhibited the degradation, while bicarbonate had a negative effect on the degradation in both processes.	(Zhang et al., 2016)
Erythromycin (ERY)	UV/PS	LP-Hg lamp (4.57 x 10^{-6} E^{-1} s^{-1}), type of water: secondary wastewater effluent, toxicity test with *Escherichia coli*, phytotoxicity test with S. *alba*, L. *sativum*, and S. *saccharatum*	Total inactivation of *Escherichia coli* within 90 min. The final treated effluent had a lower phytotoxicity (<10%) compared to the untreated wastewater. Transformation by-products identified.	(Michael-Kordatou et al., 2015)
Perfluorooatanoic acid	UV/PS	LP-Hg lamp (2.88 x 10^{-7} E^{-1} L^{-1} s^{-1}), type of water: ultrapure water and real water sample, effect of chloride	Chloride inhibited the degradation and was oxidized to chlorate.	(Qian et al., 2016)
Ibuprofen	UV/PS UV/H_2O_2	LP-Hg lamp (0.5 mW cm^{-2}), type of water: wastewater, MF filtrate, RO permeate	UV/PS was more effective than UV/H_2O_2 for ibuprofen removal in RO permeate. But, UV/PS was less effective in secondary effluent.	(Kwon et al., 2015)
β-Lactam	UV/PS	LP-Hg lamp (0.1 mW cm^{-2})	Quantitative determination of the respective contribution of sulfate and hydroxyl radical. Transformation by-products identified.	(He et al., 2014b)
Antipyrine	UV/PS UV/H_2O_2	LP-Hg lamp (75 W)	UV/H_2O_2 was more effective than UV/PS for antipyrine removal.	(Tan et al., 2013)
Polyvinyl alcohol (PVA)	UV/PS	UV365 (8 W), effect of pH, PS dose, and background water matrix	The degradation rate followed the order of pH 3 > pH 7 > pH 11. Chloride and bicarbonate had negative effect on the degradation rate.	(Lin et al., 2013)
Bromate control	UV/PS	LP-Hg lamp (2.19 x 10^{-6} E^{-1} L^{-1} s^{-1}), effect of bromide and PS dose, type of water: ultrapure water and real water sample	The bromate formation decreased over 90% with increasing pH from 7 to above 9. Less bromate was formed in the real water compared to ultrapure water.	(Fang and Shang, 2012)

Similar to the studies of UV/H_2O_2 AOP, more research works have been conducted to investigate the effect of pH, background water matrix etc. on the performance of UV/PS AOP. In some studies, the degradation rates of the organic pollutants decreased with increasing pH (Lin et al., 2013; Luo et al., 2016). However, the degradation rate of oxytetracycline (OTC) at near neutral condition (5.5-8.5) was higher than those at acidic and basic conditions (Liu et al., 2016). Most research data indicated that Cl^- inhibited the degradation of organic pollutants as it acted as the scavenger of $SO_4^{\cdot-}$ (Lin et al., 2013; Liu et al., 2016; Zhang et al., 2016). Nevertheless, the degradation rate of 2,4-Di-tert-butylphenol (2,4-D) increased with the increase of Cl^- (Wang et al., 2016). Two possible reasons were proposed to explain this phenomenon. First, the generated chlorine species such as $Cl^{\cdot}$ was also reactive to 2,4-D. Second, the generated chlorine species such as $Cl^{\cdot}$ and $Cl_2^{\cdot-}$ could promote the propagation reaction to produce more $SO_4^{\cdot-}$. Furthermore, HCO_3^- had a negative effect on the degradation kinetics in the most UV/PS AOP studies as it was a strong scavenger of $SO_4^{\cdot-}$ (Lin et al., 2013; Luo et al., 2016; Zhang et al., 2016). But, a slight increase of the degradation rate of oxytetracycline (OTC) in the UV/PS process was observed in the presence of HCO_3^-, as the generated $CO_3^{\cdot-}$ could selectively react with OTC (Liu et al., 2016).

As mentioned previously, $SO_4^{\cdot-}$ can be transformed to $HO^{\cdot}$ to some extent. There are some studies about the qualitative and quantitative determination of the respective contribution of $SO_4^{\cdot-}$ and $HO^{\cdot}$ for the organic pollutant degradation in the UV/PS process. For example, Michael-Kordatou et al (2015) used different alcohols such as t-butanol and ethanol to differentiate the respective contributions of $SO_4^{\cdot-}$ and $HO^{\cdot}$ qualitatively, as these two alcohols have different reactivities with $SO_4^{\cdot-}$ and $HO^{\cdot}$. Luo et al (2016) established a mathematical model to estimate the steady-state concentration of $SO_4^{\cdot-}$ and $HO^{\cdot}$. On this basis, the respective contributions of $SO_4^{\cdot-}$ and $HO^{\cdot}$ for 2,4,6-trichloroanisole degradation was predicted. He et al (2014b) used the probe compounds such nitrobenzene and m-toluic acid to determine the steady-state concentration of $SO_4^{\cdot-}$ and $HO^{\cdot}$ at a specific condition. Accordingly, the

respective contributions of $SO_4^{\cdot-}$ and $HO^{\cdot}$ for β-lactam antibiotics degradation were determined quantitatively.

Identification of the transformation by-products in the UV/PS process have also been conducted in most recent studies (Michael-Kordatou et al., 2015; Liu et al., 2016; Luo et al., 2016). For example, Liu et al (2016) investigated the degradation mechanism of oxytetracycline (OTC) using LC-QTOF-MS. The authors used t-butanol as the scavenger of $HO^{\cdot}$ to exclude the contribution from $HO^{\cdot}$ in a control experiment. Same transformation by-products were detected for both UV/PS and UV/PS/t-butanol system. 4 different degradation pathways were proposed including hydroxylation (+ 16 Da), demethylation (-16 Da), decarboxylation (- 28 Da), and dehydration (- 18 Da) (Figure 2.11).

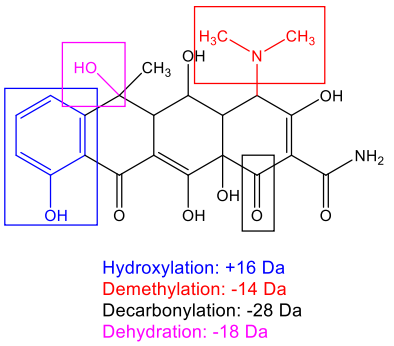

Figure 2.11 Degradation mechanism of oxytetracycline (OTC) by $SO_4^{\cdot-}$ (Liu et al., 2016).

Compared to UV/H_2O_2 AOP, limited number of studies was conducted for toxicity test during UV/PS treatment process. Michael-Kordatou et al (2015) performed phytotoxicity test during the UV/PS treatment of erythromycin in wastewater. The phytotoxicity in the final treated effluent decreased slightly (<10%) compared to that in the untreated wastewater. The authors supposed that the phytotoxicity against the test plants such as S. *alba*, L. *sativum*, and S. *saccharatum* was potentially associated with the dissolved effluent organic matters and their oxidation by-products. The authors also observed the total inactivation of *Escherichia coli* within 90 min.

There is a concern of BrO_3^- formation in the application of $SO_4^{\bullet-}$ for organic pollutants removal, as Br^- present in the source water can be oxidized by $SO_4^{\bullet-}$ to toxic BrO_3^-, which is regulated by U.S. EPA, European commission standards, and WHO at maximum contaminant level of 10 μg L^{-1} for drinking water. Besides the addition of a secondary treatment unit after $SO_4^{\bullet-}$ oxidation to remove the formed BrO_3^-, kinetic control with pH adjustment and chemical addition such as HCO_3^- have been employed to control BrO_3^- formation (Oh et al., 2016). Fang et al (2012) reported that BrO_3^- formation in the UV/PS process was almost the same at pH 4-7, but it decreased over 90% when pH increased from 7 to above 9.

Furthermore, comparative evaluation of UV/PS and UV/H_2O_2 AOP for organic pollutants removal has been conducted in some studies (Tan et al., 2013; Kwon et al., 2015; Zhang et al., 2016). Zhang et al (2016) reported that the degradation rates of azathioprine in the UV/PS process in different types of water including DI water, treated drinking water, and secondary effluent were higher than those in the UV/H_2O_2 process. In contrast, the degradation of antipyrine in the UV/H_2O_2 process in laboratory synthetic water was faster than that in the U/PS process (Tan et al., 2013). Kwon et al (2015) reported that the rate of ibuprofen (IBF) degradation in RO permeate treated with the UV/PS process was higher than that with the UV/H_2O_2 process. However, UV/H_2O_2 process was more effective than UV/PS process for ibuprofen removal in the secondary effluent. The authors evaluated the effect of the individual matrix species (HCO_3^-, Cl^-, NOM etc.) on the degradation kinetics using synthetic solution. It was found that HCO_3^- and NOM exhibited stronger negative effects on the UV/PS process than the UV/H_2O_2 process.

2.2.4 Literature summary for UV direct and indirect photolysis of DBPs

To the best knowledge of the author, UV direct and indirect photolysis has been investigated for removal of DBPs such as THMs, HAAs, halonitromethanes, haloactonitriles, and nitrosoamines etc. As shown in Table 2.9, brominated DBPs and nitrosoamines are more susceptible to UV direct photolysis as compared to

chlorinated DBPs. On the other hand, $HO^{\cdot}$-based UV indirect photolysis such as UV/H_2O_2 AOP looks promising to remove DBPs effectively. However, there is no report about removal of DBP by $SO_4^{\cdot-}$. Little is known about removal of I-DBPs by UV direct and indirect photolysis.

Table 2.9 Literature summary for UV direct and indirect photolysis of DBPs

DBPs	Conditions	Pseudo-first-order rate constant (min^{-1}) and/or quantum yield (Φ)	References
$CHCl_3$	UV 253.7 nm; pH 7.5, 20 ^oC	-[a]	(Nicole et al., 1991)
$CHCl_2Br$		Φ = 0.43±0.1	
$CHClBr_2$		Φ = 0.43±0.1	
$CHBr_3$		Φ = 0.43±0.1	
THMs	UV 112-400 nm; pH 2.5-10; 0.1% H_2O_2	92-100% removal	(Rudra et al., 2005)
$CHBr_3$	UV 254 nm; neutral pH	1.02 x 10^{-4}	(Castro and Belser, 1981)
$CHBr_3$	UV 266-324 nm; air, 31 ^oC	Φ = 0.76	(Bayes et al., 2003)
$CHBr_3$	UV 248 nm; air	Φ = 0.2-0.3	(Zou et al., 2004)
$CHBr_3$	UV 240 nm; water	Φ = 0.43	(Kwok et al., 2004)
$CHCl_3$	UV 253.7 nm only; UV 253.7 nm/H_2O_2 (6 mg L^{-1}); 24±1 ^oC	-(0.09)	(Jo et al., 2011)
$CHCl_2Br$		0.13(0.13)[b]	
$CHClBr_2$		0.60(0.78)	
$CHBr_3$		1.68(1.74)	
$CHCl_3$	UV 150-400 nm	0.020±0.002	(Hansen et al., 2013)
$CHCl_2Br$		0.070±0.008	
$CHClBr_2$		0.205±0.022	
$CHBr_3$		0.394±0.026	
BrH_2CCO_2H	UV 253.7 nm only; UV 253.7 nm/H_2O_2 (6 mg L^{-1}); 24±1 ^oC	0.13(0.066)	(Jo et al., 2011)
Br_2HCCO_2H		0.90(0.78)	
Br_3CCO_2H		4.44(3.84)	
ClH_2CCO_2H		-(0.035)	
Cl_2HCCO_2H		-(0.030)	
Cl_3CCO_2H		-(0.017)	
ClH_2CCO_2H	UV 253.7 nm/ Na_2SO_3 (126 mg L^{-1}); pH 9.2; 25 ^oC.	3.7560±0.0685 (μM min^{-1})	(Li et al., 2012a)
$Cl_3C(NO_2)$	UV 254 nm; neutral pH; 20 ^oC	8.33x10^{-3}	(Castro and Belser, 1981)
$Cl_3C(NO_2)$	UV 199-400 nm; 20 ^oC	3.41x10^{-3}-4.80x10^{-2}	(Allston et al., 1978)
$Cl_3C(NO_2)$	UV 150-400 nm	0.523±0.145	(Hansen et al., 2013)

$BrH_2C(NO_2)$ $Br_2HC(NO_2)$ $Cl_2HC(NO_2)$ $Cl_3HC(NO_2)$	UV 254 nm; pH 3-10	Φ = 0.114 Φ = 0.409 Φ = 0.327 Φ = 0.46±0.03	(Fang et al., 2013)
Cl_2HCCN Cl_3CCN ClBrHCCN Br_2HCCN	UV 150-400 nm	0.024±0.006 0.130±0.021 0.094±0.010 0.200±0.021	(Hansen et al., 2013)
Cl_2HCCN	$UV_{solar}/TiO_2/O_3$; UV_{solar}, 300-800 nm, 33.8 W m^{-2}; TiO_2, 1 g L^{-1}; O_3, 1.13 g L^{-1} h^{-1}, 20 ^oC.	0.033 min^{-1}	(Shin et al., 2013)
NDMA[c]	UV 200-300 nm; pH 3 and 10; 1 µmol L^{-1}	2.6 Φ = 0.30	(Stefan and Bolton, 2002)
NDMA	UV 254 nm only; UV 254 nm/ H_2O_2 (100 mg L^{-1})	0.16 (0.17), Φ = 0.30	(Sharpless and Linden, 2003)
NDMA	UV 200-300 nm only; UV 200-300 nm/ H_2O_2 (100 mg L^{-1})	0.36 (0.31), Φ = 0.30	
NPyr NPip	UV 253.7 nm; pH 7.1	0.8687 1.0787	(Xu et al., 2009)
BrO_3^-	UV 254 nm only, pH 7; UV 254 nm/ Na_2SO_3 (7.8 mg L^{-1}), pH 7	0.05 (0.038)	(Jung et al., 2014)
BrO_3^-	UV 200-600 nm only, pH 7; UV 200-600 nm/ Na_2SO_3 (7.8 mg L^{-1}), pH 7	0.017 (0.056)	(Jung et al., 2014)
ClH_2CCN Cl_2HCCN Cl_3CCN Br_2HCCN	UV 185 nm and UV 254 nm	Φ_{254}= 0.2 x 10^{-3} Φ_{254}= 0.38 x 10^{-3} Φ_{254}= 0.58 x 10^{-3} Φ_{254}= 0.028	(Kiattisaksiri et al., 2016)

a. Dashes denote that no reaction was observed;
b. The values in the bracket represent the pseudo-first-order rate constants obtained in the UV/H_2O_2 process;
c. NDMA: N-Nitrosodimethylamine; Npyr: N-Nitrosopyrrolidine; Npip: N-Nitrosopiperidine.

CHAPTER 3 Materials and methods

3.1 Reagents and sample preparation

Dichloroiodomethane ($CHCl_2I$, 95+%), chlorobromoiodomethane (CHClBrI, 95+%), dibromoiodomethane ($CHBr_2I$, 90-95%), chlorodiiodomethane ($CHClI_2$, 90-95%), and bromodiiodomethane ($CHBrI_2$, 95+%), iodochloroacetic acid ($IClCHCO_2H$, 99+%), iodobromoacetic acid ($IBrCHCO_2H$, 90+%), and diiodoacetic acid (I_2CHCO_2H, 95+%) were purchased from Cansyn Chemical Corp (Canada). Iodoform (CHI_3, 99%), bromoform ($CHBr_3$, 97%), nitrobenzene (NB, ≥99%), p-nitrobenzoic acid (pNBA, 98%), p-chlorobenzoic acid (pCBA, 99%), and m-toluic acid (mTA, 99%) were purchased from Sigma-Aldrich (Singapore). HPLC grade methanol was purchased from Merck (Singapore). Iodoacetic acid (ICH_2CO_2H, 99%), $Na_2S_2O_8$ (99%), and H_2O_2 (35% w/w aqueous solution) were purchased from Alfa Aesar (Singapore). Synthetic solution for UV direct photolysis and UV-based advanced oxidation were prepared using deionized (DI) water (Millipore, USA). For quantitative chromatographic analysis, stock standard solutions were prepared in methanol by weighing approximately 10 mg of individual neat I-THMs and iodoacids into a 10-mL volumetric flask and diluting to volume. The secondary standard solutions were prepared by dilution of the primary standard to 100 μg L^{-1}, 10 mg L^{-1}, and 100 mg L^{-1}, respectively.

3.2 Chemical analysis

3.2.1 Analytical method for determination of I-THMs

A reliable and sensitive method for analysis of I-THMs at ng L^{-1} level in water sample was developed using automatic purge-and-trap (P&T) extraction (Tekmar, Atomx) coupled with GC (Agilent, 6890A)/MS (Agilent, 5973C). Water sample was heated at 65 ^oC in P&T in order to improve the sensitivity of I-THMs. Trap #1, Tenax was used as the sorbent material. A DB-624 column (J&W) with helium as carrier gas was used. The oven temperature program was as follows: 45 ^oC for 2 min, then increased at a rate of 10 ^oC/min to 100 ^oC, held at 100 ^oC for 2 min, then ramped up to 200 ^oC at 5 ^oC/min, to 250 at 20 ^oC/min, and held at 250 ^oC for 5 min.

1,2-dibromopropane was used as an internal standard (IS). GC spectrum of 6 I-THM and IS was displayed in Figure 3.1.

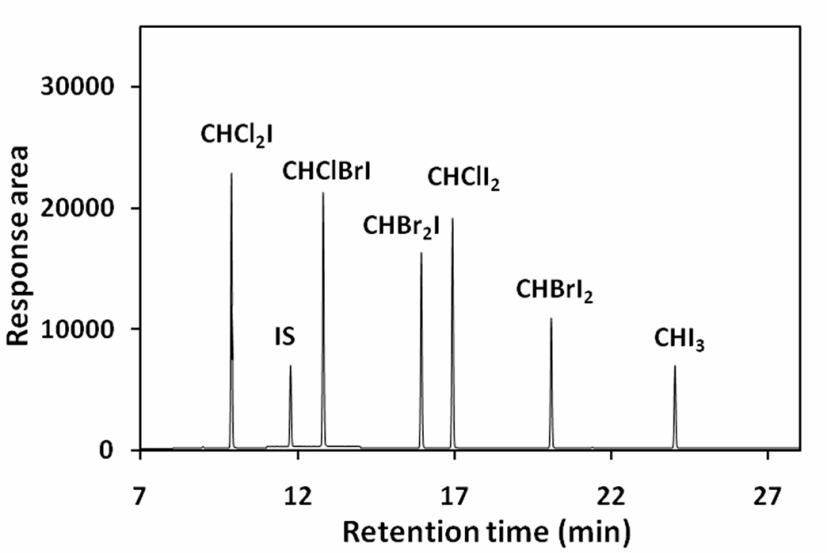

Figure 3.1 Gas Chromatography of 6 I-THMs and internal standard (1,2-dibromopropane) obtained by P&T-GC/MS in SIM mode.

Selective ion monitoring (SIM) mode was operated in MS for quantitative analysis of I-THMs. The selected ions for quantitative analysis and some related physico-chemical properties of 6 I-THMs were presented in Table 3.1. In order to evaluate the accuracy of the developed P&T-GC/MS method for quantitative analysis of I-THMs, the linearity, repeatability, reproducibility, and limit of quantification were determined and presented in Table 3.2.

Table 3.1 Selected ions for quantification and related physico-chemical properties of 6 I-THMs

Species	MW	b.p. (^oC)	$logK_{ow}$[b]	H[c]	Selected ions
$CHCl_2I$	210.8	139	2.78	0.50	82.9[a], 84.9, 126.9, 174.8
CHClBrI	254.0	172	2.99	0.30	126.9[a], 128.8, 130.8,174.8
$CHBr_2I$	299.7	189	3.20	0.25	126.9, 170.8, 172.8[a], 174.8
$CHClI_2$	302.3	199	3.31	0.20	126.9, 174.8[a], 176.8, 301.6
$CHBrI_2$	246.7	234	3.52	0.15	126.9, 139.9, 218.8[a], 220.8
CHI_3	393.7	218	3.83	0.10	126.9, 139.8, 266.8[a], 393.7
IS[d]	201.9	140-142	–	–	121[a],123

a. Target ions for quantification, other ions used for confirmation; b. Calculated with the Prolog P computer program; c. H: Henry's Law constant (dimensionless); d. IS: 1,2-dibromopropane; The physico-chemical properties of 6 I-THMs were cited from literature (Cancho et al., 2000).

Table 3.2 Validation data regarding linearity, repeatability, reproducibility and limit of quantification (LOQ)

Species	Linearity range (ng L^{-1})	Coefficient determination(r^2)	50 ng L^{-1}		LOQ (ng L^{-1})
			Recovery (%)[a]	RSD (%)[b]	
$CHCl_2I$	20–2000	0.997	86–118(11)	8	3
CHClBrI	20–2000	0.994	88–108(7)	7	4
$CHBr_2I$	20–2000	0.998	91–113(8)	8	5
$CHClI_2$	20–2000	0.996	90–107(6)	6	3
$CHBrI_2$	20–2000	0.999	89–110(8)	9	4
CHI_3	20–2000	0.992	82–125(15)	10	6

a. Repeatability values (inter-day precision), expressed as relative standard deviation (RSD), were given in brackets (n=7); b. Intra-day precision (n=7).

3.2.2 Analytical methods for determination of other targets

Micro liquid-liquid extraction with methyl tert-butyl ether (MTBE) at acidic condition was adopted for extraction of iodoacids, and both NaCl and H_2SO_4 were added to water samples to improve the extraction efficiency. The extracted iodoacids reacted with MeOH in the presence of H_2SO_4 at 50 ^oC for 2 h to produce the corresponding methyl esters, which were then determined by GC (Agilent, 6890A)/ECD (Electron Capture Detector) according to U.S. EPA method 552. A DB-225 column (J&W) with helium as carrier gas was used. Brominated/chlorinated THMs were analyzed according to U.S. EPA method 8260C. Nitrobenzene (NB), p-nitrobenzoic acid (pNBA), p-chlorobenzoic acid (pCBA), and m-toluic acid (mTA) were determined by HPLC with a photodiode array detector (Agilent, 1100 serial). Br^-, I^- and IO_3^- were detected by an ion chromatography (IC) coupled with ICP-MS (Agilent, G3151A). Formic acid (HCO_2H), oxalic acid, Cl^-, and SO_4^{2-} were analyzed by IC coupled with thermal conductivity detector (Dionex, ICS-3000). Formaldehyde (HCHO) was determined by headspace sampler coupled with GC (Agilent, 7890A)/FID (Flame Ionization Detector). Total organic carbon (TOC) was analyzed by a TOC analyzer (Shimadzu, TOC-V_{CSH}). UV absorption of I-THMs, iodoacids, and THMs were measured by a UV/Vis spectrophotometer (Shimadzu, UV-2550). H_2O_2 concentration was measured by a WTW Photolab S12.

3.3 UV Photoreactor

Photodegradation experiments were conducted in a 740 mL cylindrical glass reactor filled with 740 mL of fresh I-THMs or iodoacids aqueous solution at room temperature. A low-pressure mercury vapor lamp (nominal power 5W, manufactured by Philips) primarily emitting irradiation at 254 nm was placed coaxially with the reactor in a quartz sleeve (Figure 3.2). A small stir bar was placed at the bottom of the reactor to ensure completely mixed batch conditions.

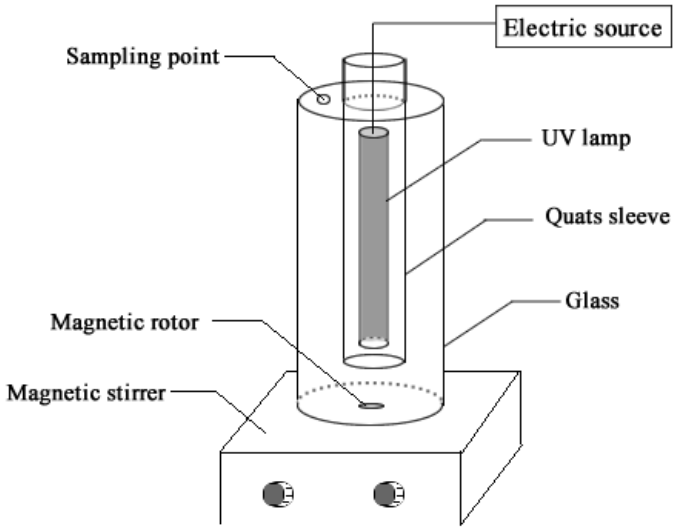

Figure 3.2 Schematic of the photoreactor used in this study.

3.4 Determination of the average photonic intensity per volume (I_o) and optical path length (b) of the photoreactor

Based on the Beer-Lambert Law and the definition of quantum yield, the overall direct photolysis rate of the organic pollutant could be described as follows.

$$-\frac{dC}{dt} = \Phi I_o (1 - e^{-2.303\varepsilon bC}) \qquad (3.1)$$

Equation 3.1 can be simplified in two cases according to the value of the exponential term as shown below (Beltrán et al., 1995).

If $2.303\varepsilon Cb > 2$

$$-\frac{dC}{dt} = \Phi I_o \quad (3.2)$$

If $2.303\varepsilon Cb < 0.02$

$$-\frac{dC}{dt} = 2.303\Phi I_o \varepsilon bC \quad (3.3)$$

Equations 3.2 and 3.3 can be used to determine the average photonic intensity per volume (I_o) and optical path length (b) of the photoreactor, respectively. In this study, hydrogen peroxide was used as the actinometer.

Direct photolysis of H_2O_2 at a high concentration of 0.062 mol L^{-1} was conducted to determine the average photonic intensity per volume (I_o) of the photoreactor. Equation 3.2 indicates that direct photolysis of H_2O_2 at a high concentration follows zero-order kinetics. Thus, a plot of C_f/C_i versus irradiation time should lead to a straight line with slope of ΦI_o as shown in Figure 3.3. The average photonic intensity per volume (I_o) was determined as 3.19×10^{-6} E L^{-1} s^{-1}.

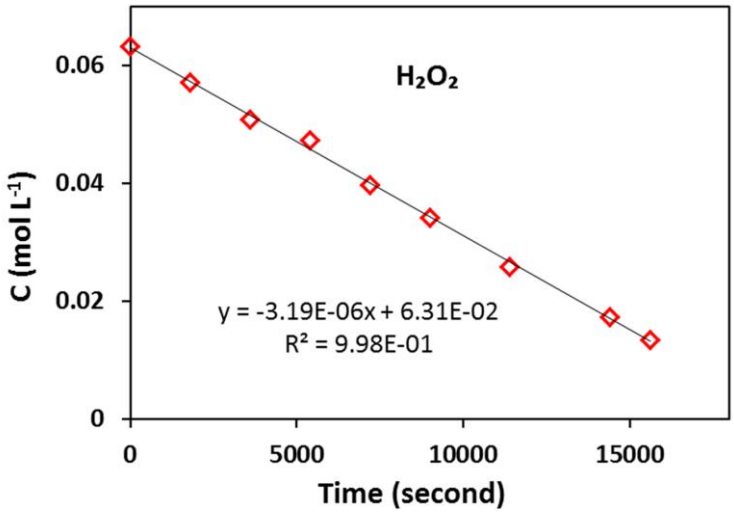

Figure 3.3 Determination of the average photonic intensity per volume (I_o) of the photoreactor used in the present study.

Direct photolysis of H_2O_2 at a low concentration of 3.50 mg L^{-1} was conducted to determine the optical path length of the photoreactor. Equation 3.3 indicates that direct photolysis of H_2O_2 at a low concentration follows first-order kinetics. Thus, a plot of $-\ln(C_f/C_i)$ versus irradiation time should lead to a straight line with slope of $2.303\Phi I_o \varepsilon b$ as shown in Figure 3.4. With the obtained Φ, I_o, and ε, the optical path length (b) was determined as 2.6 cm.

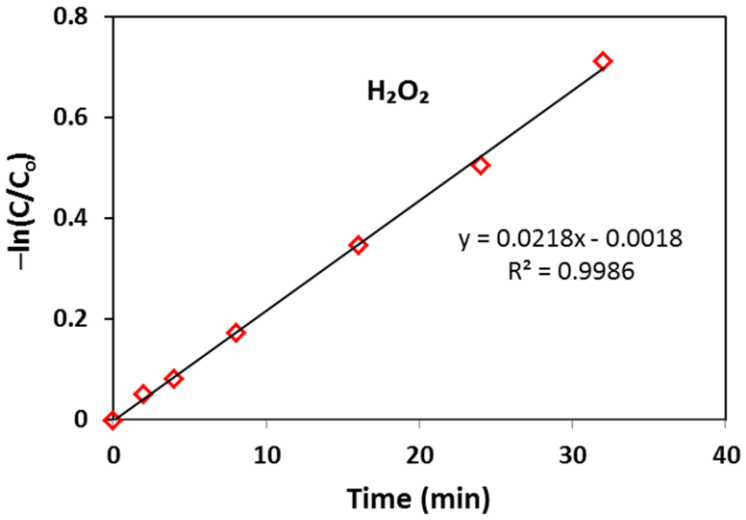

Figure 3.4 Determination of optical path length (b) of the photoreactor used in the present study.

3.5 Statistical analysis

To address experimental uncertainty, the statistical significance of the difference between the obtained results was analyzed using One-Sample t-Test. The QSAR models were established by simple and multiple linear regressions analysis in Microsoft Excel 2010. The value of the regression coefficient, R^2, is used to determine the goodness of fit of the linear relationship. In the QSAR modeling study for direct photolysis of I-DBPs, logarithm of direct photolysis rate constant ($\log k_m$) was selected as the dependent variable, while the bond strength (BS) of the carbon-halogen bond to be broken in the rate-determining step, the electronic effect constants (σ), and the steric effect constants (E_s) of all substituents to carbon centre were selected as independent variables.

CHAPTER 4. Photodegradation of I-THMs in aqueous solution by UV254 irradiation

In the first part of this study, photolysis with germicidal UV254 nm was applied to remove I-THMs, since carbon-halogen bonds could be photo-cleaved under UV254 irradiation (energy of C-I, C-Br, and C-Cl bonds are 209, 280, and 397 kJ mol^{-1}, respectively, which are lower than photon energy of 472 kJ mol^{-1} for UV254) (Weast et al., 1986; Jones and Carpenter, 2005) and there are evident UV absorption of I-THMs (i.e., molar absorption coefficients of 6 I-THMs at UV254 range from 167 to 1131 M^{-1} cm^{-1}). Direct photolysis of I-THMs and other THMs was firstly investigated and compared. The effect of common matrix species such as NO_3^-, HA, HCO_3^-, SO_4^{2-}, and Cl^- on the direct photolysis kinetics of I-THMs was also evaluated. Subsequently, UV direct photolysis of I-THMs in different types of water including DI water, treated water, surface water, and secondary effluent was examined. Finally, a QSAR model was established based on the experimental results of direct photolysis of I-THMs and brominated trihalomethanes (B-THMs).

4.1 Experiment details

Photodegradation of 6 I-THMs in the multi-species system (each at initial concentration of 100 μg L^{-1}) in DI water under UV254 irradiation was conducted in triplicate. For comparison, photodegradation of 6 I-THMs in the single-species system (each at initial concentration of 100 μg L^{-1}) was conducted once under the same conditions. Photodegradation of 6 I-THMs and 4 brominated/chlorinated THMs ($CHCl_3$, $CHCl_2Br$, $CHClBr_2$, and $CHBr_3$) in the multi-species system under UV254 irradiation was also performed once. Aliquots were sampled at predetermined time intervals and analyzed immediately by P&T-GC/MS.

4.2 Results and Discussion

4.2.1 UV absorbance

The efficiency of the photodegradation process of an organic pollutant is influenced by its light absorption and quantum yield at the wavelength in question (Prados-

Joya et al., 2011). To assess the applicability of photodegradation of I-THMs under UV254 irradiation, molar absorption coefficients (ε) of I-THMs and THMs were measured. The molar absorption coefficients of the non-chlorinated I-THMs including CHI_3, $CHBrI_2$ and $CHBr_2I$ are very close, approximately 1100 M^{-1} cm^{-1}, and are higher than those of the chlorinated I-THMs (Table 4.1). In general, molar absorption coefficients of I-THMs and THMs followed the order of $CHI_3 \approx CHBrI_2 \approx CHBr_2I > CHClI_2 > CHBr_3 \approx CHClBrI > CHClBr_2 \approx CHCl_2I > CHCl_2Br > CHCl_3$. The result suggests that the photodegradation of I-THMs under UV254 irradiation is viable due to their evident UV absorbances.

4.2.2 Direct photolysis of I-THMs in DI water: kinetic analysis

Direct photolysis of 6 I-THMs and 3 B-THMs followed the first-order kinetics (Figure 4.1). There is an insignificant difference in the degradation rate constants of 6 I-THMs obtained in the multi-species system and single-species system (Table 4.1). No change of concentration of 6 I-THMs in control solution at room temperature was observed within 60 min. Additionally, experimental results showed that pH (5 and 10) and the initial concentration of I-THMs (10-400 μg L^{-1}) had no significant effect on the direct photolysis rates of I-THMs (Figure 4.2). Thus, pH adjustment was not considered and the initial concentration of 100 μg L^{-1} for each I-THM species was used in the subsequent investigations. The direct photolysis rate constants of the non-chlorinated I-THMs ($CHBr_2I$, $CHBrI_2$, and CHI_3) are almost identical, which are higher than those of the chlorinated I-THMs ($CHCl_2I$, CHClBrI, and $CHClI_2$) and the 3 B-THMs (Table 4.1). The direct photolysis rate constant of $CHCl_2I$ is the lowest among 6 I-THMs. It was also observed that the direct photolysis rate constants of CHClBrI and $CHCl_2I$ are comparable to those of $CHBr_3$ and $CHClBr_2$, respectively. Hence, it can be said that I-THMs still become relatively recalcitrant to UV254 direct irradiation when Cl atom is also present in the molecule. In general, the direct photolysis rates of I-THMs and THMs followed the order of $CHBr_2I \approx CHBrI_2 \approx CHI_3 > CHClI_2 > CHClBrI \approx CHBr_3 > CHCl_2I \approx CHClBr_2 > CHCl_2Br > CHCl_3$ (Table 4.1).

Table 4.1 Summary of time-based first-order rate constant (k), fluence-based first-order rate constant (k_f), regression coefficient (R^2), quantum yield (Φ), and removal percentages (R_{254}) of 6 I-THMs and 4 THMs at different treatment conditions in DI water

Compound	k (min^{-1})	k (min^{-1})	$k_f \cdot 10^4$	R^2	ε	Φ^a	% I-THMs and THMs removal (R_{254})	
			($cm^2\ mJ^{-1}$)		($M^{-1}\ cm^{-1}$)		40 mJ cm^{-2}	140 mJ cm^{-2}
	(single-species)	(multi-species)	(multi-species)				(multi-species)	(multi-species)
$CHCl_2I$	0.10	0.093(±0.009)	3.95(±0.39)[b]	0.997	167	0.50(±0.05)	1.56(±0.15)	5.41(±0.52)
CHClBrI	0.27	0.26(±0.02)	11.21(±0.92)	0.993	423	0.54(±0.04)	4.38(±0.35)	14.61(±1.11)
$CHClI_2$	0.36	0.36(±0.02)	15.32(±1.08)	0.989	604	0.52(±0.04)	5.94(±0.40)	19.42(±1.23)
$CHBr_2I$	0.58	0.58(±0.07)	24.75(±2.93)	0.992	1131	0.45(±0.05)	9.41(±1.07)	29.41(±2.97)
$CHBrI_2$	0.53	0.52(±0.04)	22.26(±1.95)	0.990	1068	0.43(±0.04)	8.51(±0.71)	26.92(±2.02)
CHI_3	0.52	0.51(±0.04)	21.84(±1.78)	0.988	1118	0.40(±0.03)	8.35 (±0.65)	26.49(±1.86)
$CHBr_3$	-	0.27(±0.03)	11.34(±1.30)	0.995	448	0.52(±0.06)	4.43(±0.50)	14.78(±1.56)
$CHClBr_2$	-	0.10	4.25	0.996	228.5	0.38	1.69	5.82
$CHCl_2Br$	-	0.02	0.85	0.991	42.3	0.48	0.34	1.19
$CHCl_3$	-	-[c]	-	-	0.1	-	-	-

a. H_2O_2 as actinometer; b. Standard deviations were obtained from at least duplicate datasets; c.There was no observable loss of $CHCl_3$ in this study within 60 min of experimental run.

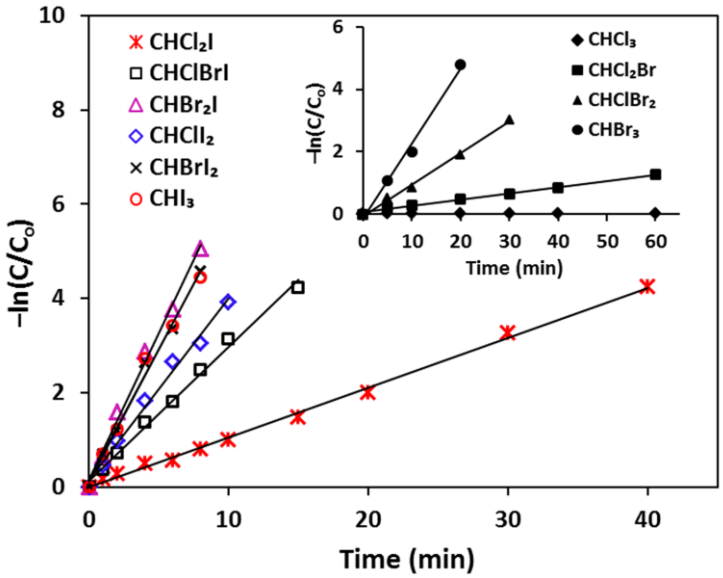

Figure 4.1 Linear plots for UV254 direct photolysis of 6 I-THMs; inset: linear plots for UV254 direct photolysis of 4 THMs.

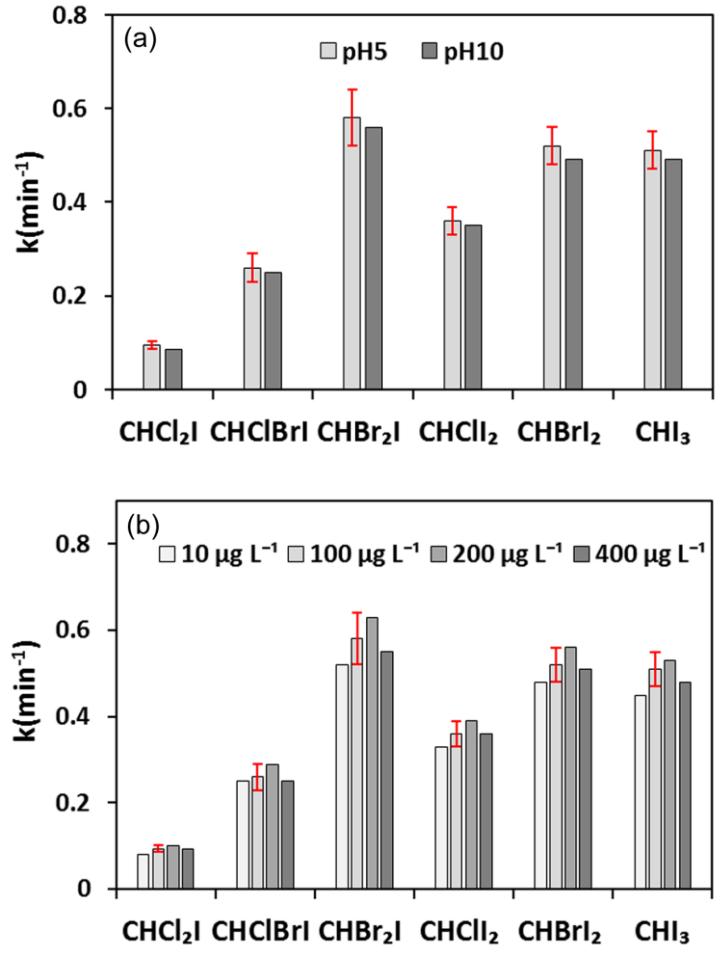

Figure 4.2 Effect of pH (a) and initial concentration (b) on the direct photolysis of 6 I-THMs.

4.2.3 Determination of quantum yield (Φ) of I-THMs

According to the Beer-Lambert Law and the definition of quantum yield, the overall direct photolysis rate of the organic pollutants could be described as follows (Fang et al., 2013).

$$-\frac{dC}{dt} = \Phi I_o (1 - e^{-2.303\varepsilon Cb}) \quad (4.1)$$

where C is the concentration of the specific organic pollutant in mol L^{-1}; dC/dt is the photodegradation rate of the specific organic pollutant in mol L^{-1} s^{-1}; Φ is the quantum yield at the wavelength in question in mol E^{-1}; ε is the molar absorption coefficient at the wavelength in question in M^{-1} cm^{-1}; I_o is the average photonic intensity per volume of the photoreactor used in this study in E L^{-1} s^{-1}; and b is the optical path length in cm. When the UV absorbance of the organic pollutant (a = εCb) is very low (i.e., 2.303εCb < 0.02), $e^{-2.303\varepsilon Cb}$ in Equation 4.1 can be simplified as 1-2.303εCb through Taylor expansion. Additionally, as the photodegradation follows the first-order kinetics (Equation 4.2), the determination of quantum yield in the diluted solution under monochromatic wavelength irradiation can be written as Equation 4.3 (Prados-Joya et al., 2011; Fang et al., 2013).

$$-\frac{dC}{dt} = kC \quad (4.2)$$

$$\Phi = \frac{k}{2.303 I_o \varepsilon b} \quad (4.3)$$

where k is the time-based first-order rate constant in s^{-1}.

As mentioned previously, using H_2O_2 as an actinometer (Beltrán et al., 1995), the average photonic intensity per volume (I_o) and effective optical path length (b) of the photoreactor used in the this study were determined as 3.19 x 10^{-6} E L^{-1} s^{-1} and 2.6 cm, respectively, which correspond to the photon flux (q_p) of 8.30 x 10^{-9} E cm^{-2} s^{-1} and UV intensity of 3.92 mW cm^{-2}. The derived quantum yields of 6 I-THMs ranged from 0.37 to 0.58 (Table 4.1), which indicates a high efficiency of quantum process in the I-THMs photodegradation under UV254 irradiation.

With the known average photonic intensity per volume (I_o) and optical path length (b) for a specific configuration of photoreactor, it is obvious from Equation 4.3 that the direct photolysis rate of the organic pollutant is proportional to quantum yield (Φ) and molar absorption coefficient (ε), which are two fundamental parameters that govern the direct photolysis rate (Figure 4.3).

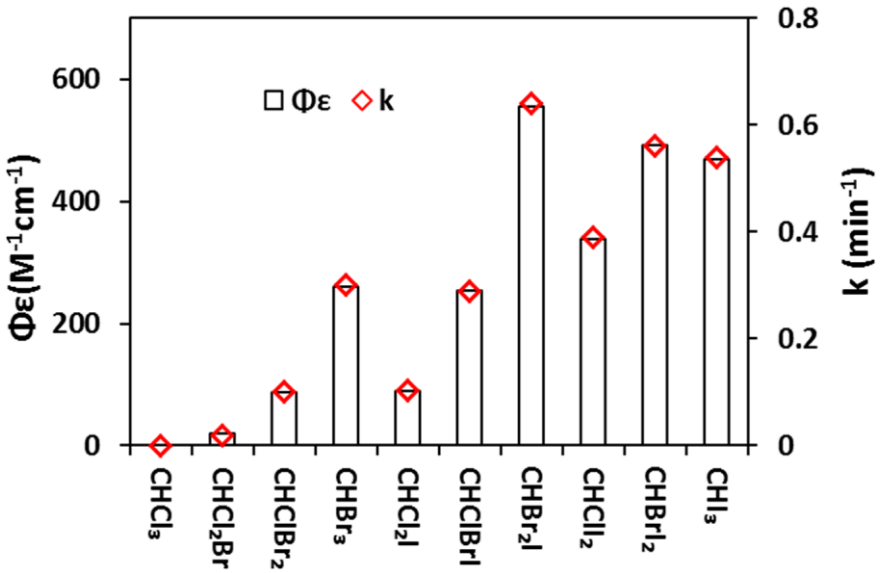

Figure 4.3 Correspondence between first-order rate constants (k) and the product of molar absorption coefficients (ε) and quantum yield (Φ) for UV254 direct photolysis of 6 I-THMs and 4 THMs.

Since fluence-based first-order rate constant (k_f) is independent of the fluctuation in photon flux (q_p) of the UV lamp, it allows for direct comparison with the photodegradation rate constants obtained with different photoreactors (Canonica et al., 2008; Prados-Joya et al., 2011). For comparison purpose, k_f values are calculated through dividing the time-based first-order rate constant (k) by the photon flux and photon energy emitted by the UV lamp according to Equation 4.4. The obtained k_f values for I-THMs were summarized in Table 4.1.

$$k_f = \frac{k}{q_p \cdot hc/\lambda} \tag{4.4}$$

where k_f is the fluence-based first-order rate constant in $cm^2\ mJ^{-1}$; k is the time-based first-order rate constant in s^{-1}; q_p is the photon flux emitted by the lamp in E $cm^{-2}\ s^{-1}$; hc/λ is the photon energy at a specific wavelength in kJ mol^{-1}.

To assess the applicability of UV254 irradiation in I-THMs photodegradation in real water treatment process, the removal efficiency of I-THMs were determined under a specific UV dose. The irradiation doses of 40 and 140 mJ cm^{-2} are chosen because they define typical range used in disinfection application (Baeza and Knappe, 2011). As the UV intensity of the present lamp is ~ 3.92 mW cm^{-2}, the time required to reach the irradiation doses of 40 and 140 mJ cm^{-2} are 10.2 and 35.7 s, respectively. The removal percentage of I-THMs (R_{254}) can be calculated according to Equation 4.5.

$$R_{254} = (1 - e^{-kt})\% \quad (4.5)$$

As seen from Table 4.1, R_{254} of 6 I-THMs at UV doses of 40 and 140 mJ cm^{-2} are less than 10 and 30%, respectively. Although I-THMs are susceptible to photodegradation under UV254 irradiation with first-order rate constants in the range of 0.1-0.6 min^{-1} (half-life times of 1 to 8 min), UV dose for disinfection in real water treatment process is still impractical for a significant removal of I-THMs. Thus, a higher irradiation dose (934-5824 mJ cm^{-2} for 90% removal of 6 I-THMs) than the usual dose for UV disinfection or a UV-based AOP is required to significantly photodegrade I-THMs.

4.2.4 Photodegradation end-products identification

A previous study has shown that the life times of $CHBr_3$ intermediate photoproducts in water were in picoseconds and special equipment (like Picosecond Time-Resolved Resonance Raman (ps-TR^3) Spectroscopy) was required to identify them (Kwok et al., 2004). In the present study, through identification of the end-products, the possible direct photolysis pathway of I-THMs could be identified. The photodegradation end-products in this study were Cl^-, Br^-, and I^- (Figure 4.4). There was a good mass balance between total amount of produced halides and the introduced halogens in I-THMs (i.e., 92-109% recovery). No formation of ClO_3^-, BrO_3^-, and IO_3^- was observed. Additionally, TOC decreased concomitantly during

the photodegradation process (Figure 4.4), indicating that the I-THMs could be mineralized via UV254 direct photolysis. However, it is worth mentioning that the HCO_2H is also identified as the end-product, which was also reported in the previous study regarding direct photolysis of $CHBr_3$ (Kwok et al., 2004). HCO_2H increased slightly during the photodegradation process and reached 40 µg L^{-1} at the end (Figure 4.4), which accounts for less than 5% of TOC concentration initially spiked in the reaction solution. It suggests that HCO_2H is the minor end-product in the direct photolysis of I-THMs. Moreover, formaldehyde (HCHO) was not detected during the photodegradation process.

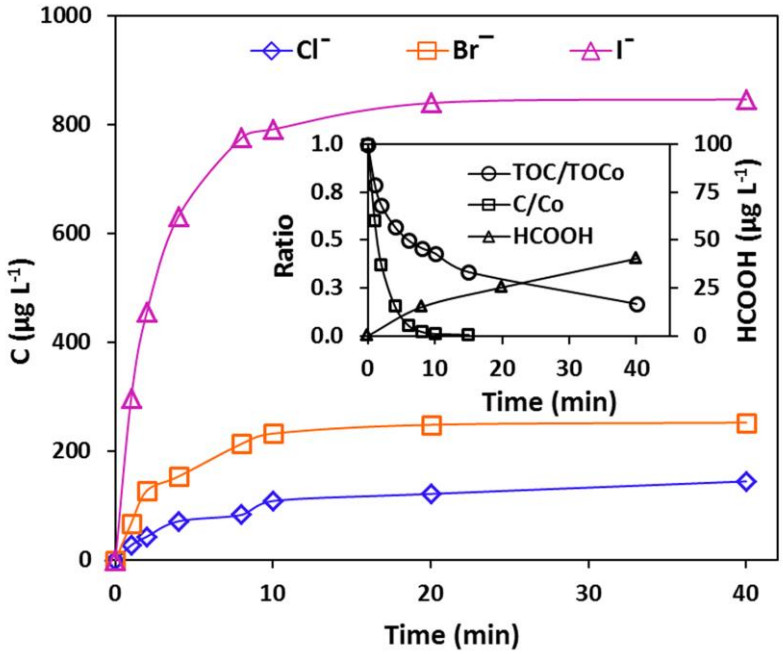

Figure 4.4 Time course of halide formation during direct photolysis of 6 I-THMs ($CHCl_2I$, CHClBrI, $CHBr_2I$, $CHClI_2$, $CHBrI_2$, and CHI_3, each at initial concentration of 200 µg L^{-1}); inset: Time course of TOC reduction, CHI_3 reduction and HCO_2H formation during direct photolysis of CHI_3 (initial concentration around 10 mg L^{-1}).

According to previous studies, UV240 nm could cleave the primary C-Br bond of $CHBr_3$, but the photon energy was insufficient to induce secondary dissociation of the $CHBr_2$ radical formed (McGivern et al., 2000; Kwok et al., 2004). In the present study, the energy of UV254 photon (472 kJ mol^{-1}) is higher than those of C-X bonds (209, 280, and 397 kJ mol^{-1} for C-I, C-Br, and C-Cl, respectively) (Weast et

al., 1986). Homolytic photo-cleavage of C-I bond upon UV254 absorption could be the first step of I-THMs photolysis. As described in the section 4.2.3, the direct photolysis rate constants of I-THMs are proportional to their corresponding molar absorption coefficients and quantumn yield. It suggests that the first-step reaction (photo-cleavage of C-I bond) is the rate-determining step for direct photolysis of I-THMs. Isobromoform (BrCHBr-Br) has been previously identified as the intermediate in the second step of $CHBr_3$ photodegradation, and subsequently a water-catalyzed mechanism proceeds to transform isobromoform into its following intermediates which will react with water molecule through OH insertion/HBr elimination resulting in complete conversion to HBr, CO (major product) and HCO_2H (minor product) (Kwok et al., 2004). Thus, in the present study, photo-cleavage of C-I bond by UV254 followed by a series of water-catalyzed reactions might be the possible photodegradation pathway for I-THMs in water.

4.2.5 Direct photolysis of I-THMs in the presence of matrix species

Further investigation was performed to evaluate the effects of common matrix species including NO_3^-, HA, HCO_3^-, SO_4^{2-}, and Cl^- on the direct photolysis of 6 I-THMs. In the following discussion, the degradation rates of each I-THM under different conditions are compared to those observed under the reference condition (DI water, initial concentration of 100 μg L^{-1}, and pH around 5). When the p value is less than 0.01 in One-Sample t-Test, it suggests that the direct photolysis rate constant of the I-THM species under the specific condition is significantly different from that obtained under the reference condition.

The direct photolysis rate constant of $CHCl_2I$ in the presence of 5 mg L^{-1} NO_3^- is comparable to that obtained in DI water (Figure 4.5(a)). However, when the concentration of NO_3^- was increased from 20 to 200 mg L^{-1}, the degradation rate of $CHCl_2I$ increased correspondingly. The degradation rate constant of $CHCl_2I$ reaches 0.31 min^{-1} in the presence of 200 mg L^{-1} NO_3^-, which is 3 times higher than that obtained in DI water. However, NO_3^- had much less influence on the photodegradation of the other 5 I-THMs which are highly susceptible to UV254

photolysis compared to $CHCl_2I$ (Table 4.1). The direct photolysis rate constants of the 5 I-THMs increased by less than one-fold as compared to those observed in DI water even the concentration of NO_3^- was increased to 200 mg L^{-1}.

It is reported that some chemicals such as salicylic acid and benzoic acid are employed as molecular probe for trapping $HO^{\bullet}$ to form the stable and quantifiable products (Jankowski et al., 2000; Yang et al., 2004; Wu et al., 2007b). On the basis of this methodology, some studies demonstrated that direct photolysis of NO_3^- under UV irradiation could generate $HO^{\bullet}$ (Yang et al., 2004; Boucheloukh et al., 2012; Ji et al., 2012). Indeed, the formation of $HO^{\bullet}$ in the UV direct photolysis of NO_3^- follows a complex pathway. The primary reactions in NO_3^- photolysis are the generation of the radical anion $O^{\bullet-}$ and nitrite ion, which continues to produce the radical anion $O^{\bullet-}$ under UV irradiation. Subsequently, the radical anion $O^{\bullet-}$ is rapidly reacting with water molecule to form the highly reactive $HO^{\bullet}$. Generally, the reaction pathway for generation of $HO^{\bullet}$ via direct photolysis of NO_3^- can be simplified as follows (Keen et al., 2012).

$$NO_3^- + h\nu \rightarrow NO_2^{\bullet} + O^{\bullet-} \quad (4.6)$$

$$NO_3^- + h\nu \rightarrow NO_2^- + \frac{1}{2}O_2 \quad (4.7)$$

$$NO_2^- + h\nu \rightarrow NO^{\bullet} + O^{\bullet-} \quad (4.8)$$

$$O^{\bullet-} + H_2O \rightarrow HO^{\bullet} + HO^- \quad (4.9)$$

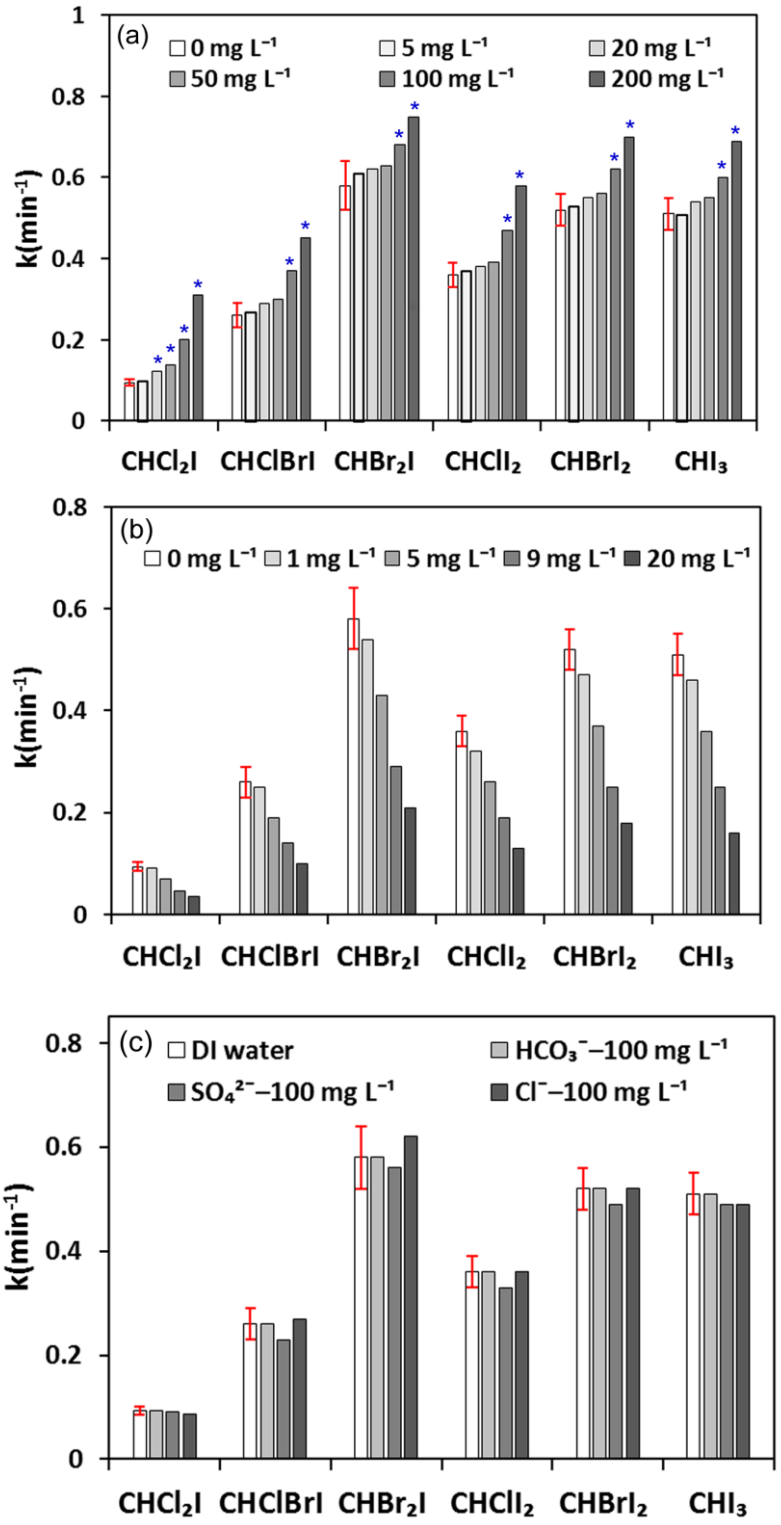

Figure 4.5 (a). Effect of $NaNO_3$ on the direct photolysis of 6 I-THMs, asterisk (*) represents $p < 0.01$, which implies that the k value is significantly different from the k values obtained in DI water; (b). Effect of HA on the direct photolysis of 6 I-THMs; (c). Effect of $NaHCO_3$, Na_2SO_4, and NaCl on the direct photolysis of 6 I-THMs; Error bars denote standard deviations obtained from at least duplicate datasets.

However, due to weak UV254 absorption of NO_3^- (Figure 4.6), $HO^{\cdot}$ was generated at a low quantum yield (Mack and Bolton, 1999; Keen et al., 2012). This can explain why the photodegradation rate of the 5 I-THMs ($CHClBrI$, $CHBr_2I$, $CHClI_2$, $CHBrI_2$, and CHI_3) only increased slightly in the presence of NO_3^- in this study. Additionally, it is believed that the main reason for the more significant effect of NO_3^--induced indirect photolysis of $CHCl_2I$ is that the efficiency of its direct photolysis is low (i.e., its k value is 3 to 6 times lower than those of other 5 species). In other words, the effect of indirect photolysis due to $HO^{\cdot}$ attack in the presence of NO_3^- for other 5 species is possibly masked by their efficient direct photolysis.

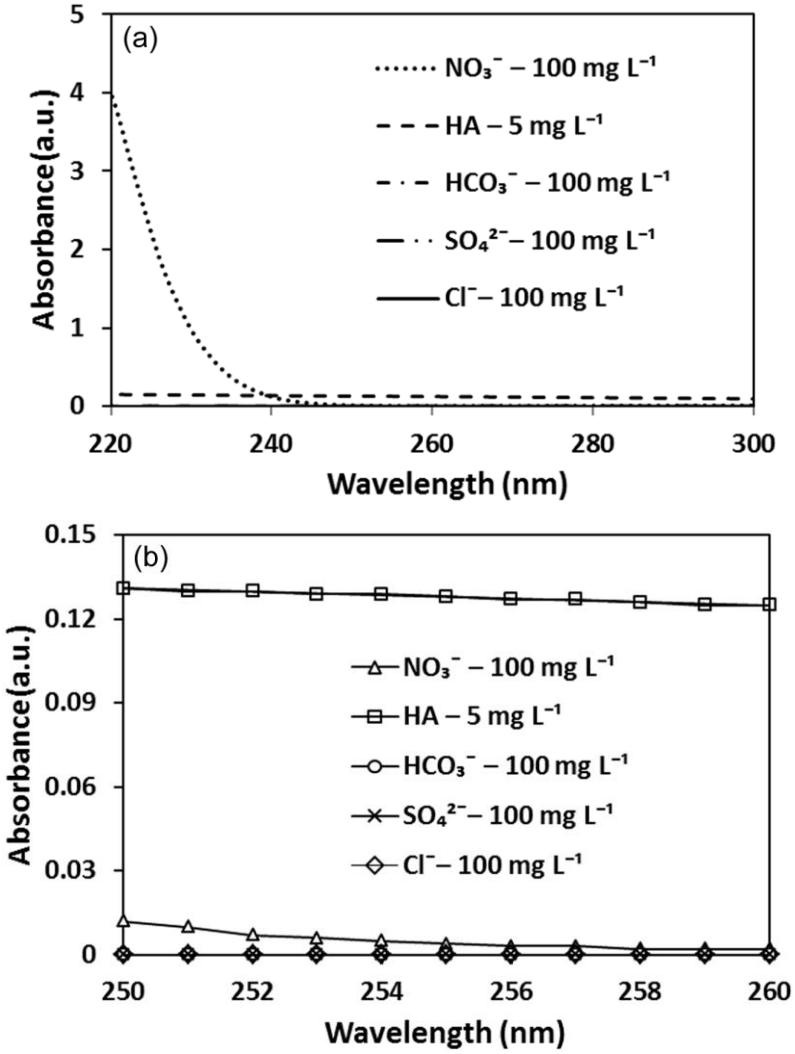

Figure 4.6 (a). Absorbance of $NaNO_3$, HA, $NaHCO_3$, Na_2SO_4, and NaCl in DI water at the concentrations used in this study in the range of 220 to 300 nm; (b).

Absorbance of $NaNO_3$, HA, $NaHCO_3$, Na_2SO_4, and NaCl in DI water at the concentrations used in this study in the range of 250 to 260 nm.

It has been reported that natural organic matter (NOM) present in water has two opposite effects on photodegradation of the organic pollutants (De la Cruz et al., 2012). On the one hand, it can inhibit the direct photolysis due to inner filtering of UV light by NOM. On the other hand, with exposure to UV irradiation, a photosensitizer present in NOM can be promoted to its reactive triplet state (^{3}NOM*) or singlet state (^{1}NOM*), which can react with the organic pollutant (De la Cruz et al., 2012; Marin et al., 2012). Moreover, ^{3}NOM* also can react with molecular oxygen present in water to generate singlet molecular oxygen, $^1O_2$ that will subsequently attack the organic pollutant (De la Cruz et al., 2012). In the latter case, the formation of reactive oxygen species (ROS, e.g. ^{3}NOM*, ^{1}NOM*, and $^1O_2$) leads to increase of the photodegradation rate of the organic pollutant. In this study, humic acid (HA) was selected as a matrix species to investigate the effect of NOM on I-THMs photodegradation, as HA is considered as the main component of NOM (Prados-Joya et al., 2011). HA consists of a great number of aromatic rings and oxygen-related functional groups, which could strongly absorb UV light (Steelink, 2002). Experimental results showed that the photodegradation rates of 6 I-THMs decreased with increasing HA from 1 to 20 mg L^{-1} (Figure 4.5(b)). The presence of HA significantly reduced the photodegradation rates of 6 I-THMs to the same extent. This result suggests that filtering and screening of UV light by HA reduces the fraction of UV light absorbed by I-THMs, which results in the decease of the photodegradation rates of I-THMs. In other words, indirect photolysis in the presence of a photosensitizer such as HA could be less significant than the competitive UV absorption effect for I-THMs photodecay.

In contrast, when HCO_3^-, SO_4^{2-}, or Cl^- was spiked into the reaction solution, the phenomenon of filtering and screening of UV254 light as well as the ROS attacking of I-THMs was not observed, because these 3 anions at the concentration of 100 mg L^{-1} have no UV254 absorbance (Figure 4.6). As such, HCO_3^-, SO_4^{2-}, and Cl^- had no statistically significant effect on the photodegradation kinetics of I-THMs (Figure 4.5(c)).

4.2.6 Direct photolysis of I-THMs in different types of water

The viability of UV254 irradiation to photodegrade I-THMs in different types of water including DI water, surface water (SW), treated water (TW, collected from a water treatment plant, Singapore), and secondary effluent (SE, collected from a wastewater treatment plant, Singapore) was also evaluated. The characteristics of the water samples used are presented in Table 4.2.

Table 4.2 Characteristics of different types of water used in this study

Water	pH	Turbidity (NTU)	TOC (as C)[b]	Total alkalinity[c]	NO_3^- [b]	SO_4^{2-} [b]	Cl^- [b]
DI	6.0	<0.1[a]	0.080	<5	<0.05	<0.045	<5
SW	6.4	100	2.40	8	3.38	4.14	9
TW	8.0	0.22	0.79	13	3.20	21.6	10
SE	6.7	5.3	9.70	36	45.2	45.1	86

a. It represents that the result is below detection limit; b. unit: mg L^{-1}; c. as $CaCO_3$.

The degradation rates of 6 I-THMs in the surface water and secondary effluent decreased dramatically, while their degradation rates in the treated water were comparable to those obtained in DI water (Figure 4.7). According to the preceding discussion, the effect of pH, HCO_3^-, SO_4^{2-}, Cl^- and NO_3^- with concentration less than 5 mg L^{-1} on I-THMs photodegradation could be excluded in the study using real water sample as water matrix. The reduction of photodegradation rates in surface water could be mainly attributed to its high turbidity which shielded target I-THMs from UV254 irradiation. Although the concentration of NO_3^- in the secondary effluent was very high (45.2 mg L^{-1}), the increase of photodegradation rate of I-THMs was not evident, as high concentration of $HO^{\cdot}$ scavengers such as HCO_3^- and NOM were also present in the secondary effluent (Table 4.2). On the other hand, high concentration of NOM present in the secondary effluent led to the decrease of photodegradation rates of I-THMs due to competitive absorption of UV254 irradiation by NOM. It suggested that direct photolysis was still the predominant mechanism for I-THMs photodegradation in the real water samples but the indirect photolysis due to generation of ROS was not evident. It can be said

that UV photolysis is more suitable as a post-treatment after filtration to control I-THMs.

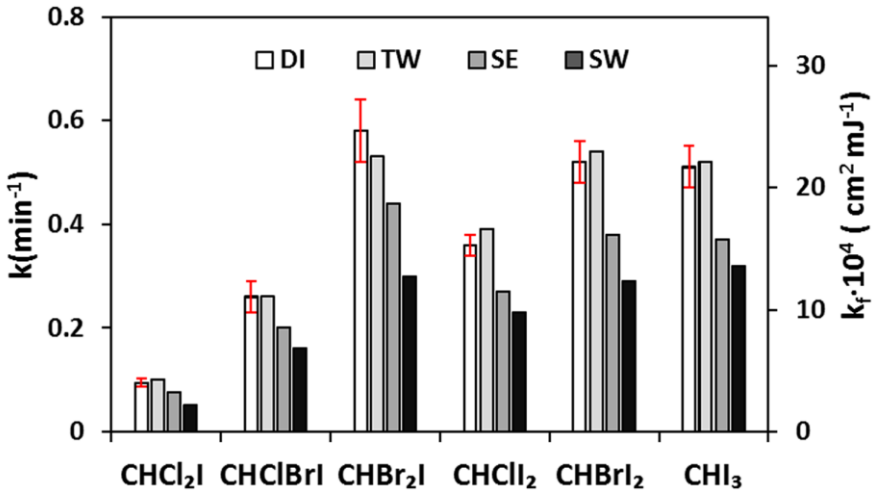

Figure 4.7 Effect of different types of water on photodegradation of 6 I-THMs (TW: treated water, SW: surface water, SE: secondary effluent). Error bars denote standard deviations obtained from at least triplicate datasets.

4.2.7 QSAR modeling

Quantitative structure-activity relationship (QSAR) is often used to explore the relationship between chemical structures and biological or chemical activity of the compounds studied. In QSAR application, it is assumed that the reactivity differences of similar compounds are due to the type, number, as well as the steric and electronic effects of their functional groups (Chen et al., 2010). An empirical equation is usually used to describe the QSAR model as follows.

$$P = \sum_{i=1,j=1}^{i=n,j=n} a_{ij} D_{ij} + b \qquad (4.10)$$

where P is the property of interest such as first-order rate constant, quantum yield etc.; a_{ij} and b are the constants obtained from simple and multiple linear regression; D_{ij} are the molecular descriptors characterizing the structure of the compounds studied (Dyekjær and Jónsdóttir, 2004; Ioele et al., 2009).

To derive a QSAR model for direct photolysis of I-THMs and B-THMs, the logarithm of measured first-order rate constants ($\log k_m$) are correlated with a

number of molecular descriptors by simple and multiple linear regressions analysis. k_m is selected as the dependent variable as it is related to the chemical structure of the compound studied and can be regarded as an indicator to compare chemical reactivity of a serial of structurally similar compounds under a specific reaction condition. 3 molecular descriptors are selected as the independent variables since they give an indication of the bond to be broken, steric and electronic effect of the substituents that determine the chemical reactivity of the compound studied. These 3 molecular descriptors include the bond strength (BS) of the carbon-halogen bond to be broken in the rate-determining step, the summation of the electronic effect constants (σ), and the summation of the steric effect constants (E_s) of all substituents to carbon centre. The combined effects of multiple halides in a halo-organic are assumed to be the summative effects of individual halides in it (Zhang and Minear, 2002; Chen et al., 2010).Values of BS, σ, and E_s of 6 I-THMs and 3 B-THMs used to establish the QSAR model are presented in Table 4.3.

Table 4.3 Values of molecular descriptors used in this study for establishing the QSAR models and experimentally measured $\log k_m$, predicted $\log k_p$ by QSAR model 7, as well as the difference between $\log k_m$ and $\log k_p$, Δ

Species	BS[a]	E_s[b]	σ[b]	$\log k_m$	$\log k_p$	Δ
$CHCl_2Br$	280	–3.08	1.36	–1.699	–1.576	0.123
$CHClBr_2$	280	–3.28	1.31	–0.998	–1.130	0.132
$CHBr_3$	280	–3.48	1.26	–0.569	–0.684	0.115
$CHCl_2I$	209	–3.32	1.32	–1.027	–1.084	0.057
CHClBrI	209	–3.52	1.27	–0.585	–0.638	0.053
$CHBr_2I$	209	–3.72	1.22	–0.237	–0.192	0.045
$CHClI_2$	209	–3.76	1.23	–0.444	–0.679	0.235
$CHBrI_2$	209	–3.96	1.18	–0.284	–0.233	0.051
CHI_3	209	–4.20	1.14	–0.292	–0.274	0.019

a. Bond strength of C-X bonds to be broken in the rate-determining step were cited from literature (Weast et al., 1986); b. E_s and σ values of halogen atoms were cited from literature (Hansch and Leo, 1995);

The results of a number of correlations between $\log k_m$ and individual BS, σ, E_s, as well as the combinations of these molecular descriptors are summarized in Table 4.4. The value of the regression coefficient, R^2, is used to determine the degree of correlation between these descriptors and $\log k_m$. For simple linear regression case, each of these 3 molecular descriptors is used separately. R^2 values obtained are 0.40, 0.74, and 0.80 for BS, E_s, and σ, respectively. For multiple linear regression

case, when any 2 molecular descriptors are correlated with $\log k_m$, there is no significant improvement in the correlation and R^2 values are still below 0.84 for all cases. The best correlation is obtained when a combination of these 3 descriptors (BS, σ, and E_s) is used, with $R^2 = 0.95$ (model 7 in Table 4.4). In addition, F test in the multiple linear regression analysis shows that all coefficients in the QSAR model 7 are significant at the 95% confidence level. It suggests that these 3 molecular descriptors have a combined effect on the direct photolysis of I-THMs and B-THMs.

Table 4.4 Correlations of the logarithm of the measured first-order rate constant ($\log k_m$) with a number of molecular descriptors

Item	Model	R^2
1	$\log k_m = -0.0086BS + 1.32$	0.40
2	$\log k_m = -1.17E_s - 4.89$	0.74
3	$\log k_m = -6.13\sigma + 7.02$	0.80
4	$\log k_m = -0.0016BS - 1.07E_s - 4.15$	0.76
5	$\log k_m = -0.0020BS - 5.50\sigma + 6.67$	0.81
6	$\log k_m = 1.88E_s - 15.6\sigma + 25.6$	0.84
7	$\log k_m = -0.0075BS + 4.97E_s - 28.8\sigma + 55$	0.95

QSAR model 7 (Table 4.4) is in turn used to predict the direct photolysis rate of I-THMs and B-THMs. The QSAR-predicted $\log k_p$, experimentally measured $\log k_m$, as well as the difference between $\log k_m$ and $\log k_p$ (Δ) are presented in Table 4.3. The correspondence between $\log k_m$ and $\log k_p$ is also displayed in Figure 4.8. Generally, QSAR-predicted values agree with the experimental results, except for $CHClI_2$ which shows 0.235-log relative standard deviation. Additionally, the predicted first-order rate constant of $CHCl_3$ by the QSAR model 7 is 0.0013 min^{-1}, which corresponds to half-time of 9 hours. It indicates that $CHCl_3$ is more stable than I-THMs under UV254 irradiation, because the life-time of 6 I-THMs is in the range of 1 to 8 min. However, there was no observable loss of $CHCl_3$ in this study within 60 min of experimental run. The deviation suggests that further research is needed to explore more parameters to give a better description of I-THMs and THMs photodegradation process.

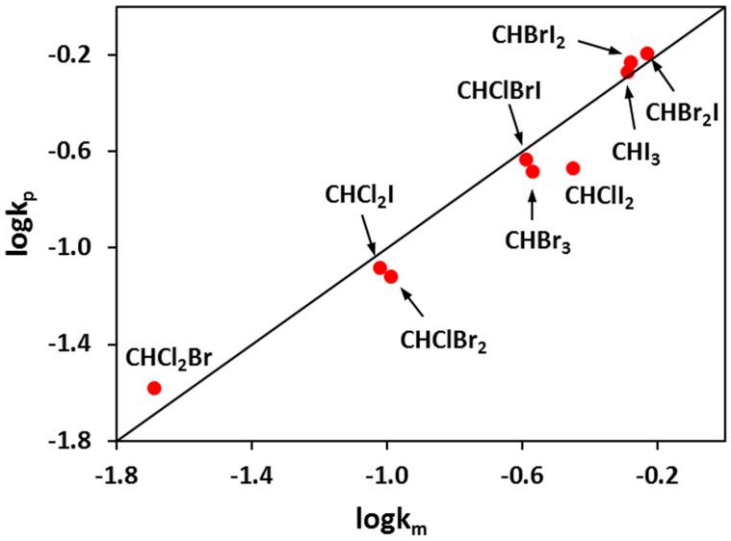

Figure 4.8 Correspondence between experimentally measured $logk_m$ and predicted $logk_p$ values by QSAR model 7 for 6 I-THMs and 3 B-THMs.

4.3 Conclusion

UV254 direct photolysis of I-THMs followed the first-order kinetics with rate constants in the range of 0.1-0.6 min^{-1}. The quantum yields of 6 I-THMs ranged from 0.37 to 0.58, when H_2O_2 was used as an actinometer. It was observed that I-THMs could be mineralized with release of halides. Experimental results also showed that NO_3^- had a slightly positive effect on the photodegradation kinetics possibly due to generation of $HO^{\cdot}$ at a low quantum yield via direct photolysis of NO_3^-, while HA reduced the photodegradation rates due to its competitive UV absorption. In contrast, HCO_3^-, SO_4^{2-}, and Cl^- had no significant effect on I-THMs photodegradation, as these 3 species have no UV254 absorption. Based on the above investigation of matrix species effect, it could be deduced that the decrease of photodegradation rate of 6 I-THMs in surface water and secondary effluent are mainly attributed to high turbidity and NOM, respectively. Additionally, it is determined that the removal efficiency of the direct photolysis of 6 I-THMs at a disinfection dose of 140 mJ cm^{-2} is less than 30%. Finally, a good QSAR model with R^2 = 0.95 was established based on the correlation between $logk_m$ and the combination of 3 molecular descriptors, namely bond strength (BS) of the carbon-

halogen bond to be broken, the electronic effect (σ) and the steric effect (E_s) of all substituents to carbon centre. It suggests that these 3 parameters have a significant combined effect on the overall direct photolysis of I-THMs and B-THMs.

CHAPTER 5 Kinetic modeling and energy efficiency of UV/H_2O_2 treatment of I-THMs

As discussed in the first part of this study, UV direct irradiation at a dose of 140 mJ cm^{-2} for disinfection is insufficient to significantly degrade I-THMs. Thus, in the second part of this study, photodegradation of I-THMs by the UV/H_2O_2 process was extensively investigated for its process kinetics, degradation products and energy efficiency. $CHCl_2I$ and CHI_3 commonly detected in drinking water were selected as the model compounds. $CHCl_2I$ is the most recalcitrant to UV254 direct photolysis as shown in the first part of this study (chapter 4), while CHI_3 is the most cytotoxic among 6 I-THMs (Richardson et al., 2008). The impact of some operational variables such as pH, H_2O_2 dose, and matrix species such as HA, HCO_3^-, SO_4^{2-}, Cl^-, NO_3^- on the photodegradation kinetics were evaluated. The parameters including pseudo-first-order rate constants, second-order rate constants of $HO^{\cdot}$ reacting with I-THMs, UV absorbance of the reaction solution were determined to characterize the photodegradation process. A steady-state kinetic model was established to predict the destruction of I-THMs in different types of water. Furthermore, in order to provide the requisite data for process scale-up, economic analysis, and energetic comparison with other treatment technologies such as ozonation and other AOPs, electrical energy per order (EE/O) was calculated to evaluate the efficiency of the UV/H_2O_2 process and to determine the optimal H_2O_2 dose. Finally, the end-products of I-THMs degradation by the UV/H_2O_2 process were identified.

5.1 Experimental details

Photodegradation of the individual $CHCl_2I$ and CHI_3 by UV/H_2O_2 were conducted in two separate series of experiments. The UV/H_2O_2 advanced oxidation experiments were conducted using different types of water with addition of H_2O_2 and pH adjustment before exposure to UV irradiation. The water matrices used in this study included DI water, laboratory synthesized water (LSW), and surface water (SW). The typical doses of H_2O_2 used were 2, 6, and 15 mg L^{-1} or otherwise indicated. The initial pH of the reaction solution was adjusted to 7 (3 or 11) by 0.1

mol L^{-1} H_2SO_4 and NaOH solution. The initial concentration of the individual I-THM (CHI_3 or $CHCl_2I$) in the UV/H_2O_2 process was 0.5 µmol L^{-1} or otherwise indicated. A competition kinetic approach was used to determine the second-order rate constants of I-THMs reacting with $HO^{\cdot}$ using p-xylene as the reference compound. The initial concentrations of the individual I-THM (CHI_3 or $CHCl_2I$), p-xylene, and H_2O_2 in DI water were 0.5 µmol L^{-1}, 0.5 µmol L^{-1}, and 58.8 µmol L^{-1}, respectively. As a base-line study, UV direct photolysis of reaction solution containing individual I-THMs including $CHCl_2I$ and CHI_3 in DI water was evaluated at different UV doses to determine the direct photolysis rate constant. Aliquots were sampled at predetermined time intervals and analyzed immediately by P&T-GC/MS.

5.2 Results and discussion

Both $CHCl_2I$ and CHI_3 photodegradation in the UV/H_2O_2 process followed the pseudo-first-order kinetics (Figure 5.1). The degradation rates increased dramatically in the UV/H_2O_2 process due to generation of $HO^{\cdot}$, as compared to direct photolysis. Without UV irradiation, there was no reduction of $CHCl_2I$ and CHI_3 concentration in the presence of 6 mg L^{-1} H_2O_2 over 60 min in a control experiment (Figure 5.1). Apparently, $CHCl_2I$ and CHI_3 can be removed effectively by UV/H_2O_2, due to a combined effect of $HO^{\cdot}$-assisted indirect photolysis and direct photolysis, rather than direct oxidation by H_2O_2.

The indirect photolysis can be affected by many factors including pH, H_2O_2 dose, matrix species in water (Crittenden et al., 2012) etc. Therefore, these factors were further investigated in order to holistically evaluate the efficiency of I-THMs photodegradation under different conditions.

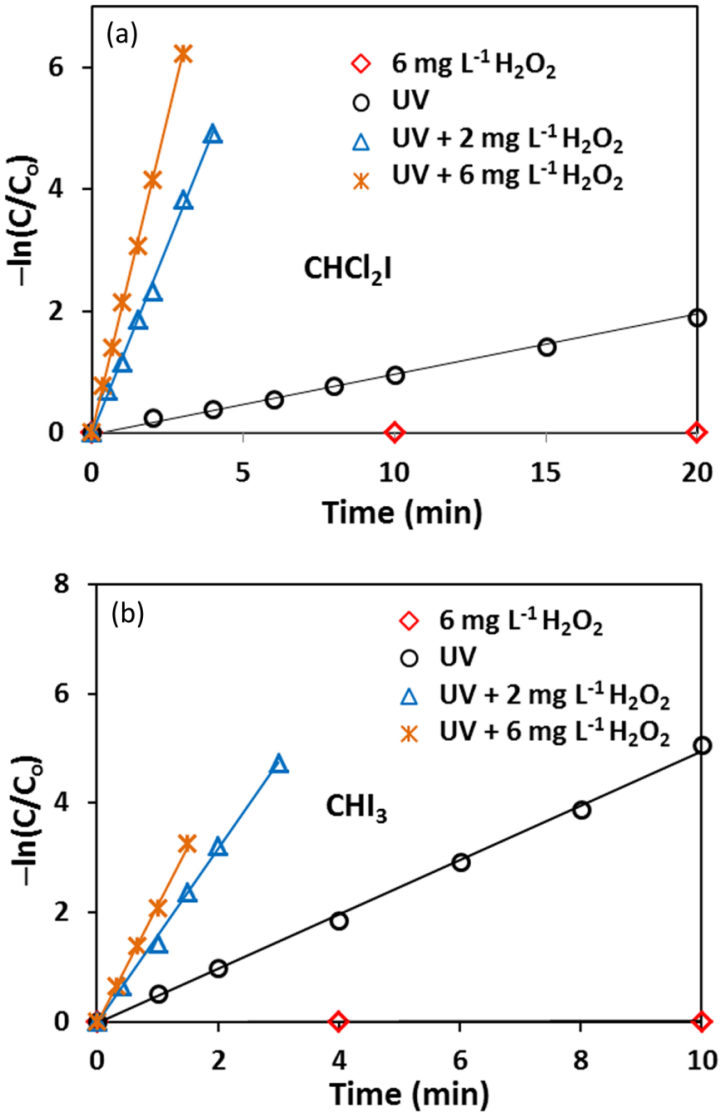

Figure 5.1 Linear plot for degradation of $CHCl_2I$ (a) and CHI_3 (b) under different treatment conditions (I-THMs: 0.5 µmol L^{-1}).

5.2.1 Effect of pH

The effect of pH on $CHCl_2I$ and CHI_3 photodegradation was studied by conducting experiment at pH 3, 7 and 11. The degradation rate at pH 3 was slightly higher than that at pH 7, possibly due to a higher redox potential of $HO^{\cdot}/H_2O$ at pH 3. For example, according to Equation 5.1 (derived from Nernst equation), the redox potential of $HO^{\cdot}/H_2O$ at pH 3, 7, and 11 are 2.62, 2.39, and 2.15 V, respectively (for $E^{o}_{HO^{\cdot}/H_2O} = 2.80\,V$).

$$E_{HO^{\cdot}} = E^{o}_{HO^{\cdot}/H_2O} - 0.059pH \quad (5.1)$$

On the other hand, the degradation rate at pH 11 decreased dramatically, as compared to that at pH 7 (Figure 5.2). The major cause for this reduction should be $HO^{\cdot}$ scavenging by hydroperoxide anion (HO_2^-). As pK_a is 11.8 for H_2O_2/HO_2^-, an alkaline condition is favorable for the generation of HO_2^- in the UV/H_2O_2 process. Although HO_2^- can promote the formation of $HO^{\cdot}$, it can also act as a strong scavenger of $HO^{\cdot}$ and react with $HO^{\cdot}$ approximately 280 times faster than H_2O_2 (Table 5.1, reactions 2 and 3). Furthermore, the redox potential of $HO^{\cdot}/H_2O$ decreases under an alkaline condition. Considering that most treatment processes are operated at circumneutral condition, the reaction solution would be adjusted to pH 7 in the following experiments.

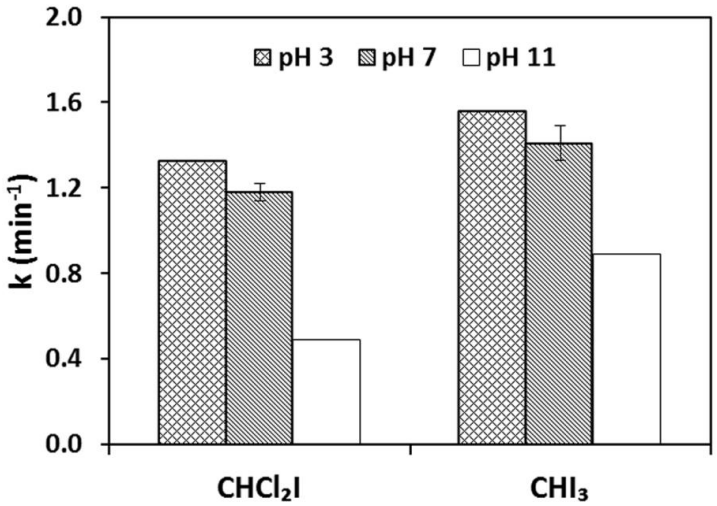

Figure 5.2 Effect of pH on the photodegradation kinetics of $CHCl_2I$ and CHI_3 in DI water (I-THMs: 0.5 μmol L^{-1}; H_2O_2: 2.0 mg L^{-1}). Error bars denote standard deviations obtained from at least duplicate datasets.

Table 5.1 Relevant chemical reactions in the UV/H_2O_2 process

Item	Reactions	Rate constant (M^{-1} s^{-1})	Reference
1	$HO^{\cdot} + NOM \rightarrow product$	2.5 x 10^4 L mg^{-1} s^{-1} as organic carbon	(Larson and Zepp, 1988)
2	$HO^{\cdot} + H_2O_2 \rightarrow H_2O + HO_2^{\cdot}$	2.7 x 10^7	(Buxton et al., 1988)
3	$HO^{\cdot} + HO_2^{-} \rightarrow HO^{-} + HO_2^{\cdot}$	7.5 x 10^9	(Buxton et al., 1988)
4	$HO^{\cdot} + HO_2^{\cdot} \rightarrow H_2O + O_2$	6.6 x 10^9	(Sehested et al., 1968)
5	$HO^{\cdot} + CO_3^{2-} \rightarrow CO_3^{\cdot-} + HO^{-}$	3.9 x 10^8	(Buxton et al., 1988)
6	$HO^{\cdot} + HCO_3^{-} \rightarrow CO_3^{\cdot-} + H_2O$	8.5 x 10^6	(Buxton et al., 1988)
7	$HO^{\cdot} + CHCl_2I \rightarrow product$	8.0 x 10^9	This study
8	$HO^{\cdot} + CHI_3 \rightarrow product$	8.9 x 10^9	This study

5.2.2 Effect of initial dose of H_2O_2

The degradation rates of I-THMs including $CHCl_2I$ and CHI_3 were also affected by the concentration of H_2O_2 in the UV/H_2O_2 process. At a low concentration of H_2O_2, the degradation rate of $CHCl_2I$ was limited (Figure 5.3), as only a small amount of $HO^{\cdot}$ was generated. Nevertheless, the degradation rate of CHI_3 was still relatively high even at a low concentration of H_2O_2 due to its effective direct photolysis. With the increase of H_2O_2 dose, the amount of $HO^{\cdot}$ increased correspondingly, which led to the enhanced degradation rates of $CHCl_2I$ and CHI_3. However, the degradation rates decreased slightly in the presence of excess of H_2O_2 which could act as a scavenger of $HO^{\cdot}$ and produce the less reactive radical, $HO_2^{\cdot}$ (Table 5.1, reaction 2). Additionally, H_2O_2 at a high concentration can act as a competitive UV absorber (screening effect) which reduces the direct photolysis rates of the organic pollutants (Wu et al., 2007a).

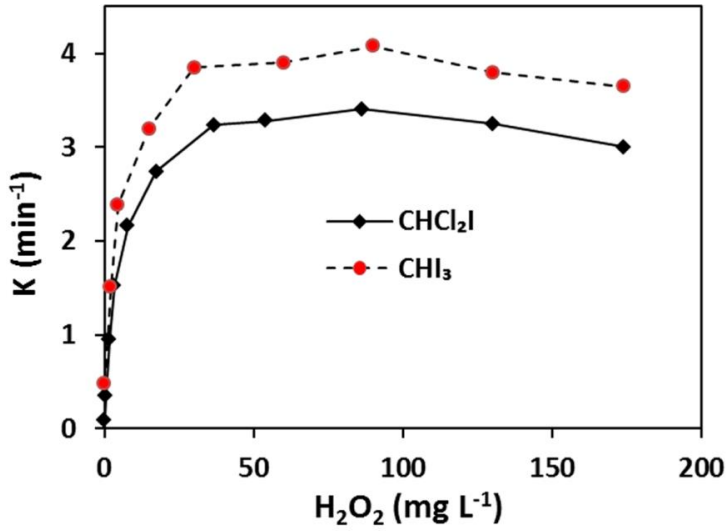

Figure 5.3 Effect of initial dose of H_2O_2 on the photodegradation kinetics of $CHCl_2I$ and CHI_3 in DI water (I-THMs: 0.5 µmol L^{-1}; pH 7).

5.2.3 Effect of matrix species

Further investigation was conducted to evaluate the impact of matrix species on the photodegradation rates in the UV/H_2O_2 process. HCO_3^-, SO_4^{2-}, Cl^-, NO_3^-, and HA were selected as matrix species as they are commonly found in natural water systems as well as wastewater.

As pK_{a1} = 6.3 and pK_{a2} = 10.3 for $H_2CO_3 / HCO_3^- / CO_3^{2-}$ system (Snoeyink and Jenkins, 1980), the predominant species at pH 7 is HCO_3^-. $HO^{\bullet}$ can react with HCO_3^- to produce less reactive species, $CO_3^{\bullet-}$ (Table 5.1, reaction 6). Thus, the presence of HCO_3^- had a negative effect on the photodegradation rates of $CHCl_2I$ due to its strong scavenging effect (Figure 5.4(a)).

The redox potential of $HO^{\bullet}/H_2O$ at pH 7 is almost similar to that of $NO_3^{\bullet} / NO_3^-$, while it is a bit lower than that of $SO_4^{\bullet-} / SO_4^{2-}$ (Table 5.2). Thus, the scavenging effect of $HO^{\bullet}$ by both SO_4^{2-} and NO_3^- can be ignored. In the presence of SO_4^{2-} from 1 to 4 mmol L^{-1}, the degradation rates of $CHCl_2I$ remained constant (Figure 5.4(a)). However, in the presence of NO_3^-, a slight increment of the degradation rate was

observed. One possible reason for this improvement is that additional $HO^{\bullet}$ can be produced at a low quantum yield via direct photolysis of NO_3^- (Equation 5.2) (Keen et al., 2012).

$$NO_3^- + hv \rightarrow NO_2^{\bullet} + O^{\bullet -} \quad (5.2a)$$

$$O^{\bullet -} + H_2O \rightarrow HO^{\bullet} + OH^- \quad (5.2b)$$

Table 5.2 Relevant redox potentials of some radicals

Couple	E/V	Remark	Reference
$HO^{\bullet} / H_2O$	2.62 2.39 2.15	pH 3 pH 7 pH 11	Nernst equation
$CO_3^{\bullet -} / CO_3^{2-}$	1.50	−	(Oppenlander, 2003)
$CO_3^{\bullet -} / HCO_3^-$	1.78	pH 7	(Medinas et al., 2007)
$SO_4^{\bullet -} / SO_4^{2-}$	2.6-3.1	−	(Eberson, 1982)
$Cl^{\bullet} / Cl^-$	2.41	−	(Huie et al., 1991)
$NO_3^{\bullet} / NO_3^-$	2.30-2.60	−	(Oppenlander, 2003)

The redox potential of $Cl^{\bullet}/Cl^-$ is also similar to that of $HO^{\bullet}/H_2O$ at pH 7 (Table 5.2). It suggests that the scavenging effect of Cl^- is limited. However, some previous studies reported that Cl^- could react with $HO^{\bullet}$ to produce $ClHO^{\bullet -}$, which could protonate to produce $HClHO^{\bullet}$ under the acidic condition (Liao et al., 2001; Deng et al., 2013; Yang et al., 2014). Subsequently, $HClHO^{\bullet}$ would be further converted to less reactive chlorine species such as $Cl^{\bullet}$. In contrast, there was a backward reaction ($ClHO^{\bullet -} \rightarrow HO^{\bullet} + Cl^-$) at pH > 7.2 (Liao et al., 2001; Deng et al., 2013; Yang et al., 2014). It indicates that the scavenging effectiveness of Cl^- is offset by the release of $HO^{\bullet}$ from the transient intermediate ($ClHO^{\bullet -}$) under the basic condition (Deng et al., 2013). The above phenomenon explains the observation that the photodegradation rates of $CHCl_2I$ at pH 7 were not affected in the presence of Cl^-. To check the reactivity of $Cl^{\bullet}$ with I-THMs, photodegradation of $CHCl_2I$ by UV/H_2O_2 in the presence of 4 mmol L^{-1} Cl^- at pH 3 was conducted. According to the above explanation, $Cl^{\bullet}$ could be generated under an acidic condition. The

degradation rate of $CHCl_2I$ decreased obviously in the presence of 4 mmol L^{-1} Cl^- at pH 3, as compared to that obtained without Cl^- at pH 3 (Figure. 5.4(b)). It suggests that $Cl^{\cdot}$ reacts slowly with $CHCl_2I$, as compared to $HO^{\cdot}$. Based on the above results, both H_2SO_4 and NaOH solutions (0.1 mol L^{-1}) were selected to adjust the pH of reaction solution in this study.

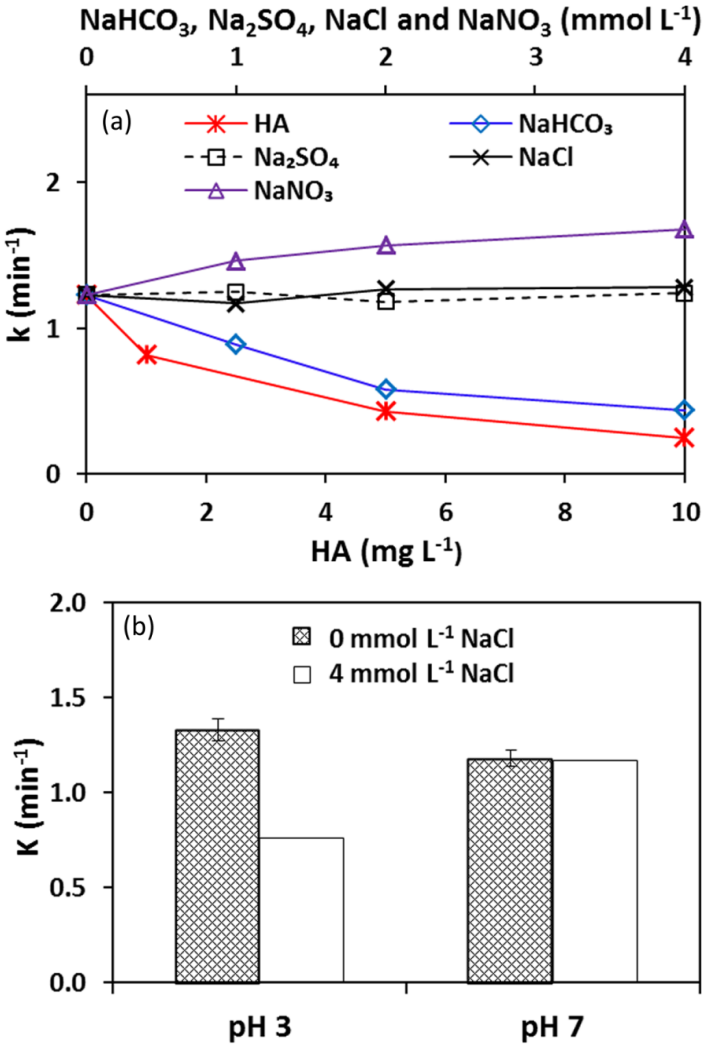

Figure 5.4 (a). Effect of matrix species including $NaHCO_3$, Na_2SO_4, NaCl, $NaNO_3$, and HA on the photodegradation kinetics in DI water at pH 7; (b). Effect of Cl^- on the photodegradation kinetics in DI water at pH 3 and 7 ($CHCl_2I$: 0.5 µmol L^{-1}; H_2O_2: 2 mg L^{-1}).

HA had a negative effect on the photodegradation rates. On the one hand, the filtering of UV light by HA reduced the fraction of UV light absorbed by $CHCl_2I$ and H_2O_2, which led to the reduced rate of direct photolysis. On the other hand, HA

could act as a strong scavenger of $HO^{\cdot}$ (Crittenden et al., 1999). These two effects resulted in a significant inhibition of the photodegradation of $CHCl_2I$ in the presence of HA (Figure 5.4(a)).

5.2.4 Mathematical modeling of UV/H_2O_2 process

The parameters such as quantum yield, molar absorption coefficient, second-order rate constant, UV absorbance of the reaction solution, average photonic intensity per volume (I_o) and the optical path length (b) of the photoreactor etc. were incorporated into a mathematical model to predict the impact of the matrix species on $CHCl_2I$ and CHI_3 photodegradation in different types of water.

In the UV/H_2O_2 process, the overall degradation involves both direct photolysis and $HO^{\cdot}$-assisted indirect photolysis (Rosenfeldt and Linden, 2004; Pereira et al., 2007).

$$-\frac{dC}{dt} = (k_d + k_i)C \tag{5.3}$$

where k_d is the pseudo-first-order rate constant of direct photolysis in s^{-1}; k_i is the pseudo-first-order rate constant of $HO^{\cdot}$-assisted indirect photolysis in s^{-1}.

With the obtained Φ and ε of target compound as well as I_o and b of the photoreactor, direct photolysis rate of target compound in a water matrix comprising various UV absorbers can be described by Equations 5.4 and 5.5 (Crittenden et al., 2012).

$$-\frac{dC}{dt} = \Phi I_o f(1 - e^{-2.303\varepsilon bC}) = \Phi I_o \frac{\varepsilon b(1 - e^{-2.303A})}{A} C \tag{5.4}$$

$$k_d = \Phi I_o \frac{\varepsilon b(1 - e^{-2.303A})}{A} \tag{5.5}$$

$$k_d = 2.303\Phi I_o \varepsilon b \tag{5.6}$$

where f is the fraction of light absorbed by target compound; and A is the total UV absorbance of the reaction solution ($A = \Sigma_{i=1}^{n} \varepsilon_{\lambda,i} b C_i$) . Equation 5.5 can be

simplified to Equation 5.6 when UV absorbance of the reaction solution is low (i.e., $2.303\varepsilon bC < 0.02$) (Beltrán et al., 1995).

The indirect photolysis rate (k_i) can be expressed as a function of the second-order rate constant of target compound reacting with $HO^{\cdot}$ and the steady-state concentration of $HO^{\cdot}$ (Rosenfeldt and Linden, 2004; Pereira et al., 2007).

$$k_i = k_{HO^{\cdot},I-THM} C_{HO^{\cdot}} \quad (5.7)$$

The experiments of competition kinetics were conducted to determine the second-order rate constant of $HO^{\cdot}$ reacting with $CHCl_2I$ and CHI_3. p-xylene ($k_{HO\cdot}$ = 7 x 10^9 M^{-1} s^{-1} at pH 7) was chosen as the reference compound because it essentially does not undergo direct photolysis (Buxton et al., 1988), and it is easy to be analyzed together with target I-THMs by P&T-GC/MS. As described above, $CHCl_2I$ and CHI_3 underwent considerable direct photolysis. Hence, such effect should be taken into consideration in determining the second-order rate constant in the UV/H_2O_2 process. The degradation rates of I-THMs and p-xylene could be expressed by Equations 5.8 and 5.9, respectively.

$$k_{obs,I-THM} = k_{HO^{\cdot},I-THM} C_{HO^{\cdot}} + k_d \quad (5.8)$$

$$k_{obs,p-xylene} = k_{HO^{\cdot},p-xylene} C_{HO^{\cdot}} \quad (5.9)$$

where $k_{obs,\ I\text{-}THM}$ and $k_{obs,\ p\text{-}xylene}$ are the observed pseudo-first-order rate constants of I-THM and p-xylene in the UV/H_2O_2 process in s^{-1}, respectively; $C_{HO\cdot}$ is the steady-state concentration of $HO^{\cdot}$ in mol L^{-1}; and k_d is the direct photolysis rate constant of I-THMs in s^{-1}. Substituting Equation 5.9 into 5.8, $k_{HO\cdot,\ I\text{-}THM}$ can be calculated as follows:

$$k_{HO^{\cdot},I-THM} = \frac{k_{obs,I-THM} - k_d}{k_{obs,p-xylene}} k_{HO^{\cdot},p-xylene} \quad (5.10)$$

The derived second-order rate constants of $HO^{\cdot}$ reacting $CHCl_2I$ and CHI_3 are 8.0 x 10^9 and 8.9 x 10^9 M^{-1} s^{-1}, respectively (Table 5.1). Considering that the typical

second-order rate constants of the organic compounds reacting with $HO^{\cdot}$ vary from 10^6 to 10^{10} M^{-1} s^{-1} (Schwarzenbach et al., 1993), I-THMs appear to be the fast-reacting compounds with $HO^{\cdot}$.

The steady-state concentration of $HO^{\cdot}$ can be estimated by a simplified pseudo-steady-state method whereby the concentration of $HO^{\cdot}$ is assumed constant (at the respective initial concentration) over the reaction period. It can be calculated as the ratio of the formation of $HO^{\cdot}$ to the consumption of $HO^{\cdot}$ according to Equation 5.11 (Rosenfeldt and Linden, 2004).

$$C_{HO\cdot} = \frac{\Phi_{HO\cdot} I_o f_{H_2O_2} (1 - e^{-2.303A})}{\sum k_{HO\cdot,S} C_S} \quad (5.11)$$

where $\Phi_{HO\cdot}$ is the quantum yield of the production of $HO^{\cdot}$ by the photolysis of H_2O_2 (assumed to be 1.0 mol E^{-1}) (Rosenfeldt and Linden, 2007); $k_{HO\cdot,S}$ is the second-order rate constant of scavenger reacting with $HO^{\cdot}$ in M^{-1} s^{-1} (Table 5.1); C_S is the concentration of scavenger in mol L^{-1} and all of the components are assumed at their constant concentrations over the reaction period; other terms are as defined previously.

The predicted kinetics is compared with the experimental results for different types of water in the present study. Firstly, the comparison was conducted using laboratory synthesized water (LSW). As the exact composition in LSW is known, this allows proper estimation of the steady-state concentration of $HO^{\cdot}$ as a function of water quality. In this study, HA (DOC, 1 mg L^{-1}) and HCO_3^- (2 mmol L^{-1}) were spiked into DI water to prepare LSW as these two species had a significant effect on the photodegradation kinetics of $CHCl_2I$ in the UV/H_2O_2 process. The calculated total scavenging factor ($\Sigma k_{HO\cdot,S} C_S$) and the fraction of UV light absorbed by H_2O_2 are listed in Table 5.3. With the obtained parameters such as Φ, ε, I_0, b, a, $f_{H_2O_2}$, and $\Sigma k_{HO\cdot,S} C_S$, direct photolysis rate constant (k_d) and $HO^{\cdot}$-assisted indirect photolysis rate constant (k_i) could be determined according to Equations 5.5 and 5.7, respectively. As shown in Table 5.3, for $CHCl_2I$, indirect photolysis played a

dominant role in its degradation and its rate increased significantly with increasing H_2O_2 concentration. For CHI_3, both direct and indirect photolysis were important in its degradation at a low concentration of H_2O_2 (i.e., 2 mg L^{-1}), while its indirect photolysis becomes increasingly dominant with increasing H_2O_2 concentration. Because of the relatively high UV absorption capability of I-THMs and weak C-I bond, it is essential to delineate the roles of indirect photolysis and direct photolysis in the UV based-AOP. Through the kinetic model, the respective contributions from the direct photolysis and $HO^{\cdot}$-assisted indirect photolysis in the degradation of I-THMs under different reaction conditions were determined. Therefore, the model study could help to gain insights into the UV based-AOP and delineate the respective reaction kinetics for $CHCl_2I$ & CHI_3.

In general, there is a good agreement between the kinetic model predicted first-order rate constant (k_p) and experimentally measured first-order rate constants (k_m) for both $CHCl_2I$ and CHI_3 (Figure 5.5(a)). These results again indicate that NOM, alkalinity, and H_2O_2 are the major scavengers of $HO^{\cdot}$.

NOM could be degraded as the UV254 doses increases, the composition of DOC will change correspondingly. However, the steady-state concentration of $HO^{\cdot}$ is estimated based on the initial concentration of all components and is assumed to remain virtually constant over the reaction period. In fact, the concentration of $HO^{\cdot}$ increases as the contribution of the dominant scavenger such as NOM is reduced. This is one possible reason why the k_p values are slightly smaller than the k_m values. Additionally, measurement uncertainty such as the second-order rate constants for I-THMs and pseudo-first-order rate constants could also contribute to the difference between the predicted and the experimentally measured values. Even with these uncertainties, the differences between the values of k_p and k_m are less than 20%.

Table 5.3 The parameters used for establishing kinetic model as well as the predicted (k_p) and experimentally measured rate constants (k_m)

Water matrix	Species	H_2O_2 (mg L^{-1})	pH	TOC (mg L^{-1})	Total alkalinity (as $CaCO_3$, mg L^{-1})	*a* (254 nm)[b] (cm^{-1})	$f_{H_2O_2}$ x 100	$\Sigma k_{HO^{\cdot},S} C_S$ x10^{-4} (s^{-1})	$k_p = k_i + k_d$ (min^{-1})	k_m (min^{-1})
LSW[a]	$CHCl_2I$	2	7	1	200	0.0556	3.59	4.70	0.42=0.34+0.081	0.46
LSW	$CHCl_2I$	6	7	1	200	0.0610	8.19	5.07	0.83=0.75+0.080	0.92
LSW	$CHCl_2I$	15	7	1	200	0.0697	16.4	5.79	1.56=1.48+0.078	1.84
LSW	CHI_3	2	7	1	200	0.0543	3.68	4.80	0.79=0.36+0.43	0.82
LSW	CHI_3	6	7	1	200	0.0588	8.50	5.12	1.27=0.84+0.43	1.42
LSW	CHI_3	15	7	1	200	0.0661	17.3	5.84	2.06=1.64+0.42	2.28
SW[c]	$CHCl_2I$	2	7	3.9	8.70	0.0924	2.16	10.3	0.21=0.14+0.074	0.24
SW	$CHCl_2I$	6	7	3.9	8.70	0.0955	5.24	10.6	0.40=0.33+0.073	0.50
SW	$CHCl_2I$	15	7	3.9	8.70	0.1013	13.3	11.3	0.77=0.70+0.072	0.98
SW	CHI_3	2	7	3.9	8.70	0.0964	2.10	10.4	0.54=0.15+0.39	0.65
SW	CHI_3	6	7	3.9	8.70	0.0989	5.10	10.7	0.75=0.36+0.39	0.85
SW	CHI_3	15	7	3.9	8.70	0.1047	10.9	11.4	1.14=0.76+0.38	1.35

a. LSW: laboratory synthesized water;
b. *a* = absorptivity (εC, cm^{-1});
c. SW: surface water (Cl^-: 24.5 mg L^{-1}, SO_4^{2-}: 6.78 mg L^{-1}, NO_3^- as N: 0.68 mg L^{-1}

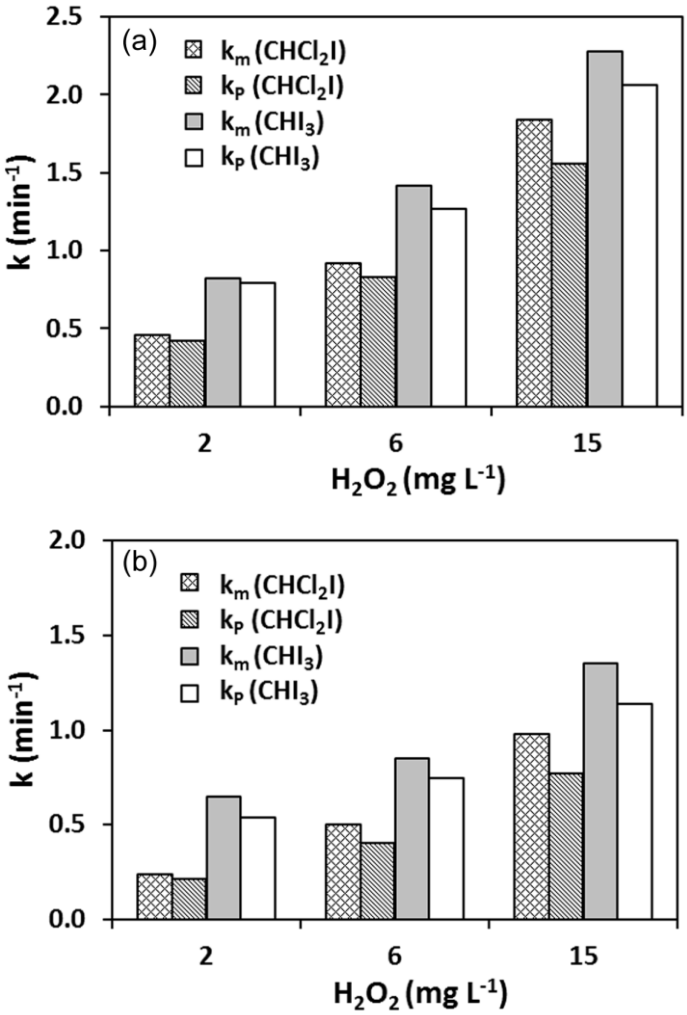

Figure 5.5 Comparison of experimentally measured (k_m) with the predicted pseudo-first-order rate constants (k_p) for CH_2I and CHI_3 in laboratory synthesized water (a) and surface water (b) (I-THMs: 0.5 µmol L^{-1}; pH 7)

To further examine how accurate this established kinetic model is in predicting the destruction of I-THMs in a natural water system, photodegradation of $CHCl_2I$ and CHI_3 by UV/H_2O_2 in surface water (SW) that was used as the source water in a waterworks in Singapore was conducted. Samples were filtered through 0.45 µm filter to remove particles, and water quality parameters of the filtrate such as pH, TOC, alkalinity, and UV254 absorbance are shown in Table 5.3. The degradation rates of both $CHCl_2I$ and CHI_3 in SW decreased significantly due to a stronger combined negative effect of the aqueous matrix species as compared to that of LSW. A good correlation between k_p and k_m is also obtained for the case of reaction in SW (Figure 5.5(b)). Generally, the kinetic model based on the pseudo-steady-state

concentration of $HO^{\cdot}$ is applicable to predict the destruction of I-THMs by the UV/H_2O_2 process in different types of water.

5.2.5 Photodegradation end-products identification

Both $CHCl_2I$ and TOC decreased concomitantly as the UV dose increased (Figure 5.6). $CHCl_2I$ was completely degraded by UV/H_2O_2 within 15 min with a corresponding TOC removal of 53%. Meanwhile, HCO_2H was formed concomitantly with TOC reduction and accounted for 37% of initial TOC at 15-min reaction. There were still some unidentified organic species in the reaction solution, which accounted for ~10 % of initial TOC. Cl^- and I^- were also identified as the end-products and their amounts continued to increase with the reaction time. There is a good mass balance (i.e., 95% recovery) between the produced halides and the introduced halogens in $CHCl_2I$. No ClO_3^- was observed over the reaction period, while trace level of IO_3^- was detected and its amount was less than 2% of the total liberated iodine species at the end of the reaction. Additionally, both formaldehyde and oxalic acid were not detectable during the photodegradation process.

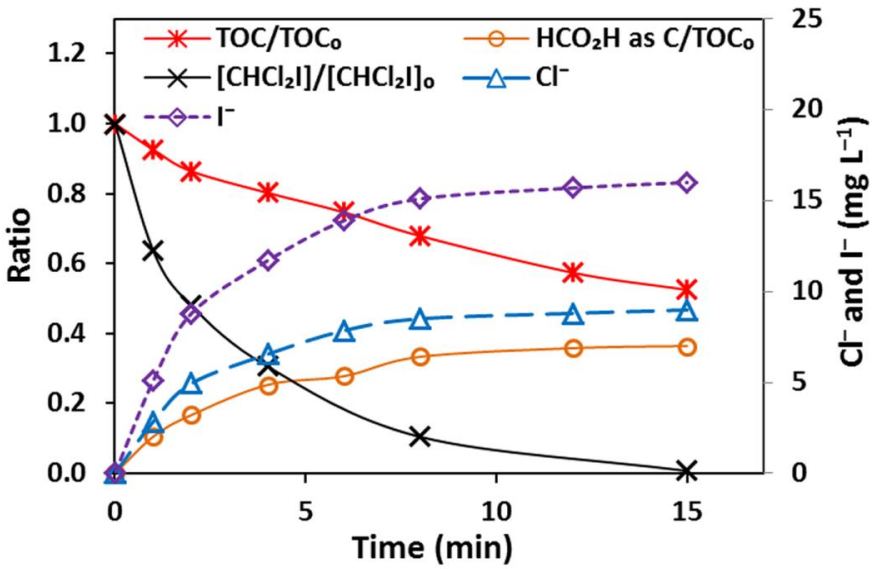

Figure 5.6 Time course of $CHCl_2I$ reduction, TOC reduction, halide formation, and HCO_2H formation during photodegradation of $CHCl_2I$ by the UV/H_2O_2 treatment. ($CHCl_2I$: 28 mg L^{-1}; H_2O_2: 45 mg L^{-1})

5.2.6 An economic analysis using EE/O concept

The electrical energy per order (EE/O) concept is applied to evaluate the efficiency of the UV/H_2O_2 process and to determine the optimal H_2O_2 dose at a given condition. The EE/O ($kWhm^{-3}order^{-1}$) is defined as the electrical energy (kWh) required to degrade the contaminants by one-order magnitude in m^3 of contaminated water (Bolton and Cater, 1994). The figures-of-merit provide the requisite reference for scale-up, economic analysis, and energy comparison with other treatment technologies such as ozonation etc. The electrical energy of UV lamp (EE/O_{UV}) and H_2O_2 consumption (H_2O_2/O) per one-order magnitude of I-THM removal in 1 m^3 water can be calculated according to Equations 5.12 and 5.13, respectively. As the energy consumption for production of H_2O_2 is 10.81 x 10^{-6} $kWhmg^{-1}$ (Rosenfeldt et al., 2006), H_2O_2/O can be expressed in terms of equivalent electric energy consumption ($EE/O_{H_2O_2}$), which has the same energy unit ($kWhm^{-3}order^{-1}$) as EE/O_{UV} (Equation 5.14). Thus, the total equivalent electrical energy consumption (EE/O_{total}) for the UV/H_2O_2 process can be calculated using Equation 5.15.

$$EE/O_{UV} = \frac{Pt1000}{V\log(\frac{C_i}{C_f})} = \frac{38.4P}{Vk}(kWhm^{-3}order^{-1}) \quad (5.12)$$

$$H_2O_2/O = \frac{C_{H_2O_2}}{\log(\frac{C_i}{C_f})}(mgL^{-1}order^{-1}) \quad (5.13)$$

$$EE/O_{H_2O_2} = 10.81 \times 10^{-3} \times H_2O_2/O\,(kWhm^{-3}order^{-1}) \quad (5.14)$$

$$EE/O_{total} = EE/O_{UV} + EE/O_{H_2O_2}(kWhm^{-3}order^{-1}) \quad (5.15)$$

where P is lamp power output in kW; t is the irradiation time in h; V is the reactor volume in L; k is the predicted first-order rate constant (k_p) in min^{-1}; C_i is the initial concentration of the target compound in mg L^{-1}; C_f is the final concentration of the target compound in mg L^{-1}; $C_{H_2O_2}$ is the concentration of H_2O_2 in the reaction solution in mg L^{-1}.

In this study, EE/O_{UV}, $EE/O_{H_2O_2}$, and EE/O_{total} are evaluated based on 90% of target $CHCl_2I$ removal. As shown in the Figure 5.7(a), the required UV lamp energy (EE/O_{UV}) decreased by increasing H_2O_2 dose. At a low dose of H_2O_2 (i.e., < 10 mg L^{-1}), EE/O_{UV} is the major contributor to EE/O_{total}, as indicated by $(EE/O_{H_2O_2})/(EE/O_{UV}) < 1$ (Figure 5.7(b)). In contrast, at a high dose of H_2O_2, the required UV energy is very limited and $EE/O_{H_2O_2}$ is the main component of EE/O_{total}. At a specific percentage of $CHCl_2I$ removal, the lowest EE/O_{total} in different water types of water follows the order of DI < LSW < SW (Figure 5.7(b)), and correspond to 0.2, 0.31, and 0.45 $kWhm^{-3}order^{-1}$, respectively. They are 8-15 times lower than the corresponding EE/O_{total} by UV direct photolysis (Table 5.4). The optimal H_2O_2 doses in DI, LSW, and SW for their lowest EE/O_{total} are estimated at 5, 12, and 16 mg L^{-1}, respectively, which correspond to the H_2O_2: $CHCl_2I$ molar ratio of 294, 705, and 941. The ratios of $EE/O_{H_2O_2}$ versus EE/O_{UV} in DI, LSW, and SW at their respective optimal H_2O_2 doses are 0.38, 0.70, and 0.55, respectively. These results further demonstrate the effect of different types of water on the process efficiency. It is worth mentioning that energy consumption is mainly due to consumption of H_2O_2 and there is no significant difference in energy consumption for different water matrices at a high dose of H_2O_2 (Figure 5.7(b)). For example, at 120 mg L^{-1} of H_2O_2, the $EE/O_{H_2O_2}$: EE/O_{UV} ratios for DI, LSW, and SW are 19, 17, and 15, respectively, while EE/O_{total} in these 3 types of water are almost the same which is ~1.3 $kWhm^{-3}order^{-1}$. The energy efficiency decrease obviously at a high dose of H_2O_2 due to scavenging of $HO^{\cdot}$ by H_2O_2. Subsequently, additional treatment such as GAC is required to remove the residual of H_2O_2, which leads to further increase of the operating cost. Thus, it is very important to optimize the H_2O_2 dose to improve the energy efficiency of the whole process.

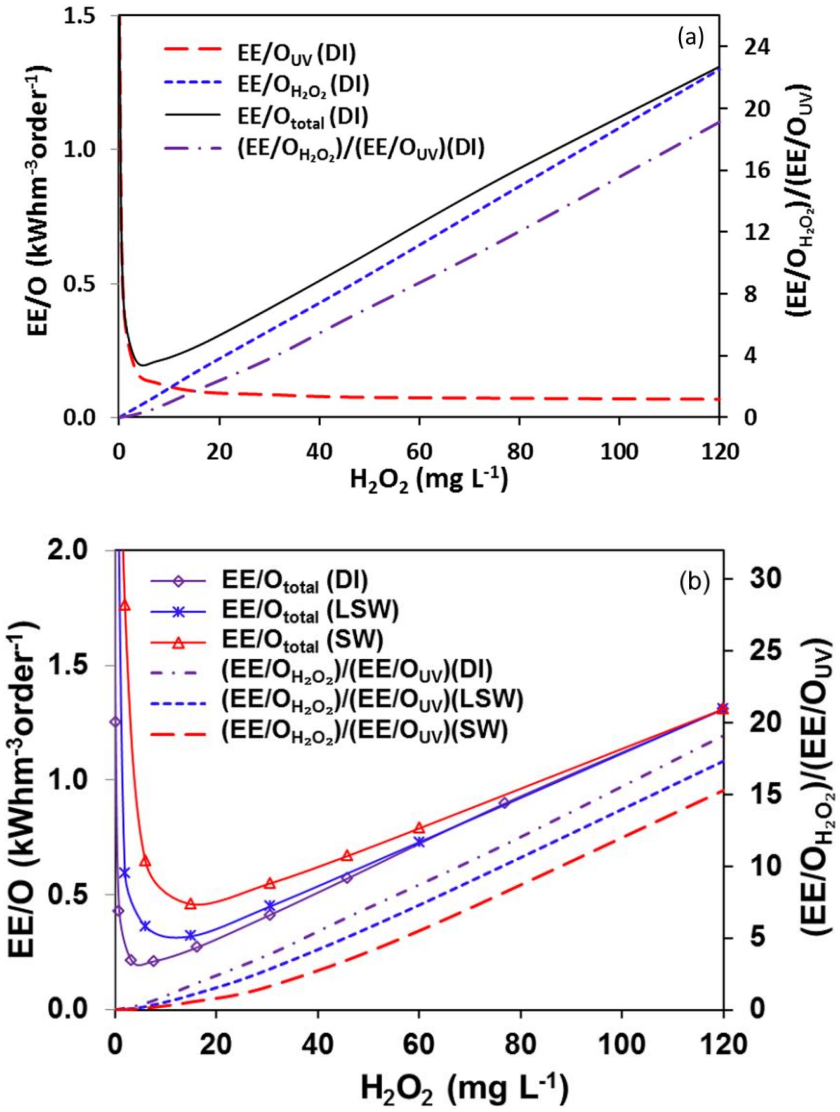

Figure 5.7 (a). Plot of EE/O_{UV}, $EE/O_{H_2O_2}$, EE/O_{total}, and $(EE/O_{H_2O_2})/(EE/O_{UV})$ versus H_2O_2 dose in DI water; (b). Plot of EE/O_{total} and $(EE/O_{H_2O_2})/(EE/O_{UV})$ versus H_2O_2 dose in DI water, LSW, and SW ($CHCl_2I$: 0.5 µmol L^{-1}; pH 7).

Table 5.4 Comparison of energy efficiency of UV and UV/H_2O_2 removal of $CHCl_2I$ in different types of water

Water matrix	UV Photolysis	UV/H_2O_2			
	EE/O_{total} [b]	Lowest EE/O_{total}	Optimal H_2O_2 dose[c]	Molar ratio (H_2O_2 : $CHCl_2I$)[a]	$(EE/O_{H_2O_2})$ /(EE/O_{UV})
DI	2.95	0.20	5	294	0.38
LSW	3.56	0.31	12	705	0.70
SW	3.92	0.45	16	941	0.55

a. $CHCl_2I$: 0.5 µmol L^{-1}; b. unit: $kWhm^{-3}order^{-1}$; c. unit: mg L^{-1}.

5.3 Conclusion

Both $CHCl_2I$ and CHI_3 underwent a fast photodegradation process in the UV/H_2O_2 process, due to synergistic effect of $HO^{\cdot}$-assisted indirect photolysis and direct photolysis. A fraction of $CHCl_2I$ could be completely mineralized within 15 min and the remaining fraction was mainly converted to HCO_2H. Cl^- and I^- were identified as the predominant end-products. Some common matrix species including HA, HCO_3^-, NO_3^-, SO_4^{2-} and Cl^- were added to study the interferences, which were negative in the case of HA and HCO_3^-, and positive for NO_3^-. Both SO_4^{2-} and Cl^- had no significant effect on the photodegradation rate of $CHCl_2I$ and CHI_3 in the UV/H_2O_2 process. A steady-state kinetic model was established to successfully predict the destruction of I-THMs by the UV/H_2O_2 process in different types of water. The optimal H_2O_2 doses in DI, LSW, and SW are estimated at 5, 12, and 16 mg L^{-1}, respectively, which correspond to the lowest EE/O_{total} of 0.2, 0.31, and 0.45 $kWhm^{-3}order^{-1}$. The $EE/O_{H_2O_2}$: EE/O_{UV} ratios for DI, LSW, and SW at their respective optimal H_2O_2 doses are 0.38, 0.70, and 0.55, respectively. These results indicate the high efficiency of the UV/H_2O_2 process for degrading I-THMs.

CHAPTER 6 Comparative evaluation of iodoacids removal by UV/H_2O_2 and UV/persulfate processes

In the final part of this study, degradation of iodoacids by UV, UV/H_2O_2, and UV/PS (persulfate, $S_2O_8^{2-}$) was extensively investigated. Firstly, UV direct photolysis of 4 iodoacids was examined. On this basis, a quantitative structure-activity relationship (QSAR) model was established and applied to predict the direct photolysis rates of 6 other commercially unavailable iodoacids. It is well known that UV/H_2O_2 process, one of the most common AOPs, has been extensively studied and applied to remove recalcitrant organic pollutants in water and advanced water treatment processes. Additionally, UV/PS process has been demonstrated to remove some carboxylic acids effectively through decarboxylation by $SO_4^{\bullet-}$. Thus, UV/H_2O_2 and UV/PS AOPs were applied to remove ICH_2CO_2H (IAA), the most photo-recalcitrant and toxic species among all iodoacids. The degradation of IAA by the UV/PS and UV/H_2O_2 processes were compared in terms of the effect of pH, oxidant dose, and matrix species such as HA and HCO_3^- on its photodegradation rate as well as the end-products and operating cost. Different types of water including DI water, treated water, surface water and secondary effluent were used as water matrix to further evaluate the effectiveness of these AOPs for IAA removal. The respective contributions of UV, $HO^{\bullet}$, and $SO_4^{\bullet-}$ for IAA removal in the UV/PS process were also determined.

6.1 Experimental details

UV direct photolysis of 4 iodoacids (each at initial concentration of 300 μg L^{-1}) in the multi-species system was conducted in DI water. UV/PS and UV/H_2O_2 treatment of IAA (1.5 μmol L^{-1}) were conducted in two separate series of experiments. The UV-based AOP experiments were conducted using different types of water with addition of oxidant and pH adjustment before exposure to UV irradiation. The water matrices used in this study included DI water, treated water (TW), surface water (SW), and secondary effluent (SE). Since most water and advanced water treatment processes in practice are operated at circumneutral

condition, the reaction solution was adjusted to pH 7 by phosphate buffer solution (5 mmol L^{-1}) in the present study unless otherwise stated. For other pH values (3, 5, 9, and 11), the pH adjustment was carried out using 0.1 mol L^{-1} H_2SO_4 or NaOH solution.

6.2 Results and discussion

6.2.1 UV direct photolysis

Direct photolysis of 4 iodoacids followed the first-order kinetics (Figure 6.1). The overall direct photolysis rate could be described by Equations 6.1 and 6.2, when the UV absorbance of the reaction solution is very low (i.e., $2.303\varepsilon bC < 0.02$) (Beltrán et al., 1995).

$$-\frac{dC}{dt} = 2.303\Phi I_o \varepsilon bC = kC \tag{6.1}$$

$$k = 2.303\Phi I_o \varepsilon b \tag{6.2}$$

where all of the terms are as defined previously.

The direct photolysis rates of 4 iodoacids follow the order of IAA < $IClCHCO_2H$ < $IBrCHCO_2H$ < I_2CHCO_2H. The degradation rate constant of the most photo-recalcitrant iodoacid, IAA is 0.057 min^{-1}, while the degradation rate constant of the most photo-labile I_2CHCO_2H is 0.71 min^{-1}. The molar absorption coefficients (ε) and the quantum yields (Φ) of the 4 iodoacids range from 389 to 1833 M^{-1} cm^{-1} and 0.13 to 0.34, respectively (Table 6.1). Apparently, the direct photolysis rates of these 4 species should be proportional to the quantum yield (Φ) and molar absorption coefficient (ε), which are two fundamental parameters that govern the direct photolysis rate (Equation 6.2).

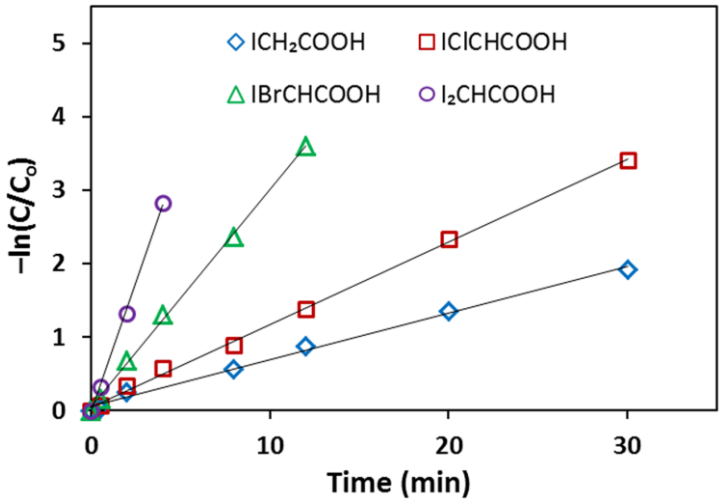

Figure 6.1 Linear plots for UV direct photolysis of 4 iodoacids in DI water.

To evaluate the feasibility of UV irradiation alone (e.g., using the existing disinfection system in waterworks) for degradation of iodoaicds, the removal efficiencies of iodoacids were determined at a UV dose of 140 mJ cm^{-2} which is upper-bound value for disinfection (Baeza and Knappe, 2011). The removal percentages of IAA, the most photo-recalcitrant species and I_2CHCO_2H, the most photo-labile species are 3.35% and 34.7%, respectively (Table 6.1). It suggests that a higher UV dose (763-9502 mJ cm^{-2} for 90% removal of the 4 iodoacids) than the usual dose for disinfection or advanced oxidation processes (AOPs) should be adopted to significantly remove iodoacids.

Table 6.1 Summary of molar absorption coefficient (ε), first-order rate constant (k), quantum yield (Φ), and removal percentages of 4 iodoacids through UV direct photolysis in DI water

Species	ε ($M^{-1}cm^{-1}$)	Φ_{254}[a]	$\varepsilon \cdot \Phi_{254}$	k (min^{-1})	$k_f \cdot 10^4$ ($cm^2\ mJ^{-1}$)[b]	R^2	R_{254} (140 mJ cm^{-2})
ICH_2CO_2H	389	0.13	51	0.057	2.43	0.994	3.35
$IClCHCO_2H$	449	0.21	94	0.11	4.68	0.997	6.39
$IBrCHCO_2H$	878	0.30	263	0.30	12.8	0.997	16.5
I_2CHCO_2H	1833	0.34	623	0.71	30.2	0.998	34.7

a. H_2O_2 as an actinometer. b. $k_f = \dfrac{k}{q_p \cdot hc/\lambda}$

6.2.2 QSAR modeling for direct photolysis of haloacids

As mentioned previously, QSAR analysis is a useful tool to correlate the chemical activity with molecular structure. Additionally, the established QSAR model can also be used to predict the chemical activity of any compound which has a similar molecular structure as the ones used to establish the model. Thus, QSAR analysis for direct photolysis of iodoacids was also conducted in order to find the relationship between the chemical activity and chemical structure as well as to predict the direct photolysis rate of the other structurally similar iodoacids which are commercially unavailable.

Similar to the method for establishing the QSAR model for direct photolysis of I-THMs and B-THMs in the chapter 4, the logarithm of measured first-order rate constants ($logk_m$) are correlated with 3 molecular descriptors by multiple linear regressions analysis to derive the QSAR model for direct photolysis of iodoacids. These 3 molecular descriptors include the bond strength (BS) of the carbon-halogen bond to be broken in the rate-determining step, the electronic effect (σ), and the steric effect (E_s) of all substituents to carbon center. E_s value for Cl, Br, and I are -0.96, -1.16, and -1.40, respectively; σ value for Cl, Br, and I are 0.47, 0.42, and 0.38, respectively (Hansch and Leo, 1995); the combined effect of multiple halides in the iodoacid are assumed to be the summation of individual effect of these halides (Table 6.2) (Zhang and Minear, 2002; Chen et al., 2010).

Table 6.2 Values of BS, E_s and σ for establishing QSAR model, and experimentally measured $logk_m$ and QSAR model predicted $logk_p$ as well as the difference between $logk_m$ and $logk_p$, Δ

Compound	BS	E_s	σ	$logk_m$	$logk_p$	Δ
ICH_2CO_2H	209	-1.40	0.38	-1.244	-1.309	0.065
$IClCHCO_2H$	209	-2.36	0.85	-0.959	-0.918	0.041
$IBrCHCO_2H$	209	-2.56	0.80	-0.523	-0.534	0.011
I_2CHCO_2H	209	-2.80	0.76	-0.155	-0.114	0.041
$BrCH_2CO_2H$	280	-1.16	0.42	-1.852	-1.835	0.017
Br_2CHCO_2H	280	-2.32	0.84	-1.000	-1.061	0.061
Br_3CCO_2H	280	-3.48	1.26	-0.290	-0.286	0.004
ICl_2CCO_2H	209	-3.32	1.32	-	-0.528	-
$IClBrCCO_2H$	209	-3.52	1.27	-	-0.144	-
IBr_2CCO_2H	209	-3.72	1.22	-	0.213	-
I_2ClCCO_2H	209	-3.76	1.23	-	0.277	-
I_2BrCCO_2H	209	-3.96	1.18	-	0.661	-
I_3CCO_2H	209	-4.20	1.14	-	1.082	-

Besides the above 4 iodoacids, other 3 bromine-containing haloacetic acids were included in order to have sufficient datasets to establish the QSAR model. Through correlating $\log k_m$ with the combination of BS, E_s and σ by multiple linear regression analysis, a QSAR model for direct photolysis of haloacetic acids was well established with regression coefficient, $R^2 = 0.993$ (Equation 6.3).

$$\log k = -0.0015BS - 1.41E_s - 2.05\sigma - 2.19 \quad (6.3)$$

The QSAR model was in turn used to predict the direct photolysis rate of the 7 haloacids studied. The QSAR model-predicted $\log k_p$ agree well with the experimentally measured $\log k_m$ (Figure 6.2). The differences between $\log k_p$ and $\log k_m$ for these 7 haloacids are less than 0.1-log relative standard deviations (Table 6.2).

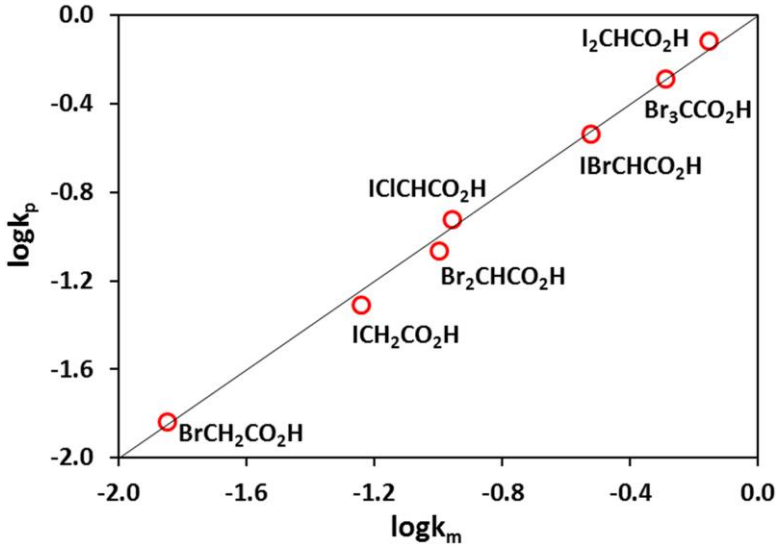

Figure 6.2 Comparison between experimentally measured $\log k_m$ and QSAR model-predicted $\log k_p$ for haloacids.

The QSAR model was also used to predict the k_p of 6 other structurally similar iodoacid which are commercially unavailable. Generally, the degradation rates of all iodoacids follow the order of IAA < $ICl CHCO_2H$ < $IBrCHCO_2H$ ≈ ICl_2CCO_2H < $IBrClCCO_2H$ < I_2CHCO_2H < IBr_2CCO_2H < I_2ClCCO_2H < I_2BrCCO_2H < I_3CCO_2H. The highest QSAR model-predicted k_p of I_3CCO_2H among all iodoacids is 12.1 min^{-1}, which is 212 times higher than the lowest degradation rate constant of IAA (0.057 min^{-1}). These results suggest that IAA is the most photo-recalcitrant

species and I_3CCO_2H is the most photo-labile species among all iodoacids. In addition to the generally low concentration of iodide in raw water, the QSAR model-predicted results could provide another possible reason why IAA has been detected and I_3CCO_2H has not been reported in the drinking water.

6.2.3 Comparison of UV/PS and UV/H_2O_2 AOPs

As mentioned above, IAA is the most recalcitrant to UV irradiation among all iodoacids and most toxic among all haloacetic acids. Thus, IAA was selected as the model compound to further investigate the efficiencies of the UV/PS and UV/H_2O_2 processes for iodoacids removal. In a control experiment, there was no change of IAA concentration in the presence of oxidant (6 mg L^{-1} H_2O_2 or 42 mg L^{-1} PS; molar fraction of oxidant/IAA = 120) without UV irradiation. The degradation of IAA in both UV/PS and UV/H_2O_2 processes also followed the pseudo-first-order kinetics (Figure 6.3). The degradation rates increased dramatically in these two AOPs due to generation of highly reactive $SO_4^{\bullet -}$ and $HO^{\bullet}$ as compared to direct photolysis. Furthermore, the degradation rates in the UV/PS process were much higher than those in the UV/H_2O_2 process under the comparable condition. For example, when the molar fractions of oxidant/IAA were 40, 120, and 300, the first-order rate constants in the UV/PS process were 2.54, 3.43, and 4.80 times higher than those in the UV/H_2O_2 process, respectively.

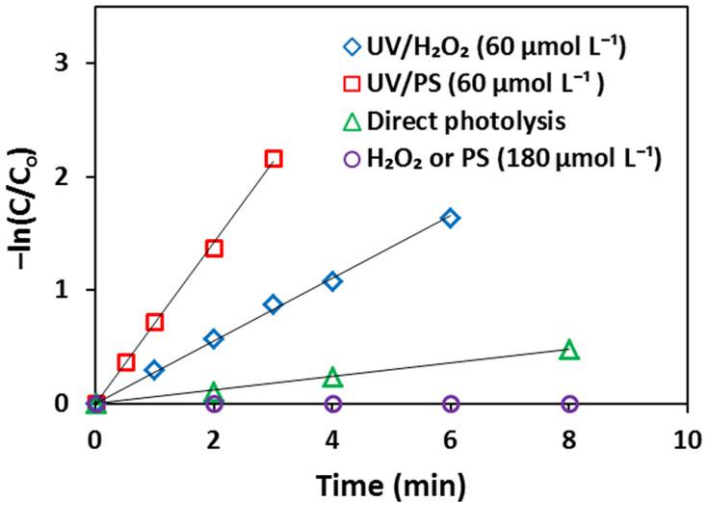

Figure 6.3 Linear plot for degradation of IAA under different treatment conditions in DI water (IAA: 1.5 µmol L^{-1}; pH 7)

To investigate the difference in the degradation rate between these two AOPs, the second-order rate constants of IAA reacting with $SO_4^{\cdot-}$ and $HO^{\cdot}$ were determined from the competition experiments using reference compounds with reported second-order rate constants at pH 7 (phosphate buffer solution, 5 mmol L^{-1}).

In the UV/H_2O_2 process, the overall degradation is attributed to direct photolysis and $HO^{\cdot}$-assisted indirect photolysis (Equation 6.4a). The indirect photolysis rate can be expressed as a function of the second-order rate constant of the reaction between IAA and $HO^{\cdot}$ and the steady-state concentration of $HO^{\cdot}$ (Equation 6.4b). The second-order rate constant of IAA reacting with $HO^{\cdot}$ was determined from the competition experiments using pCBA as reference compound. The reactions of $HO^{\cdot}$ with IAA and pCBA are assumed to proceed independently and in parallel (Equations 6.4c and 6.4d).

$$-\frac{dC}{dt} = (k_{obs,UV/IAA} + k_{obs,HO^{\cdot}/IAA})C \quad (6.4a)$$

$$k_{obs,HO^{\cdot}/IAA} = k_{HO^{\cdot},IAA} C_{HO^{\cdot},UV/H_2O_2} \quad (6.4b)$$

$$k_{obs,UV/H_2O_2/IAA} = k_{obs,UV/IAA} + k_{HO^{\cdot},IAA} C_{HO^{\cdot},UV/H_2O_2} \quad (6.4c)$$

$$k_{obs,UV/H_2O_2/pCBA} = k_{obs,UV/pCBA} + k_{HO^{\cdot},pCBA} C_{HO^{\cdot},UV/H_2O_2} \quad (6.4d)$$

Competitive kinetics:

$$k_{HO^{\cdot},IAA} = \frac{k_{obs,UV/H_2O_2/IAA} - k_{obs,UV/IAA}}{k_{obs,UV/H_2O_2/pCBA} - k_{obs,UV/pCBA}} k_{HO^{\cdot},pCBA} \quad (6.4e)$$

where $k_{obs,UV/H_2O_2/IAA}$ and $k_{obs,UV/H_2O_2/pCBA}$ are the observed overall pseudo-first-order rate constants of IAA and pCBA in the UV/H_2O_2 process in s^{-1}, respectively; $k_{obs,UV/IAA}$ and $k_{obs,UV/pCBA}$ are the direct photolysis rate constants of IAA and pCBA in s^{-1}, respectively; $k_{HO^{\cdot},IAA}$ and $k_{HO^{\cdot},pCBA}$ are the second-order rate constant of

$HO^{\cdot}$ reacting with IAA and pCBA, respectively; $C_{HO^{\cdot},UV/H_2O_2}$ is the steady-state concentration of $HO^{\cdot}$ in the UV/H_2O_2 process.

In the UV/PS process, as $SO_4^{\cdot-}$ can be converted to $HO^{\cdot}$ to some extent, the overall degradation involves direct photolysis as well as $SO_4^{\cdot-}$- and $HO^{\cdot}$-assisted indirect photolysis (Equations 6.5a and 6.5b). Since the second-order rate constant of t-butanol reacting with $SO_4^{\cdot-}$ ($k_{SO_4^{\cdot-},t\text{-}BuOH}$ = 8.4 x 10^5 M^{-1} s^{-1} at pH 7) (Clifton and Huie, 1989) is almost 3 orders of magnitude lower than that with $HO^{\cdot}$ ($k_{HO^{\cdot},t\text{-}BuOH}$ = 6.0 x 10^8 M^{-1} s^{-1} at pH 7) (Buxton et al., 1988), t-butanol was selected as the $HO^{\cdot}$ quenching reagent for the determination of the second-order rate constant of IAA reacting with $SO_4^{\cdot-}$ when mTA was used as reference compound.

$$k_{obs,UV/PS/IAA} = k_{obs,UV/IAA} + k_{SO_4^{\cdot-},IAA} C_{SO_4^{\cdot-},UV/PS} + k_{HO^{\cdot},IAA} C_{HO^{\cdot},UV/PS} \quad (6.5a)$$

$$k_{obs,UV/PS/mTA} = k_{obs,UV/mTA} + k_{SO_4^{\cdot-},mTA} C_{SO_4^{\cdot-},UV/PS} + k_{HO^{\cdot},mTA} C_{HO^{\cdot},UV/PS} \quad (6.5b)$$

With scavenging of $HO^{\cdot}$ by t-butanol, Equations 6.5a and 6.5b can be simplified to Equations 6.5c and 6.5d, respectively

$$k_{obs,UV/PS/IAA} = k_{obs,UV/IAA} + k_{SO_4^{\cdot-},IAA} C_{SO_4^{\cdot-},UV/PS} \quad (6.5c)$$

$$k_{obs,UV/PS/mTA} = k_{obs,UV/mTA} + k_{SO_4^{\cdot-},mTA} C_{SO_4^{\cdot-},UV/PS} \quad (6.5d)$$

Competitive kinetics:

$$k_{SO_4^{\cdot-},IAA} = \frac{k_{obs,UV/PS/IAA} - k_{obs,UV/IAA}}{k_{obs,UV/PS/mTA} - k_{obs,UV/mTA}} k_{SO_4^{\cdot-},mTA} \quad (6.5e)$$

where $k_{obs,UV/PS/IAA}$ and $k_{obs,UV/PS/mTA}$ are the observed overall pseudo-first-order rate constants of IAA and mTA in the UV/PS process in s^{-1}, respectively; $k_{obs,UV/IAA}$ and $k_{obs,UV/mTA}$ are the direct photolysis rate constants of IAA and mTA in s^{-1}, respectively; $k_{SO_4^{\cdot-},IAA}$ and $k_{SO_4^{\cdot-},mTA}$ are the second-order rate constant of $SO_4^{\cdot-}$

reacting with IAA and mTA, respectively; $C_{HO^{\cdot},UV/PS}$ and $C_{SO_4^{\cdot-},UV/PS}$ are the steady-state concentrations of $HO^{\cdot}$ and $SO_4^{\cdot-}$ in the UV/PS process, respectively.

For $k_{SO_4^{\cdot-},IAA}$ determination, the initial concentrations of IAA, mTA ($k_{SO_4^{\cdot-},mTA}$ = 2.0 x 10^9 M^{-1} s^{-1} at pH 7) (Neta et al., 1977), PS, and t-butanol were 1.5 µmol L^{-1}, 1.5 µmol L^{-1}, 90 µmol L^{-1}, and 1.5 mmol L^{-1}, respectively. For $k_{HO^{\cdot},IAA}$ determination, the initial concentrations of IAA, pCBA ($k_{HO^{\cdot},pCBA}$ = 4.5 x 10^9 M^{-1} s^{-1} at pH 7) (Buxton et al., 1988), and H_2O_2 were 1.5 µmol L^{-1}, 1.5 µmol L^{-1}, and 90 µmol L^{-1}, respectively. From the competition kinetic experiments, the second-order rate constant of IAA reacting with $SO_4^{\cdot-}$ and $HO^{\cdot}$ are 3.4 x 10^9 and 2.4 x 10^9 M^{-1} s^{-1}, respectively (Table 6.3). It suggests that $SO_4^{\cdot-}$ is more reactive than $HO^{\cdot}$ with IAA. However, $k_{SO_4^{\cdot-},IAA}$ is only 1.42 times higher than $k_{HO^{\cdot},IAA}$. It could not explain the difference of 2.54, 3.43, and 4.80 times in the degradation rates for these two processes when the molar fractions of oxidant/IAA were 40, 120, and 300.

Table 6.3 Respective contributions of UV, $HO^{\cdot}$, and $SO_4^{\cdot-}$ for IAA removal in the UV/PS process at a specific condition (1.5 µmol L^{-1} IAA or probe compound, 60 µmol L^{-1} oxidant, and pH 7)

	$k_{obs}(min^{-1})$			k ($x10^9$ $M^{-1}s^{-1}$)		Contribution in UV/PS process		
	UV only	UV/H_2O_2	UV/PS	$HO^{\cdot}$	$SO_4^{\cdot-}$	UV	$HO^{\cdot}$	$SO_4^{\cdot-}$
IAA	0.057	0.28	0.73	2.4[c]	3.4[c]	7.8%	14.7%	77.5%
NB	-	0.28	0.16	3.9[a]	$<10^{-3}$[b]	-	99.9%	0.1%
pNBA	-	0.19	0.12	2.6[a]	$<10^{-3}$[b]	-	99.8%	0.2%
mTA	-	0.41	0.69	7.6[c]	2[b]	-	50.7%	49.3%

a. Buxton et al., 1988; b. Neta et al., 1977; c. determined in this study.

Besides the different reactivities of $SO_4^{\cdot-}$ and $HO^{\cdot}$ with IAA, the difference in the degradation rates between these two processes could be also attributed to other factors. First, the generation yield of $SO_4^{\cdot-}$ in the UV/PS process is higher than the generation yield of $HO^{\cdot}$ in the UV/H_2O_2 process, as the radical formation quantum yield of $SO_4^{\cdot-}$ (Φ = 1.4, ε = 20 M^{-1} cm^{-1}) is higher than that of $HO^{\cdot}$ (Φ = 1.0, ε = 19.6 M^{-1} cm^{-1}) (Baxendale and Wilson, 1957; Mark et al., 1990). Second, the self-scavenging of $SO_4^{\cdot-}$ by $S_2O_8^{2-}$ in the UV/PS process is much lower than the self-scavenging of $HO^{\cdot}$ by H_2O_2 in the UV/H_2O_2 process (Table 6.4, reactions 3 versus

15). As shown in Figure 6.4, in the UV/PS process, the degradation rate increased almost linearly with PS concentration, as the scavenging effect of $S_2O_8^{2-}$ is limited. However, in the UV/H_2O_2 process, due to the stronger self-scavenging effect of H_2O_2, the increase of IAA degradation rate was limited when H_2O_2 concentration was increased.

Table 6.4 Relevant chemical reactions in the UV/PS and UV/H_2O_2 processes

Rxn	Reactions	k (M^{-1} s^{-1} or s^{-1})	Reference
1	$H_2O_2 + hv \rightarrow 2HO^{\bullet} (\Phi = 1.0)$		(Baxendale and Wilson, 1957)
2	$S_2O_8^{2-} + hv \rightarrow 2SO_4^{\bullet-} (\Phi = 1.4)$		(Mark et al., 1990)
3	$HO^{\bullet} + H_2O_2 \rightarrow H_2O + HO_2^{\bullet}$	2.7 x 10^7	(Buxton et al., 1988)
4	$HO^{\bullet} + HO_2^{-} \rightarrow HO^{-} + HO_2^{\bullet}$	7.5 x 10^9	(Buxton et al., 1988)
5	$HO^{\bullet} + CO_3^{2-} \rightarrow CO_3^{\bullet-} + HO^{-}$	3.9 x 10^8	(Buxton et al., 1988)
6	$HO^{\bullet} + HCO_3^{-} \rightarrow CO_3^{\bullet-} + H_2O$	8.5 x 10^6	(Buxton et al., 1988)
7	$HO^{\bullet} + SO_4^{2-} \rightarrow HO^{-} + SO_4^{\bullet-}$	3.5 x 10^5	(Neta et al., 1988)
8	$HO^{\bullet} + S_2O_8^{2-} \rightarrow HO^{-} + S_2O_8^{\bullet-}$	1.4 x 10^7	(Buxton et al., 1988)
9	$HO^{\bullet} + Cl^{-} \rightarrow ClOH^{\bullet-}$	4.3 x 10^9	(Buxton et al., 1988)
10	$ClOH^{\bullet-} \rightarrow HO^{\bullet} + Cl^{-}$	6.0 x 10^9	(Neta et al., 1988)
11	$ClOH^{\bullet-} + H^{+} \rightarrow HClOH^{\bullet} (pK_a = 7.2)$	3.0 x 10^{10}	(Neta et al., 1988; Liao et al., 2001)
12	$HClOH^{\bullet} \rightarrow Cl^{\bullet} + H_2O$	5.0 x 10^4	(Neta et al., 1988)
13	$HClOH^{\bullet} + Cl^{-} \rightarrow Cl_2^{\bullet-} + HO^{-}$	4.0 x 10^6	(Neta et al., 1988)
14	$Cl^{\bullet} + Cl^{-} \rightarrow Cl_2^{\bullet-}$	8.5 x 10^9	(Neta et al., 1988)
15	$SO_4^{\bullet-} + S_2O_8^{2-} \rightarrow SO_4^{2-} + S_2O_8^{\bullet-}$	6.6 x 10^5	(Neta et al., 1988)
16	$SO_4^{\bullet-} + OH^{-} \rightarrow HO^{\bullet} + SO_4^{2-}$	6.5 x 10^7	(Neta et al., 1988)
17	$SO_4^{\bullet-} + H_2O \rightarrow HO^{\bullet} + SO_4^{2-}$	< 60	(Neta et al., 1988)
18	$SO_4^{\bullet-} + HCO_3^{-} \rightarrow CO_3^{\bullet-} + HSO_4^{-}$	9.1 x 10^6	(Buxton et al., 1988)
19	$SO_4^{\bullet-} + CO_3^{2-} \rightarrow CO_3^{\bullet-} + SO_4^{2-}$	6.1 x 10^6	(Zuo et al., 1999)
20	$SO_4^{\bullet-} + Cl^{-} \rightarrow Cl^{\bullet} + SO_4^{2-}$	3.1 x 10^8	(Chawla and Fessenden, 1975)
21	$SO_4^{\bullet-} + NO_3^{-} \rightarrow NO_3^{\bullet} + SO_4^{2-}$	2.1 x 10^0	(Neta et al., 1988)

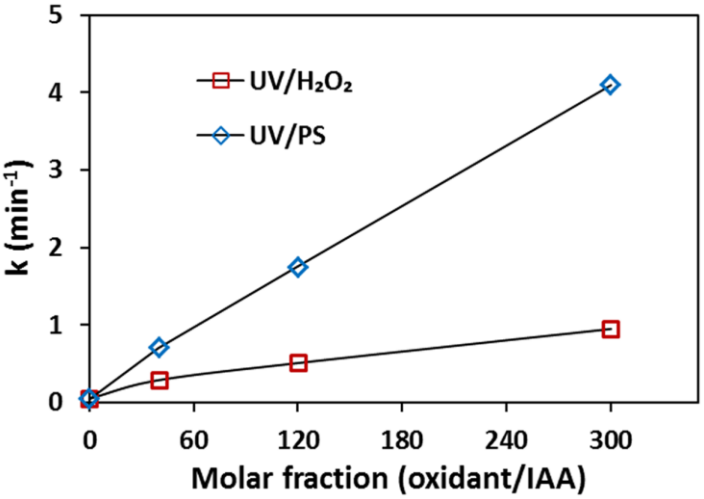

Figure 6.4 Effect of oxidant doses on IAA photodegradation rates (IAA: 1.5 µmol L^{-1}; pH 7).

6.2.4 Effect of pH

Effect of pH on photodegradation rate was examined at pH 3, 5, 7, 9, and 11. The degradation rates in both UV/PS and UV/H_2O_2 processes decreased with increasing pH (Figure 6.5). In the UV/H_2O_2 process, the degradation rates decreased slightly from pH 3 to 9, possibly due to the decrease of redox potential of $HO^{\cdot}/H_2O$ with the increase of pH. For example, according to Equation 6.6 (derived from Nernst equation), the redox potential of $HO^{\cdot}/H_2O$ at pH 3, 5, 7, 9, and 11 are 2.62, 2.51, 2.39, 2.29, and 2.15 V, respectively (for $E^{o}_{HO^{\cdot}/H_2O} = 2.80$ V).

$$E_{HO^{\cdot}} = E^{o}_{HO^{\cdot}/H_2O} - 0.059\text{pH} \quad (6.6)$$

$$H_2O_2 \rightarrow HO_2^- + H^+ (pK_a = 11.8) \quad (6.7)$$

On the other hand, the degradation rate decreased dramatically at pH 11. The major reason for this reduction is the scavenging of $HO^{\cdot}$ by hydroperoxide anion (HO_2^-), which can be generated under an alkaline condition in the UV/H_2O_2 process (Equation 6.7) (Gottschalk et al., 2010). Although HO_2^- can promote the formation of $HO^{\cdot}$, it is also a strong radical scavenger and reacts with $HO^{\cdot}$ ~ 280 times faster than H_2O_2 (Table 6.4, reactions 3 and 4).

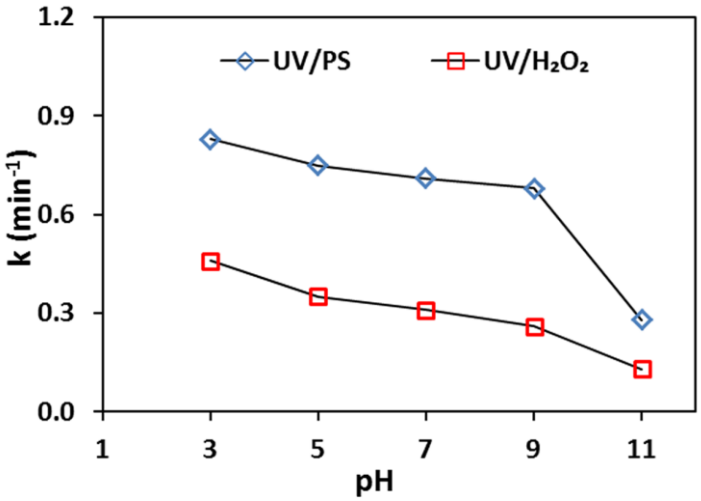

Figure 6.5 Effect of pH on IAA photodegradation rates (IAA: 1.5 μmol L^{-1}; oxidants: 60 μmol L^{-1})

In the UV/PS process, the degradation rates increased slightly under the acidic condition as less amount of $SO_4^{\bullet-}$ is transformed to $HO^{\bullet}$ at a lower pH (Table 6.4, reaction 16). Thus, $SO_4^{\bullet-}$ is the predominant radical species in the UV/PS process under the acidic condition (He et al., 2014b; Yuan et al., 2014). In contrast, at pH 11, the major radical species in the UV/PS process is $HO^{\bullet}$. As $SO_4^{\bullet-}$ is more reactive than $HO^{\bullet}$ with IAA, the degradation rates also decreased with increasing pH in the UV/PS process.

6.2.5 Effect of aqueous matrix species

Some of the matrix species which are commonly present in water can react with radicals including $SO_4^{\bullet-}$ and $HO^{\bullet}$, in competition with the organic pollutants (Criquet and Leitner, 2009). Thus, the scavenging effect of matrix species on IAA photodegradation rate at pH 7 was also investigated. HA, SO_4^{2-}, Cl^-, HCO_3^-, and NO_3^- were selected as matrix species in this study, as these species are commonly found in the natural water.

In general, SO_4^{2-}, HCO_3^-, HA, and NO_3^- had similar effects on IAA removal in both UV/PS and UV/H_2O_2 processes (Figure 6.6). In the presence of SO_4^{2-}, the

degradation rates were almost similar to those in DI water, as SO_4^{2-} reacts slowly with both $SO_4^{\bullet-}$ and $HO^{\bullet}$ and its scavenging effect can be ignored (Table 6.4, reaction 7). HCO_3^- can react with $SO_4^{\bullet-}$ and $HO^{\bullet}$ to produce less reactive species, $CO_3^{\bullet-}$ (Table 6.4, reactions 6 and 18). Thus, the degradation rate decreased in the presence of HCO_3^- due to its strong scavenging of $SO_4^{\bullet-}$ and $HO^{\bullet}$. HA had a negative effect on the photodegradation rates due to the following reasons: First, HA is a strong scavenger of $SO_4^{\bullet-}$ and $HO^{\bullet}$. Second, the attenuation of UV due to absorption by HA reduces the fraction of UV light absorbed by PS and H_2O_2, which lead to lower the production of $SO_4^{\bullet-}$ and $HO^{\bullet}$. The redox potential of $NO_3^{\bullet} / NO_3^-$ (2.3-2.6 V versus NHE) is almost similar to that of $HO^{\bullet}/H_2O$ at pH 7 (2.39 V versus NHE). It means that $HO^{\bullet}$ cannot oxidize NO_3^- to produce $NO_3^{\bullet}$. NO_3^- also reacts slowly with $SO_4^{\bullet-}$ (Table 6.4, reaction 21). Thus, the scavenging of $HO^{\bullet}$ and $SO_4^{\bullet-}$ by NO_3^- can be ignored. The degradation rates of IAA in both UV/PS and UV/H_2O_2 processes increased in the presence of NO_3^- possible due to generation of additional $HO^{\bullet}$ by direct photolysis of NO_3^- (Keen et al., 2012).

In contrast, Cl^- had different effects on the degradation rates in these two AOPs (Figure 6.6). In the UV/PS process, Cl^- can react with $SO_4^{\bullet-}$ to produce the less reactive $Cl^{\bullet}$ (Table 6.4, reaction 20), which leads to the decreased IAA degradation rate. In the UV/H_2O_2 process, Cl^- can react rapidly with $HO^{\bullet}$ to form $ClOH^{\bullet-}$ (Table 6.4, reaction 9). Under the acidic condition, $ClOH^{\bullet-}$ can be converted to $HClOH^{\bullet}$ (pK_a = 7.2 for the deprotonation of $HClOH^{\bullet}$; Table 6.4, reaction 11), which subsequently decomposes to less reactive species such as $Cl^{\bullet}$ (Table 6.4, reactions 12 and 13). On the other hand, under the neutral and basic conditions, $ClOH^{\bullet-}$ can rapidly revert back to Cl^- and $HO^{\bullet}$ (Table 6.4, reaction 10). This could explain why the photodegradation rates of IAA in the UV/H_2O_2 process were not affected by Cl^- at pH 7.

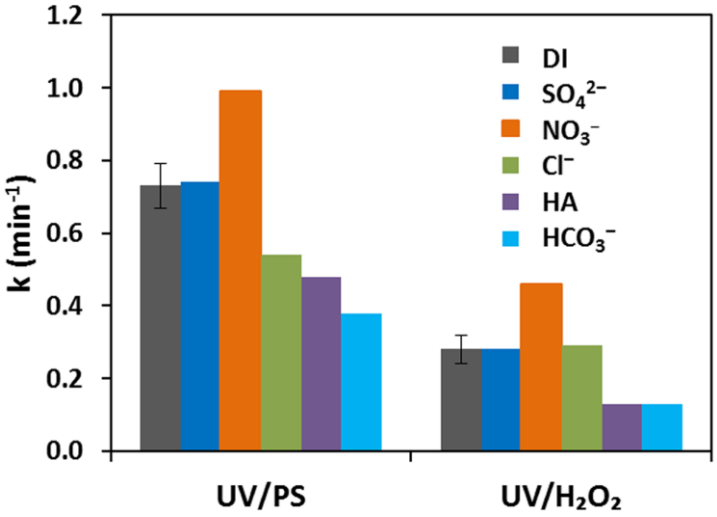

Figure 6.6 Effect of matrix species on IAA photodegradation rates (IAA: 1.5 µmol L^{-1}; oxidants: 60 µmol L^{-1}; $NaSO_4$, NaCl, $NaHCO_3$ and $NaNO_3$: 4 mmol L^{-1}; HA: 5 mg L^{-1}; pH 7). Error bars denote standard deviation obtained from at least duplicate datasets.

6.2.6 Degradation of IAA in different types of water

Photodegradation of IAA in different types of water including DI water, surface water (SW from a river, used as source water in a water treatment plant, Singapore), treated water (TW, collected from the same water treatment plant with surface water, Singapore), secondary effluent (SE, collected from a wastewater treatment plant, Singapore) was also investigated. The characteristics of the different types of water are listed in Table 6.5.

Table 6.5 Characteristics of different types of water used in this study

Water matrix	TOC[a]	Turbidity[b] (NTU)	a (254nm) (cm^{-1})	Total alkalinity	Cl^- [a]	SO_4^{2-} [a]	NO_3^- [a]
DI	0.08	< 0.1[c]	0	< 5	< 5	< 0.045	< 0.05
TW	0.99	0.22	0.010	5.93	14.3	21.6	0.12
SW	3.94	1.85	0.075	7.65	21.8	4.14	0.47
SE	10.6	0.19	0.152	54.9	145.5	45.1	6.28

a. Unit: mg L^{-1}; b. After 0.45 µm membrane filtration; c. It represents the result is below detection limit.

The IAA degradation rates in both UV/PS and UV/H_2O_2 processes decreased slightly in TW and significantly in SW and SE, as compared to those in DI water.

Its degradation rates in different types of water followed the order of SE < SW << TW < DI (Figure 6.7). These results suggest that these two UV-based AOPs are more suitable as post-filtration treatment to remove IAA, from the view point of degradation kinetics. According to the preceding discussion, the reduction of IAA degradation rate is due to the presence of the scavengers such as NOM, alkalinity, and H_2O_2 in the UV/H_2O_2 process, while NOM, alkalinity, and Cl^- are the major scavengers of $SO_4^{\bullet-}$ in the UV/PS process. Furthermore, NOM can act as a competitive UV absorber to provide screening effect, which leads to the decreased direct photolysis rate of IAA, H_2O_2, and PS. Compared to the UV/H_2O_2 process, UV/PS process is still more effective to remove IAA in all types of water studied.

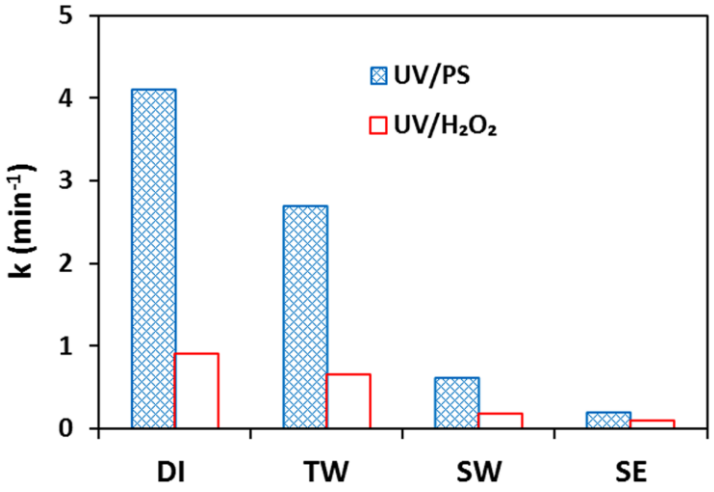

Figure 6.7 Effect of different types of water on IAA photodegradation rates (IAA: 1.5 μmol L^{-1}; oxidants: 450 μmol L^{-1}; pH 7).

6.2.7 Respective contributions of UV, $HO^{\bullet}$, and $SO_4^{\bullet-}$ for degradation of IAA

As mentioned above, $SO_4^{\bullet-}$ can be transformed to $HO^{\bullet}$ in the UV/PS process. To further identify the respective contributions of UV, $HO^{\bullet}$, and $SO_4^{\bullet-}$ for IAA degradation, a series of experiments were conducted for quantitation of $HO^{\bullet}$ and $SO_4^{\bullet-}$ generated in the UV/PS process. The second-order rate constants of NB and pNBA reacting with $SO_4^{\bullet-}$ were reported to be 3 orders of magnitude lower than those with $HO^{\bullet}$ (Table 6.3), indicating that NB and pNBA react slowly with $SO_4^{\bullet-}$.

Their degradations in the UV/PS process are mainly attributed to $HO^{\bullet}$ (Liang and Su, 2009; He et al., 2014b). Thus, NB and pNBA can be selected as probe compounds to quantify the $HO^{\bullet}$ in the UV/PS process. In contrast, some other compounds such as mTA react fast with both $HO^{\bullet}$ and $SO_4^{\bullet-}$, as suggested by its reported second-order rate constant (Table 6.3). In this study, the average steady-state concentration of $HO^{\bullet}$ in the UV/PS process was firstly determined using NB and pNBA as probe compounds (Equations 6.8 and 6.9). Subsequently, the concentration of $SO_4^{\bullet-}$ in the UV/PS process could be calculated through subtracting the contribution of UV and $HO^{\bullet}$ in mTA degradation, when mTA was used as the probe compound for $SO_4^{\bullet-}$ determination (Equations 6.10 and 6.11).

$$k_{obs,HO^{\bullet}/NB} = k_{obs,UV/PS/NB} - k_{obs,UV/NB} - k_{obs,SO_4^{\bullet-}/NB} \approx k_{obs,UV/PS/NB} - k_{obs,UV/NB} \quad (6.8)$$

$$C_{HO^{\bullet},UV/PS} = \frac{k_{obs,UV/PS/NB} - k_{obs,UV/NB}}{k_{HO^{\bullet},NB}} \quad (6.9)$$

$$k_{obs,SO_4^{\bullet-}/mTA} = k_{obs,UV/PS/mTA} - k_{obs,UV/mTA} - k_{obs,HO^{\bullet}/mTA} \quad (6.10)$$

$$C_{SO_4^{\bullet-},UV/PS} = \frac{k_{obs,UV/PS/mTA} - k_{obs,UV/mTA} - k_{HO^{\bullet},mTA} C_{HO^{\bullet},UV/PS}}{k_{SO_4^{\bullet-},mTA}} \quad (6.11)$$

where $k_{obs,UV/PS/NB}$, $k_{obs,UV/NB}$, $k_{obs,SO_4^{\bullet-}/NB}$, and $k_{obs,HO^{\bullet}/NB}$ are the observed overall pseudo-first-order rate constant, direct photolysis rate constant, $SO_4^{\bullet-}$- and $HO^{\bullet}$-assisted indirect photolysis rate constant of NB in the UV/PS process, respectively; $k_{obs,UV/PS/mTA}$, $k_{obs,UV/mTA}$, $k_{obs,SO_4^{\bullet-}/mTA}$, and $k_{obs,HO^{\bullet}/mTA}$ are the observed overall pseudo-first-order rate constant, direct photolysis rate constant, $SO_4^{\bullet-}$- and $HO^{\bullet}$-assisted indirect photolysis rate constant of mTA in the UV/PS process, respectively; $k_{HO^{\bullet},NB}$, $k_{HO^{\bullet},mTA}$, and $k_{SO_4^{\bullet-},mTA}$ are the second-order rate constants of $HO^{\bullet}$ reacting with NB and mTA as well as $SO_4^{\bullet-}$ reacting with mTA, respectively; $C_{HO^{\bullet},UV/PS}$ and $C_{SO_4^{\bullet-},UV/PS}$ are the steady-state concentrations of $HO^{\bullet}$ and $SO_4^{\bullet-}$ in the UV/PS process, respectively.

In the UV/H_2O_2 process, $HO^{\cdot}$ is the main reacting radical species. Its steady-state concentration can be calculated according to Equations 6.12 and 6.13.

$$k_{obs,HO^{\cdot}/NB} = k_{obs,UV/H_2O_2/NB} - k_{obs,UV/NB} \quad (6.12)$$

$$C_{HO^{\cdot},UV/H_2O_2} = \frac{k_{obs,UV/H_2O_2/NB} - k_{obs,UV/NB}}{k_{HO^{\cdot},NB}} \quad (6.13)$$

where $k_{obs,UV/H_2O_2/NB}$, $k_{obs,UV/NB}$, and $k_{obs,HO^{\cdot}/NB}$ are the observed overall pseudo-first-order rate constant, direct photolysis rate constant, and $HO^{\cdot}$-assisted indirect photolysis rate constant of NB in the UV/H_2O_2 process, respectively; $C_{HO^{\cdot},UV/H_2O_2}$ is the steady-state concentration of $HO^{\cdot}$ in the UV/H_2O_2 process. Similar kinetic expression for pNBA as a probe compound can also be derived for both UV/PS and UV/H_2O_2 processes.

At a specific condition (1.5 μmol L^{-1} IAA or probe compound, 60 μmol L^{-1} oxidant, and pH 7), the average steady-state concentration of $HO^{\cdot}$ and $SO_4^{\cdot-}$ in the UV/PS process were estimated as 7.48 ± 0.43 x 10^{-13} and 2.77 ±0.05 x 10^{-12} M, respectively. In the UV/H_2O_2 process, the average steady-state concentration of $HO^{\cdot}$ was estimated as 1.21 ± 0.26 x 10^{-12} M. Through inputting the derived steady-state concentration of $HO^{\cdot}$ and $SO_4^{\cdot-}$, second-order rate constant of IAA reacting with $HO^{\cdot}$ and $SO_4^{\cdot-}$, and the direct photolysis rate constant into Equation 6.5a, the predicted k_p of IAA for the UV/PS process is 0.73 ± 0.02 min^{-1}, which is agreeable with the experimentally measured k_{obs} (0.73 min^{-1}).

The respective contributions of UV, $HO^{\cdot}$, and $SO_4^{\cdot-}$ for the degradation of IAA, NB, pNBA, and mTA in the UV/PS process were determined accordingly. The results indicate that the contribution of $SO_4^{\cdot-}$ in IAA degradation in the UV/PS is predominant over the combination of $HO^{\cdot}$-assisted indirect photolysis and UV direct photolysis. For example, the respective contributions of UV, $HO^{\cdot}$, and $SO_4^{\cdot-}$ for IAA removal in the UV/PS process were determined as 7.8%, 14.7%, and 77.5%, respectively (Table 6.3). Similarly, the respective contributions of UV and $HO^{\cdot}$ for

IAA removal in the UV/H_2O_2 process were determined as 20% and 80%, respectively (Figure 6.8). As discussed in the preceding section (6.2.4), the $SO_4^{\bullet-}$/$HO^{\bullet}$ concentration ratio in the UV/PS process is pH dependent and so do their respective contributions in the IAA degradation. Compared to $SO_4^{\bullet-}$, PS is more effective to scavenge $HO^{\bullet}$ (Table 6.4, reactions 8 and 15). Thus, the concentration of $SO_4^{\bullet-}$ would increase more significantly with PS dose, as compared to the extent of $HO^{\bullet}$ increase in the UV/PS process. Consequently, the percentage of $SO_4^{\bullet-}$ contribution to the overall IAA degradation in the UV/PS process would increase with PS dose.

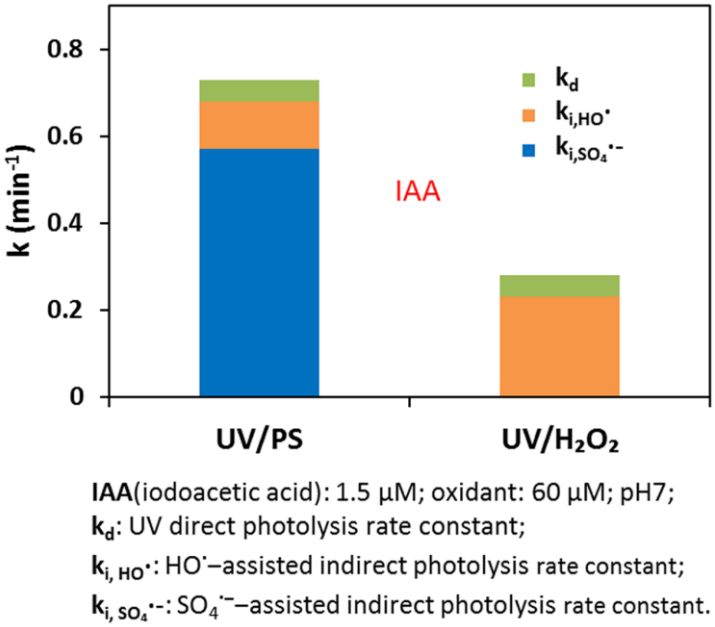

Figure 6.8 Respective contributions of UV direct photolysis and indirect photolysis for IAA removal in the UV/PS and UV/H_2O_2 processes

6.2.8 Photodegradation end-products identification

The TOC evolutions in the UV/PS and UV/H_2O_2 processes are rather different (Figure. 6.9(a)). In the UV/PS process, IAA could be completely removed within 6 min. A greater TOC removal rate was observed within the initial 3 min. Then, the reduction rate of TOC became relatively slow from 3 to 10 min, possibly due to generation of $SO_4^{\bullet-}$-resistant intermediates relative to IAA. From 10 min onward,

TOC reduced rapidly again toward the complete mineralization. In the UV/H_2O_2 process, TOC reduced gradually over the whole reaction time of 30 min. Almost 50% of the initial TOC was still present at 30 min, although IAA had been completely removed within 15 min (Figure. 6.9(a)).

In the UV/PS process, formaldehyde (HCHO) increased gradually at the initial 10 min and reached the maximum concentration of 0.84 mg-C L^{-1} (~ 16.3% of initial TOC) at 10 min (Figure. 6.9(b)). Then, it reduced dramatically and almost disappeared at 20 min. Meanwhile, formic acid (HCO_2H) and oxalic acid were below detection limits (DL: 30 µg L^{-1} for HCO_2H; DL: 50 µg L^{-1} for oxalic acid) in the UV/PS process. In the UV/H_2O_2 process, both HCHO and HCO_2H were detected, while oxalic acid was also not detected (Figure. 6.9(c)). The amount of HCHO increased gradually from 0 to 1.12 mg-C L^{-1} (~ 21.7% of initial TOC) over the initial 10 min and then decreased gradually to 0.64 mg-C L^{-1} (~ 12.4% of initial TOC) at 30 min. HCO_2H also increased over the reaction time and reached the maximum concentration of 0.48 mg-C L^{-1} (~ 9.30% of initial TOC) at 20 min and then its concentration slightly decreased to 0.44 mg-C L^{-1} (~ 8.53% of initial TOC) at 30 min. The mass of carbon from HCHO and HCO_2H at 30 min accounted for ~ 20% of initial TOC. As mentioned above, 50% of initial TOC were mineralized at 30 min. It means that the remaining 30% of initial TOC were associated with other unidentified intermediates. These results suggested that UV/PS process is more effective to remove both IAA and its degradation intermediates, which leads to a greater mineralization as compared to UV/H_2O_2 process.

Additionally, IO_3^- was identified as the predominant end-product in the UV/PS process (Figure. 6.9(d)). IO_3^- increased slightly at the initial 6 min, and then it increased dramatically from 6 min onward and reached the maximum concentration of ~ 40 mg L^{-1} (98.9% of total I in IAA) at 10 min. On the other hand, a trace level of I^- was detected around 0.16 mg L^{-1} at 1 min. Then, it gradually decreased and almost disappeared at 10 min. In the UV/H_2O_2 process, I^- was identified as the predominant end-product (Figure. 6.9(e)). Its amount increased gradually over the reaction time and reached the maximum concentration of ~ 26.5 mg L^{-1} (97.1% of

total I in IAA) at 30 min. In addition, trace level of IO_3^- was observed and its amount is less than 0.02% of I^- generated in the UV/H_2O_2 process. In general, there is a good mass balance between the produced I^- or IO_3^- and the total I in IAA in both UV/PS and UV/H_2O_2 processes.

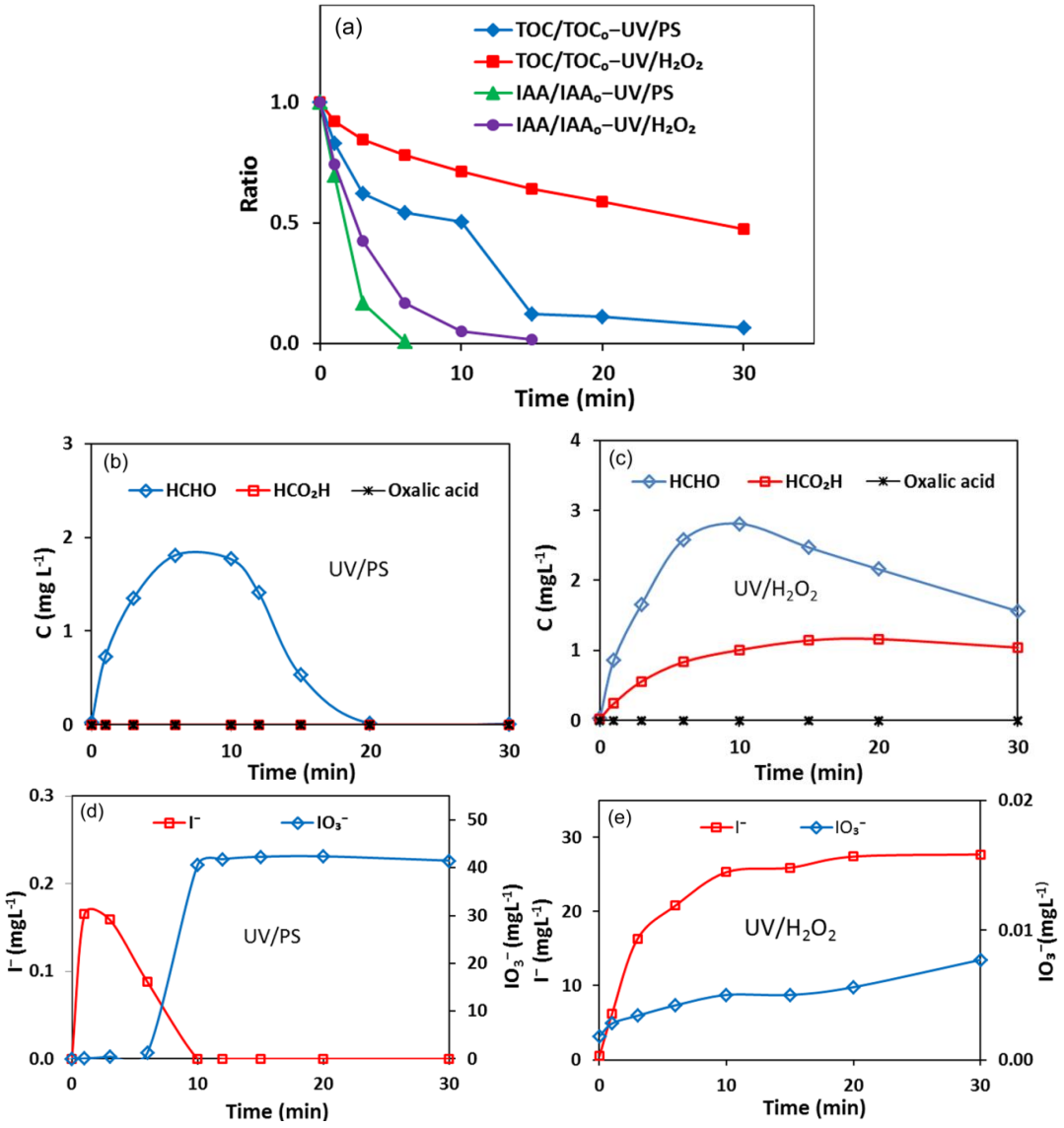

Figure 6.9 Time course of IAA and TOC reduction in the UV/PS and UV/H_2O_2 processes (a); HCHO, HCO_2H, and oxalic acid formation in the UV/PS (b) and UV/H_2O_2 (c) processes; I^- and IO_3^- formation in the UV/PS (d) and UV/H_2O_2 (e) processes (IAA 40 mg L^{-1}; molar fraction of oxidant/ IAA = 40).

6.2.9 Economic comparison of UV/PS and UV/H_2O_2 processes

The economic comparison of UV/PS and UV/H_2O_2 processes for removal of IAA was conducted based on the total cost of electrical energy and the oxidants. The electric energy consumed by UV lamp is expressed in terms of electrical energy per order (EE/O_{UV}), which is defined as the electric energy in kWh required to degrade the organic pollutant by one order of magnitude in 1 m^3 of water. The EE/O_{UV} can be determined according to Equation 6.14. Using 0.1 US$/kWh as electricity cost, the electrical energy cost and the total cost per order ($cost/O_{total}$) can be calculated according to Equations 6.15 and 6.16, respectively.

$$EE / O_{UV} = \frac{1000Pt}{Vlog(\frac{C_i}{C_f})} = \frac{38.4P}{Vk} (kWhm^{-3}order^{-1}) \quad (6.14)$$

$$\text{Electrical energy cost } (\$m^{-3}oder^{-1}) = EE/O_{UV} \times \text{electricity cost } (\$/kWh) \quad (6.15)$$

$$Cost/O_{total} (\$m^{-3}order^{-1}) = \text{electrical energy cost + oxidant cost} \quad (6.16)$$

where all of the terms are as defined previously.

Generally, the $cost/O_{total}$ is significantly lower for both UV/PS and UV/H_2O_2 processes as compared to UV direct photolysis (Table 6.6). For example, at the molar fraction of oxidant/IAA = 40, the $cost/O_{total}$ for the UV/H_2O_2 and UV/PS processes in DI water are 0.098 and 0.049 $\$m^{-3}order^{-1}$, respectively, which are 5 times and 10 times lower than that (0.481 $\$m^{-3}order^{-1}$) by UV direct photolysis. As shown in the Figure 6.10, at a relatively low concentration of oxidant (i.e., molar fraction of oxidant/IAA < 190, that is, H_2O_2 < 9.5 mg L^{-1} and PS < 66.5 mg L^{-1}), the $cost/O_{total}$ for the UV/PS processes is lower than that for the UV/H_2O_2 process. However, when the molar fraction of oxidant/IAA is ≥ 190, the $cost/O_{total}$ for the UV/PS process is higher than that for the UV/H_2O_2 process. As mentioned previously, these two UV-based AOPs are more suitable as post-filtration treatment to remove IAA. Therefore, in the clean water matrix such as DI and treated water, a relatively low concentration of oxidant in these two AOPs is sufficient to

significantly remove IAA. In this circumstance, UV/PS process is more economically competitive than UV/H_2O_2 process. For example, at the molar fraction of oxidant/IAA = 120, the cost/O_{total} (0.047 $\$m^{-3}order^{-1}$) for the UV/PS process in DI water is lower than that (0.063 $\$m^{-3}order^{-1}$) for the UV/$H_2O_2$ process (Table 6.6). Furthermore, the lowest cost/O_{total} (~ 0.040 $\$m^{-3}order^{-1}$) for the UV/PS process is also lower than the corresponding value (~ 0.053 $\$m^{-3}order^{-1}$) for the UV/$H_2O_2$ process (Figure 6.10).

Table 6.6 Economic comparison of UV, UV/PS and UV/H_2O_2 processes for IAA removal in DI water

	Molar fraction (oxidant/IAA)	EE/O ($kWhm^{-3}order^{-1}$)	Cost (US$ $m^{-3}order^{-1}$)[a]		
			UV[b]	Oxidant[c]	Total
UV	-	4.81	0.481	-	0.481
UV/H_2O_2	40	0.95	0.095	0.003	0.098
	120	0.54	0.054	0.009	0.063
	300	0.30	0.030	0.023	0.053
	600	0.23	0.023	0.046	0.069
UV/PS	40	0.39	0.039	0.010	0.049
	120	0.16	0.016	0.031	0.047
	300	0.06	0.006	0.078	0.084
	600	0.04	0.004	0.156	0.160

a. IAA: 1.5 µmol L^{-1};
b. \$0.10 $(kWh)^{-1}$ (U.S. Energy Information Administration, 2015);
c. PS: \$0.74 kg^{-1} (\$0.18 mol^{-1}); H_2O_2: \$1.5 kg^{-1} (\$0.051 mol^{-1}) (Zhang et al., 2014)

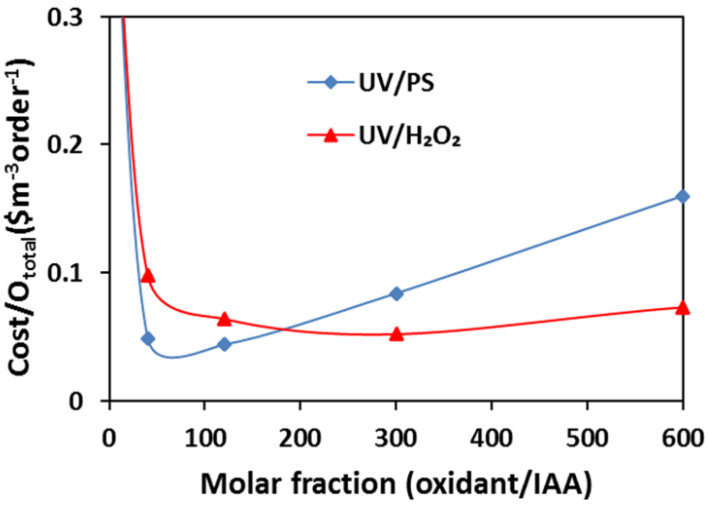

Figure 6.10 Economic comparison of UV/PS and UV/H_2O_2 processes for the removal of IAA in DI water (IAA: 1.5 µmol L^{-1}; pH 7).

6.3 Conclusion

Direct photolysis of 4 iodoacids followed first-order kinetics with rate constant in the range of 0.057 to 0.71 min^{-1}. A QSAR model was applied to predict the direct photolysis rate constant of 6 other commercially unavailable iodoacids. Subsequently, UV/PS process was applied to degrade IAA, the most photo-recalcitrant species among all iodoacids, and compared its effectiveness with UV/H_2O_2 process. The degradation rates decreased with the increase of pH in both processes. HA and HCO_3^- had inhibitory effects on IAA degradation in both processes. The degradation rate decreased in the presence of Cl^- in the UV/PS process, while Cl^- had no effect on the degradation rate in the UV/H_2O_2 process under the reaction conditions (i.e., pH 7). The degradation rates of IAA in both processes increased slightly in the presence of NO_3^- possibly due to generation of $HO^{\cdot}$ at a low quantum yield via direct photolysis of NO_3^-. The degradation rates of IAA in the UV/PS process in different types of water including DI, TW, SW, and SE were larger than the corresponding values in the UV/H_2O_2 process. A greater IAA mineralization was also observed in the UV/PS process as compared to the UV/H_2O_2 process. IO_3^- was identified as the predominant end-product in the UV/PS process, while I^- was the major end-product in the UV/H_2O_2 process. The respective contributions of UV, $HO^{\cdot}$, and $SO_4^{\cdot -}$ for IAA removal in the UV/PS process were 7.8%, 14.7%, and 77.5%, respectively. Based on total cost of the electrical energy and the oxidant, UV/PS process was more cost-effective than the UV/H_2O_2 process for IAA removal, under the reaction conditions adopted in this study.

CHAPTER 7 Conclusions and recommendations

7.1 Overall conclusion

To develop a cost-effective method for post-formation mitigation of I-DBPs, degradation of I-THMs and iodoacids by UV, UV/H_2O_2, and UV/PS was extensively investigated in this study. The major findings and conclusions from this research can be summarized as follows.

- **UV direct photolysis of I-DBPs**. UV254 direct photolysis of 6 I-THMs and 4 iodoacids followed first-order kinetics with rate constants in the range of 0.057-0.71 min^{-1}. The derived quantum yields of the 6 I-THMs and 4 iodoacids range from 0.13 to 0.58, which indicates a high efficiency of quantum process in the I-THMs and iodoacids photodegradation under UV254 irradiation.

- **Benefit of UV-based AOP compared to UV photolysis**. However, at a UV dose of 140 mJ cm^{-2} which is the upper-bound value used for disinfection, the removal percentages of 6 I-THMs and 4 iodoacids were 5.41% to 29.4% and 3.35% to 34.7%, respectively. It suggests that a higher UV dose than the usual dose for water disinfection or UV-based AOP is required to significantly photodegrade I-THMs and iodoacids.

- **Matrix species effect**. In the UV, UV/H_2O_2, and UV/PS processes, the degradation rates of I-THMs and iodoacids increased slightly in the presence of NO_3^- possibly due to generation of $HO^{\bullet}$ at a low quantum yield via direct photolysis of NO_3^-. HA lowered the photodegradation rate due to its competitive UV absorption and scavenging effect of $SO_4^{\bullet-}$ and $HO^{\bullet}$. HCO_3^-, SO_4^{2-}, and Cl^- had no significant effect on direct photolysis kinetics, as there is no UV absorption for these 3 species. On the other hand, HCO_3^- had a negative effect on $SO_4^{\bullet-}$- and $HO^{\bullet}$-assisted indirect photolysis rates, as it could act as a scavenger of $SO_4^{\bullet-}$ and $HO^{\bullet}$. SO_4^{2-} also had no

effect on the IAA photodegradation in the UV/H_2O_2 and UV/PS processes, as its scavenging effect of $SO_4^{\cdot-}$ and $HO^{\cdot}$ could be ignored. Cl^- could adversely affect the IAA degradation rate in the UV/PS process but had no effect in the UV/H_2O_2 process.

- **QSAR modeling**. A QSAR model for direct photolysis of I-THMs and B-THMs was established based on the correlation between $\log k_m$ and the combination of BS (bond strength), σ (electrical effect) and E_s (steric effect). It suggests that these 3 parameters have a significant combined effect on the overall direct photolysis of I-THMs and B-THMs. Similarly, a QSAR model for direct photolysis of iodoacids was established through correlating $\log k_m$ with the combination of BS, σ and E_s. The established QSAR model was used to predict the direct photolysis rates of 6 other structurally similar iodoacids whose standards are commercially unavailable.

- **Contribution of different reactive oxygen species (ROS)**. A steady-state kinetic model was established to successfully predict the destruction of I-THMs by the UV/H_2O_2 processes in different types of water and to determine the respective contributions from the direct photolysis and $HO^{\cdot}$-assisted indirect photolysis in the I-THMs degradation under different reaction conditions. In the UV/PS process, the steady-state concentration of $SO_4^{\cdot-}$ and $HO^{\cdot}$ were determined using some specific probe compounds. Subsequently, the respective contributions of UV, $HO^{\cdot}$, and $SO_4^{\cdot-}$ for IAA removal in the UV/PS process were determined as 7.8%, 14.7%, and 77.5%, respectively.

- **End-products of UV direct and indirect photolysis**. In the UV direct photolysis, the major fraction of CHI_3 could be completely mineralized and ~ 5% of CHI_3 was converted to HCO_2H at the end of the reaction (40 min). I^- was identified as the predominant end-products. In the UV/H_2O_2 process, when $CHCl_2I$ was used as the model compound, ~ 53% of $CHCl_2I$ could be completely mineralized and ~ 37% of $CHCl_2I$ was converted to HCO_2H at 15 min. There were still some unidentified organic species in the reaction

solution, which accounted for ~10 % of initial TOC. Both Cl^- and I^- were identified as the predominant end-products. When IAA was treated with UV/H_2O_2, ~ 50% of initial TOC were mineralized and the mass of carbon from HCHO and HCO_2H accounted for ~ 20% of initial TOC at 30 min. The remaining 30% of initial TOC were associated with other unidentified end-products. I^- was the major end-product in the UV/H_2O_2 process. In the UV/PS process, complete mineralization of IAA was observed at 30 min and IO_3^- was the predominant end-product.

- **Comparison of UV/H_2O_2 and UV/PS**. The UV/PS process is more effective than the UV/H_2O_2 process for IAA removal in different types of water due to the following reasons: (i), $SO_4^{\bullet-}$ is more reactive with IAA than $HO^{\bullet}$ (i.e., the second-order rate constants of IAA reacting with $SO_4^{\bullet-}$ and $HO^{\bullet}$ are $3.4 \times 10^9\ M^{-1}\ s^{-1}$ and $2.4 \times 10^9\ M^{-1}\ s^{-1}$, respectively); (ii), the radical formation quantum yield of $SO_4^{\bullet-}$ ($\Phi = 1.4$, $\varepsilon = 20\ M^{-1}\ cm^{-1}$) is higher than that of $HO^{\bullet}$ ($\Phi = 1.0$, $\varepsilon = 19.6\ M^{-1}\ cm^{-1}$); (iii), the self-scavenging of $SO_4^{\bullet-}$ by $S_2O_8^{2-}$ in the UV/PS process is much lower than the self-scavenging of $HO^{\bullet}$ by H_2O_2 in the UV/H_2O_2 process.

- **Economic analysis of UV photolysis and UV/H_2O_2**. Electrical energy per order (EE/O) was applied to evaluate the efficiency of the UV/H_2O_2 process for $CHCl_2I$ degradation and to optimize the H_2O_2 dose for different scenarios. The optimal H_2O_2 doses in DI water, laboratory synthesized water, and surface water were estimated as 5, 12, and 16 mg L^{-1}, respectively, which correspond to the lowest total equivalent electrical energy consumption of (EE/O_{total}) of 0.2, 0.31, and 0.45 $kWhm^{-3}order^{-1}$. The lowest EE/O_{total} in these 3 types of water with the UV/H_2O_2 process is 8-15 times lower than the corresponding EE/O_{total} with UV direct photolysis.

- **Cost comparison of UV/H_2O_2 and UV/PS**. Compared to UV/H_2O_2 process, UV/PS was observed as more cost-effective process for IAA removal based on the total cost of energy and oxidant consumption, under the reaction

conditions adopted in this study. For example, the lowest cost/O_{total} (~ 0.040 $\$m^{-3}order^{-1}$) for IAA removal in DI water with the UV/PS process is lower than the corresponding value (~ 0.053 $\$m^{-3}order^{-1}$) with the UV/$H_2O_2$ process.

7.2 Recommendation for future work

7.2.1 UV direct and indirect photolysis of other groups of I-DBPs

Besides I-THMs and iodoacids, there are some other groups of I-DBPs including iodinated halonitromethanes, iodinated haloacetonitriles, iodinated haloacetamides, and iodinated haloacetaldehyde etc. To the best knowledge of the author, there is still no well-documental study about post-formation mitigation of these groups of I-DBPs. In this context, UV-based direct and indirect photolysis can be considered to remove these groups of I-DBPs in the future study. In the meanwhile, to give a better description of the direct photolysis process of I-DBPs, more parameters besides BS, E_s and σ can be explored to establish QSAR model for a large glass of I-DBPs mentioned above.

7.2.2 Pilot study of UV-based AOP for I-DBPs removal in the plants

In the future, a pilot study of UV-based AOP for post-formation mitigation of I-DBPs can be conducted in a water treatment plant to obtain the first-hand data on treating actual effluent. This pilot study can provide the requisite date to decision maker for upgrading plant design to treat potential organic pollutants including I-DBPs. Additionally, based on results from the pilot study, a preliminary cost estimate of CAPEX and OPEX can be made for a waterworks which is planning to install a full-scale UV-based AOP application.

7.2.3 Formation study of I-DBPs

Different types of water samples including surface water, seawater, and secondary effluent have different water matrix species, such as varying concentrations of iodide, bromide, and NOM etc., which could show different I-DBPs formation

potentials. In addition, the different operations such as the type of disinfectants used or disinfectant dosing point during water treatment processes can also influence the I-DBPs formation and speciation in the product water. Most previous studies focused on the formation of I-THMs. However, little is known about the formation of other groups of I-DBPs. Therefore, the effects of chlorination, chloramination, and other oxidative processes on the formation and speciation of I-DBPs in different types of water should be investigated and compared in the future study.

Furthermore, some key factors such as characteristics of NOM, concentration of iodide and bromide, ratio of iodide to NOM etc. should be further investigated using artificial water sample as water matrix. For example, effects of different types of NOM on the formation and speciation of I-DBPs can be evaluated to identify what kinds of NOM are the major precursors for different groups of I-DBPs. On this basis, some model compounds can be selected to investigate the formation pathways of I-DBPs through identification of the I- and Br-containing reaction intermediates. The findings from the above-mentioned studies will enable developing a viable strategy for mitigation of I-DBPs formation during water treatment processes.

REFERENCES

Allard, S., Charrois, J.W.A., Joll, C.A. and Heitz, A., 2012. Simultaneous analysis of 10 trihalomethanes at nanogram per liter levels in water using solid-phase microextraction and gas chromatography mass-spectrometry. Journal of Chromatography A 1238, 15-21.

Allard, S., Nottle, C.E., Chan, A., Joll, C. and von Gunten, U., 2013. Ozonation of iodide-containing waters: Selective oxidation of iodide to iodate with simultaneous minimization of bromate and I-THMs. Water Research 47(6), 1953-1960.

Allston, T.D., Fedyk, M.L. and Takacs, G.A., 1978. Photoabsorption spectra of some halogen-substituted methyl nitrogen oxides. Journal of Photochemistry 9(2), 116-118.

Baeza, C. and Knappe, D.R.U., 2011. Transformation kinetics of biochemically active compounds in low-pressure UV Photolysis and UV/H_2O_2 advanced oxidation processes. Water Research 45(15), 4531-4543.

Barrett, J., Debenham, D.F. and Glauser, J., 1965. The electronic spectrum and photolysis of S-nitrosotoluene-α-thiol. Chemical Communications (London) (12), 248-249.

Baxendale, J.H. and Wilson, J.A., 1957. The photolysis of hydrogen peroxide at high light intensities. Transactions of the Faraday Society 53, 344-356.

Bayes, K.D., Toohey, D.W., Friedl, R.R. and Sander, S.P., 2003. Measurements of quantum yields of bromine atoms in the photolysis of bromoform from 266 to 324 nm. Journal of Geophysical Research D: Atmospheres 108(3), ACH 4-1 - ACH 4-6.

Bellar, T.A., Lichtenbert, J.J. and Kroner, R.C., 1974. The occurrence of organohalides in chlorinated drinking waters. Journal - American Water Works Association 66, 703-706.

Beltrán, F.J., Ovejero, G., García-Araya, J.F. and Rivas, J., 1995. Oxidation of polynuclear aromatic hydrocarbons in water. 2. UV radiation and ozonation in the presence of UV radiation. Industrial and Engineering Chemistry Research 34(5), 1607-1615.

Bichsel, Y. and von Gunten, U., 1999. Oxidation of iodide and hypoiodous acid in the disinfection of natural waters. Environmental Science and Technology 33(22), 4040-4045.

Bichsel, Y. and von Gunten, U., 2000. Formation of iodo-trihalomethanes during disinfection and oxidation of iodide-containing waters. Environmental Science and Technology 34(13), 2784-2791.

Bolton, J.R. and Cater, S.R., 1994. Homogeneous Photodegradation of Pollutants in Contaminanted Water-An Introduction. Aquatic and Surface Photochemistry; Lewis Publishers Inc: Boca Raton., 467-490.

Boucheloukh, H., Sehili, T., Kouachi, N. and Djebbar, K., 2012. Kinetic and analytical study of the photo-induced degradation of monuron by nitrates and nitrites under irradiation or in the dark. Photochemical and Photobiological Sciences 11(8), 1339-1345.

Brass, H.J., Feige, M.A., Halloran, T., Mello, J.W., Munch, D. and Thomas, R.F., 1977. The national organic monitoring survey: samplings and analyses for purgeable organic compounds. In: Drinking Water Quality Enhancement Through Source Protection, ed. Pojasek R. B., p. 398. Ann Arbor Science Publishers, Michigan.

Braun, A.M., Maurette, M.T. and Oliveros, E., 1991. Photochemical Technology. John Wiley & Sons, New York.

Brillas, E., Sirés, I. and Oturan, M.A., 2009. Electro-fenton process and related electrochemical technologies based on fenton's reaction chemistry. Chemical Reviews 109(12), 6570-6631.

Buxton, V.G., Helman, W.P. and Ross, A.b., 1988. Critical Review of rate constants for reactions of hydrated electrons, hydrogen atoms and hydroxyl radicals in Aqueous Solution. Journal of Physical and Chemical Reference Data 17(2), 513-886.

Cancho, B., Fabrellas, C., Diaz, A., Ventura, F. and Galceran, M.T., 2001. Determination of the odor threshold concentrations of iodinated trihalomethanes in drinking water. Journal of Agricultural and Food Chemistry 49(4), 1881-1884.

Cancho, B., Ventura, F., Galceran, M., Diaz, A. and Ricart, S., 2000. Determination, synthesis and survey of iodinated trihalomethanes in water treatment processes. Water Research 34(13), 3380-3390.

Cancho, B., Ventura, F. and Galceran, M.A.T., 1999. Solid-phase microextraction for the determination of iodinated trihalomethanes in drinking water. Journal of Chromatography A 841(2), 197-206.

Canonica, S., Meunier, L. and von Gunten, U., 2008. Phototransformation of selected pharmaceuticals during UV treatment of drinking water. Water Research 42(1-2), 121-128.

Cardador, M.J., Fernández-Salguero, J. and Gallego, M., 2015. Simultaneous quantification of trihalomethanes and haloacetic acids in cheese by on-line static headspace gas chromatography-mass spectrometry. Journal of Chromatography A.

Castro, C.E. and Belser, N.O., 1981. Photohydrolysis of methyl bromide and chloropicrin. Journal of Agricultural and Food Chemistry 29(5), 1005-1008.

Cédat, B., de Brauer, C., Métivier, H., Dumont, N. and Tutundjan, R., 2016. Are UV photolysis and UV/H_2O_2 process efficient to treat estrogens in waters? Chemical and biological assessment at pilot scale. Water Research 100, 357-366.

Chan, K.H. and Chu, W., 2009. Degradation of atrazine by cobalt-mediated activation of peroxymonosulfate: Different cobalt counteranions in homogenous process and cobalt oxide catalysts in photolytic heterogeneous process. Water Research 43(9), 2513-2521.

Chawla, O.P. and Fessenden, R.W., 1975. Electron spin resonance and pulse radiolysis studies of some reactions of $SO_4^{-\cdot}$ The Journal of Physical Chemistry 79(24), 2693-2700.

Chen, B., 2011. Hydrolytic stabilities of halogenated disinfection byproducts: Review and rate constant quantitative structure-property relationship analysis. Environmental Engineering Science 28(6), 385-394.

Chen, B., Lee, W., Westerhoff, P.K., Krasner, S.W. and Herckes, P., 2010. Solar photolysis kinetics of disinfection byproducts. Water Research 44(11), 3401-3409.

Clifton, C.L. and Huie, R.E., 1989. Rate constants for hydrogen abstraction reactions of the sulfate radical,$SO_4^{-\cdot}$. Alcohols. International Journal of Chemical Kinetics 21(8), 677-687.

Criquet, J. and Leitner, N.K.V., 2009. Degradation of acetic acid with sulfate radical generated by persulfate ions photolysis. Chemosphere 77(2), 194-200.

Crittenden, J.C., Howe, K., Hand, D.W., Trussell, R.R. and Tchobanoglous, G., 2012. *MWH*'s Water Treatment: Principles and Design. John Wiley & Sons: New York.

Crittenden, J.C., Hu, S., Hand, D.W. and Green, S.A., 1999. A kinetic model for UV/H_2O_2 process in a completely mixed batch reactor. Water Research 33(10), 2315-2328.

Davies, M.J., Gilbert, B.C., Barry Thomas, C. and Young, J., 1985. Electron spin resonance studies. Part 69. Oxidation of some aliphatic carboxylic acids, carboxylate anions, and related compounds by the sulphate radical anion ($SO_4^{-\cdot}$). Journal of the Chemical Society, Perkin Transactions 2 (8), 1199-1204.

De la Cruz, N., Giménez, J., Esplugas, S., Grandjean, D., De Alencastro, L.F. and Pulgarín, C., 2012. Degradation of 32 emergent contaminants by UV and neutral photo-fenton in domestic wastewater effluent previously treated by activated sludge. Water Research 46(6), 1947-1957.

Deng, J., Shao, Y., Gao, N., Xia, S., Tan, C., Zhou, S. and Hu, X., 2013. Degradation of the antiepileptic drug carbamazepine upon different UV-based advanced oxidation processes in water. Chemical Engineering Journal 222, 150-158.

Devi, P., Das, U. and Dalai, A.K., 2016. In-situ chemical oxidation: Principle and applications of peroxide and persulfate treatments in wastewater systems. Science of the Total Environment.

Dogliotti, L., 1967. Flash photolysis of persulfate ions in aqueous solutions. Study of the sulfate and ozonide radical allions. Journal of Physical Chemistry 71(8), 2511-2516.

Dyekjær, J.D. and Jónsdóttir, S.Ó., 2004. QSPR models for various physical properties of carbohydrates based on molecular mechanics and quantum chemical calculations. Carbohydrate Research 339(2), 269-280.

Eberson, L., 1982. Electron-Transfer Reactions in Organic Chemistry. in: *Advances in Physical Organic Chemisty*, (Eds) V. Gold, D. Bethell, Volume 18, Academic Press, pp. 79-185.

Fang, J.Y., Ling, L. and Shang, C., 2013. Kinetics and mechanisms of pH-dependent degradation of halonitromethanes by UV photolysis. Water Research 47(3), 1257-1266.

Fang, J.Y. and Shang, C., 2012. Bromate formation from bromide oxidation by the UV/persulfate process. Environmental Science and Technology 46(16), 8976-8983.

Farré, M.J., Doederer, K., Gernjak, W., Poussade, Y. and Weinberg, H. 2012 Disinfection by-products management in high quality recycled water. Water Science and Technology: Water Supply, pp. 573-579.

Femia, J., Mariani, M., Zalazar, C. and Tiscornia, I., 2013. Photodegradation of chlorpyrifos in water by UV/H_2O_2 treatment: Toxicity evaluation. Water Science and Technology 68(10), 2279-2286.

Gallard, H., Allard, S., Nicolau, R., Von Gunten, U. and Croué, J.P., 2009. Formation of iodinated organic compounds by oxidation of iodide-containing waters with manganese dioxide. Environmental Science and Technology 43(18), 7003-7009.

García-Galán, M.J., Anfruns, A., Gonzalez-Olmos, R., Rodríguez-Mozaz, S. and Comas, J., 2016. UV/H_2O_2 degradation of the antidepressants venlafaxine and O-desmethylvenlafaxine: Elucidation of their transformation pathway and environmental fate. Journal of Hazardous Materials 311, 70-80.

Gottschalk, C., Libra, J.A. and Saupe, A., 2010. Ozonation of Water and Waster Water. Publisher: WILEY-VCH.

Hansch, C. and Leo, A., 1995. Exploring QSAR: Hydrophobic, Electronic, and Steric constants. In: Heller, S. R. (Ed.), American Chemical Society Professional Reference Book. Washington, DC.

Hansen, K.M.S., Zortea, R., Piketty, A., Vega, S.R. and Andersen, H.R., 2013. Photolytic removal of DBPs by medium pressure UV in swimming pool water. Science of the Total Environment 443, 850-856.

Hansson, R.C., Henderson, M.J., Jack, P. and Taylor, R.D., 1987. Iodoform taste complaints in chloramination. Water Research 21(10), 1265-1271.

He, X., de la Cruz, A.A., O'Shea, K.E. and Dionysiou, D.D., 2014a. Kinetics and mechanisms of cylindrospermopsin destruction by sulfate radical-based advanced oxidation processes. Water Research 63, 168-178.

He, X., Mezyk, S.P., Michael, I., Fatta-Kassinos, D. and Dionysiou, D.D., 2014b. Degradation kinetics and mechanism of β-lactam antibiotics by the activation of H_2O_2 and $Na_2S_2O_8$ under UV-254nm irradiation. Journal of Hazardous Materials 279, 375-383.

He, X., Zhang, G., De La Cruz, A.A., O'Shea, K.E. and Dionysiou, D.D., 2014c. Degradation mechanism of cyanobacterial toxin cylindrospermopsin by hydroxyl radicals in homogeneous UV/H_2O_2 process. Environmental Science and Technology 48(8), 4495-4504.

Heit, G., Neuner, A., Saugy, P.Y. and Braun, A.M., 1998. Vacuum-UV (172 nm) actinometry. The quantum yield of the photolysis of water. Journal of Physical Chemistry A 102(28), 5551-5561.

Huie, R.E., Clifton, C.L. and Neta, P., 1991. Electron transfer reaction rates and equilibria of the carbonate and sulfate radical anions. Radiation Physics and Chemistry 38(5), 477-481.

Ioele, G., De Luca, M., Oliverio, F. and Ragno, G., 2009. Prediction of photosensitivity of 1,4-dihydropyridine antihypertensives by quantitative structure-property relationship. Talanta 79(5), 1418-1424.

Jankowski, J.J., Kieber, D.J., Mopper, K. and Neale, P.J., 2000. Development and intercalibration of ultraviolet solar actinometers. Photochemistry and Photobiology 71(4), 431-440.

Ji, Y., Zeng, C., Ferronato, C., Chovelon, J.M. and Yang, X., 2012. Nitrate-induced photodegradation of atenolol in aqueous solution: Kinetics, toxicity and degradation pathways. Chemosphere 88(5), 644-649.

Jo, C.H., Dietrich, A.M. and Tanko, J.M., 2011. Simultaneous degradation of disinfection byproducts and earthy-musty odorants by the UV/H_2O_2 advanced oxidation process. Water Research 45(8), 2507-2516.

Jones, C.E. and Carpenter, L.J., 2005. Solar photolysis of CH_2I_2, CH_2ICI, and CH_2IBr in water, saltwater, and seawater. Environmental Science and Technology 39(16), 6130-6137.

Jones, D.B., 2009. The formation and control of iodinated trihalomethanes in drinking water treatment. Thesis for master degree, Clemson University.

Jones, D.B., Saglam, A., Song, H. and Karanfil, T., 2012a. The impact of bromide/iodide concentration and ratio on iodinated trihalomethane formation and speciation. Water Research 46(1), 11-20.

Jones, D.B., Saglam, A., Triger, A., Song, H. and Karanfil, T., 2011. I-THMs Formation and Speciation: Performed Monochloramine versus Prechlorination Followed by Ammonia Addition. Environmental Science and Technology 45(24), 10429-10437.

Jones, D.B., Song, H. and Karanfil, T., 2012b. The effects of selected preoxidation strategies on I-THM formation and speciation. Water Research 46(17), 5491-5498.

Jung, B., Nicola, R., Batchelor, B. and Abdel-Wahab, A., 2014. Effect of low- and medium-pressure Hg UV irradiation on bromate removal in advanced reduction process. Chemosphere 117(1), 663-672.

Keen, O.S., Love, N.G. and Linden, K.G., 2012. The role of effluent nitrate in trace organic chemical oxidation during UV disinfection. Water Research 46(16), 5224-5234.

Khiahi, D., Ventura, F., Chinn, R. and Barrett, S., 1999. The occurrence of iodinated trihalomethanes in drinking water. Presented at ACS National Meeting.

Kiattisaksiri, P., Khan, E., Punyapalakul, P. and Ratpukdi, T., 2016. Photodegradation of haloacetonitriles in water by vacuum ultraviolet irradiation: Mechanisms and intermediate formation. Water Research 98, 160-167.

Kochany, J. and Bolton, J.R., 1991. Mechanism of photodegradation of aqueous organic pollutants. 1. EPR spin-trapping technique for the determination of •OH radical rate constants in the photooxidation of chlorophenols following the photolysis of H_2O_2. Journal of Physical Chemistry 95(13), 5116-5120.

Krasner, S.W., Weinberg, H.S., Richardson, S.D., Pastor, S.J., Chinn, R., Sclimenti, M.J., Onstad, G.D. and Thruston Jr, A.D., 2006. Occurrence of a new generation of disinfection byproducts. Environmental Science and Technology 40(23), 7175-7185.

Kruithof, J.C. and Martijn, B.J. 2013 UV/H_2O_2 treatment: An essential process in a multi barrier approach against trace chemical contaminants. Water Science and Technology: Water Supply, pp. 130-138.

Kwok, W.M., Zhao, C., Li, Y.L., Guan, X., Wang, D. and Phillips, D.L., 2004. Water-Catalyzed Dehalogenation Reactions of Isobromoform and Its Reaction Products. Journal of the American Chemical Society 126(10), 3119-3131.

Kwon, M., Kim, S., Yoon, Y., Jung, Y., Hwang, T.M., Lee, J. and Kang, J.W., 2015. Comparative evaluation of ibuprofen removal by UV/H_2O_2 and UV/$S_2O_8^{2-}$ processes for wastewater treatment. Chemical Engineering Journal 269, 379-390.

Larson, R.A. and Zepp, R.G., 1988. Environmental chemistry. Reactivity of the carbonate radical with aniline derivatives. Environmental Toxicology and Chemistry 7(4), 265-274.

Li, X., Ma, J., Liu, G., Fang, J., Yue, S., Guan, Y., Chen, L. and Liu, X., 2012a. Efficient reductive dechlorination of monochloroacetic acid by sulfite/UV process. Environmental Science and Technology 46(13), 7342-7349.

Li, Y., Song, W., Fu, W., Tsang, D.C.W. and Yang, X., 2015. The roles of halides in the acetaminophen degradation by UV/H_2O_2 treatment: Kinetics, mechanisms, and products analysis. Chemical Engineering Journal 271, 214-222.

Li, Y., Whitaker, J.S. and McCarty, C.L., 2012b. Analysis of iodinated haloacetic acids in drinking water by reversed-phase liquid chromatography/electrospray

ionization/tandem mass spectrometry with large volume direct aqueous injection. Journal of Chromatography A 1245, 75-82.

Liang, C. and Su, H.W., 2009. Identification of sulfate and hydroxyl radicals in thermally activated persulfate. Industrial and Engineering Chemistry Research 48(11), 5558-5562.

Liao, C.H., Kang, S.F. and Wu, F.A., 2001. Hydroxyl radical scavenging role of chloride and bicarbonate ions in the H_2O_2/UV process. Chemosphere 44(5), 1193-1200.

Lin, C.C., Lee, L.T. and Hsu, L.J., 2013. Performance of UV/$S_2O_8^{2-}$ process in degrading polyvinyl alcohol in aqueous solutions. Journal of Photochemistry and Photobiology A: Chemistry 252, 1-7.

Lin, C.C., Lin, H.Y. and Hsu, L.J., 2016. Degradation of ofloxacin using UV/H_2O_2 process in a large photoreactor. Separation and Purification Technology 168, 57-61.

Liu, X., Wei, X., Zheng, W., Jiang, S., Templeton, M.R., He, G. and Qu, W., 2013. An Optimized Analytical Method for the Simultaneous Detection of Iodoform, Iodoacetic Acid, and Other Trihalomethanes and Haloacetic Acids in Drinking Water. PLoS ONE 8(4).

Liu, Y., He, X., Duan, X., Fu, Y. and Dionysiou, D.D., 2015. Photochemical degradation of oxytetracycline: Influence of pH and role of carbonate radical. Chemical Engineering Journal 276, 113-121.

Liu, Y., He, X., Fu, Y. and Dionysiou, D.D., 2016. Kinetics and mechanism investigation on the destruction of oxytetracycline by UV-254 nm activation of persulfate. Journal of Hazardous Materials 305, 229-239.

Luo, C., Jiang, J., Ma, J., Pang, S., Liu, Y., Song, Y., Guan, C., Li, J., Jin, Y. and Wu, D., 2016. Oxidation of the odorous compound 2,4,6-trichloroanisole by UV activated persulfate: Kinetics, products, and pathways. Water Research 96, 12-21.

Mack, J. and Bolton, J.R., 1999. Photochemistry of nitrite and nitrate in aqueous solution: A review. Journal of Photochemistry and Photobiology A: Chemistry 128(1-3), 1-13.

Madhavan, V., Levanon, H. and Neta, P., 1978. Decarboxylation by $SO_4^{\cdot-}$ radicals. Radiation Research 76(1), 15-22.

Marin, M.L., Santos-Juanes, L., Arques, A., Amat, A.M. and Miranda, M.A., 2012. Organic photocatalysts for the oxidation of pollutants and model compounds. Chemical Reviews 112(3), 1710-1750.

Mark, G., Schuchmann, M.N., Schuchmann, H.P. and von Sonntag, C., 1990. The photolysis of potassium peroxodisulphate in aqueous solution in the presence of tert-butanol: a simple actinometer for 254 nm radiation. Journal of Photochemistry and Photobiology, A: Chemistry 55(2), 157-168.

McGivern, W.S., Derecskei-Kovacs, A., North, S.W. and Francisco, J.S., 2000. Computationally Efficient Methodology to Calculate C-H and C-X (X = F, Cl, and Br) Bond Dissociation Energies in Haloalkanes. Journal of Physical Chemistry A 104(2), 436-442.

Medinas, D.B., Cerchiaro, G., Trindade, D.F. and Augusto, O., 2007. The carbonate radical and related oxidants derived from bicarbonate buffer. IUBMB Life 59(4-5), 255-262.

Michael-Kordatou, I., Iacovou, M., Frontistis, Z., Hapeshi, E., Dionysiou, D.D. and Fatta-Kassinos, D., 2015. Erythromycin oxidation and ERY-resistant Escherichia coli inactivation in urban wastewater by sulfate radical-based oxidation process under UV-C irradiation. Water Research 85, 346-358.

Mitrović, J.Z., Radović, M.D., Andelković, T.D., Bojić, D.V. and Bojić, A.L., 2014. Identification of intermediates and ecotoxicity assessment during the UV/H_2O_2 oxidation of azo dye Reactive Orange 16. Journal of Environmental Science and Health - Part A Toxic/Hazardous Substances and Environmental Engineering 49(5), 491-502.

Neta, P., Huie, A.B. and Ross, A.B., 1988. Rate constants for reactions of inorganic radicals in aqueous solution. Journal of Physical and Chemical Reference Data 17(3), 1027-1284.

Neta, P., Madhavan, V., Zemel, H. and Fessenden, R.W., 1977. Rate constants and mechanism of reaction of $SO_4^{\cdot-}$ with aromatic compounds. Journal of the American Chemical Society 99(1), 163-164.

Nicole, I., De Laat, J., Dore, M., Duguet, J.P. and Suty, H., 1991. Degradation of trihalomethanes in dilute aqueous solution by UV irradiation - Determination of the quantum yield of photolysis at 253.7 NM. Environmental Technology 12(1), 21-31.

Norman, R.O.C., Storey, P.M. and West, P.R., 1970. Electron spin resonance studies. Part XXV. Reactions of the sulphate radical anion with organic compounds. Journal of the Chemical Society B: Physical Organic, 1087-1095.

Oh, W.D., Dong, Z. and Lim, T.T., 2016. Generation of sulfate radical through heterogeneous catalysis for organic contaminants removal: Current development, challenges and prospects. Applied Catalysis B: Environmental 194, 169-201.

Oppenlander, T., 2003. Photochemical purification of water and air. Publisher: WILEY-VCH.

Pereira, V.J., Weinberg, H.S., Linden, K.G. and Singer, P.C., 2007. UV degradation kinetics and modeling of pharmaceutical compounds in laboratory grade and surface water via direct and indirect photolysis at 254 nm. Environmental Science and Technology 41(5), 1682-1688.

Plewa, M.J., Wagner, E.D., Richardson, S.D., Thruston Jr, A.D., Woo, Y.T. and McKague, A.B., 2004. Chemical and biological characterization of newly discovered iodoacid drinking water disinfection byproducts. Environmental Science and Technology 38(18), 4713-4722.

Prados-Joya, G., Sánchez-Polo, M., Rivera-Utrilla, J. and Ferro-garcía, M., 2011. Photodegradation of the antibiotics nitroimidazoles in aqueous solution by ultraviolet radiation. Water Research 45(1), 393-403.

Pressman, J.G., Richardson, S.D., Speth, T.F., Miltner, R.J., Narotsky, M.G., Hunter Iii, E.S., Rice, G.E., Teuschler, L.K., McDonald, A., Parvez, S., Krasner, S.W., Weinberg, H.S., McKague, A.B., Parrett, C.J., Bodin, N., Chinn, R., Lee, C.F.T. and Simmons, J.E., 2010. Concentration, chlorination, and chemical analysis of drinking water for disinfection byproduct mixtures health effects research: U.S. EPAs four lab study. Environmental Science and Technology 44(19), 7184-7192.

Qian, Y., Guo, X., Zhang, Y., Peng, Y., Sun, P., Huang, C.H., Niu, J., Zhou, X. and Crittenden, J.C., 2016. Perfluorooctanoic Acid Degradation Using UV-Persulfate Process: Modeling of the Degradation and Chlorate Formation. Environmental Science and Technology 50(2), 772-781.

Rahn, R.O., 1997. Potassium Iodide as a Chemical Actinometer for 254 nm Radiation: Use of lodate as an Electron Scavenger. Photochemistry and Photobiology 66(4), 450-455.

Richardson, S.D., Fasano, F., Ellington, J.J., Crumley, F.G., Buettner, K.M., Evans, J.J., Blount, B.C., Silva, L.K., Waite, T.J., Luther, G.W., McKague, A.B., Miltner, R.J., Wagner, E.D. and Plewa, M.J., 2008. Occurrence and mammalian cell toxicity of iodinated disinfection byproducts in drinking water. Environmental Science and Technology 42(22), 8330-8338.

Richardson, S.D., Plewa, M.J., Wagner, E.D., Schoeny, R. and DeMarini, D.M., 2007. Occurrence, genotoxicity, and carcinogenicity of regulated and emerging disinfection by-products in drinking water: A review and roadmap for research. Mutation Research - Reviews in Mutation Research 636(1-3), 178-242.

Rook, J.J., 1974. Formation of haloforms during chlorination of natural waters, . Water Treatment Examination 23, 234-243.

Rosenfeldt, E.J. and Linden, K.G., 2004. Degradation of endocrine disrupting chemicals bisphenol A, ethinyl estradiol, and estradiol during UV photolysis and advanced oxidation processes. Environmental Science and Technology 38(20), 5476-5483.

Rosenfeldt, E.J. and Linden, K.G., 2007. The $R_{OH,UV}$ concept to characterize and the model UV/H_2O_2 process in natural waters. Environmental Science and Technology 41(7), 2548-2553.

Rosenfeldt, E.J., Linden, K.G., Canonica, S. and von Gunten, U., 2006. Comparison of the efficiency of {radical dot}OH radical formation during ozonation and the advanced oxidation processes O_3/H_2O_2 and UV/H_2O_2. Water Research 40(20), 3695-3704.

Rozas, O., Vidal, C., Baeza, C., Jardim, W.F., Rossner, A. and Mansilla, H.D., 2016. Organic micropollutants (OMPs) in natural waters: Oxidation by UV/H_2O_2 treatment and toxicity assessment. Water Research 98, 109-118.

Rudra, A., Thacker, N.P. and Pande, S.P., 2005. Hydrogen peroxide and ultraviolet irradiations in water treatment. Environmental Monitoring and Assessment 109(1-3), 189-197.

Schwarzenbach, R.P., Gschwend, P.M. and Imboden, D.M., 1993. Photochemical transformation reactions. . In: Environmental Organic Chemistry. John Wiley and Sons, Inc., New York, , 436-484.

Schwarzenbach, R.P., Gschwend, P.M. and Imbond, D.M., 2003. Enviromental organic chemistry-second edition. John Wiley & Sons, Inc. New York.

Sehested, K., Rasmussen, O.L. and Fricke, H., 1968. Rate constants of OH with HO_2, O_2^-, and $H_2O_2^+$ from hydrogen peroxide formation in pulse-irradiated oxygenated water. Journal of Physical Chemistry 72(2), 626-631.

Sharpless, C.M. and Linden, K.G., 2003. Experimental and model comparisons of low- and medium-pressure Hg lamps for the direct and H_2O_2 assisted UV photodegradation of N-nitrosodimethylamine in simulated drinking water. Environmental Science and Technology 37(9), 1933-1940.

Shin, D., Jang, M., Cui, M., Na, S. and Khim, J., 2013. Enhanced removal of dichloroacetonitrile from drinking water by the combination of solar-photocatalysis and ozonation. Chemosphere 93(11), 2901-2908.

Smith, E.M., Plewa, M.J., Lindell, C.L., Richardson, S.D. and Mitch, W.A., 2010. Comparison of byproduct formation in waters treated with chlorine and iodine: Relevance to point-of-use treatment. Environmental Science and Technology 44(22), 8446-8452.

Snoeyink, V.L. and Jenkins, D., 1980. Water Chemsity. John Wiley & Sons: New York.

Steelink, C., 2002. Investigating humic acids in soils. Analytical Chemistry 74(11), 327A-333A.

Stefan, M.I. and Bolton, J.R., 2002. UV direct photolysis of N-nitrosodimethylamine (NDMA): Kinetic and product study. Helvetica Chimica Acta 85(5), 1416-1426.

Tan, C., Gao, N., Deng, Y., Zhang, Y., Sui, M., Deng, J. and Zhou, S., 2013. Degradation of antipyrine by UV, UV/H_2O_2 and UV/PS. Journal of Hazardous Materials 260, 1008-1016.

Tsitonaki, A., Petri, B., Crimi, M., Mosbk, H., Siegrist, R.L. and Bjerg, P.L., 2010. In situ chemical oxidation of contaminated soil and groundwater using persulfate: A review. Critical Reviews in Environmental Science and Technology 40(1), 55-91.

U.S. EPA, 1979. National interim primary drinking water regulations: control of trihalomethanes in drinking water: final rules, Fed. Reg. 44, 68624-68705.

U.S. EPA, 1998. National primary drinking water regulations: disinfectants and disinfection byproducts; final rule, Fed. Reg. 63, 69390–69476.

U.S. EPA, 2006. National primary drinking water regulations: stage 2 disinfectants and disinfection byproducts rule, Fed. Reg. . 71, 387-493.

Wang, Q., Shao, Y., Gao, N., Chu, W., Shen, X., Lu, X., Chen, J. and Zhu, Y., 2016. Degradation kinetics and mechanism of 2,4-Di-tert-butylphenol with UV/persulfate. Chemical Engineering Journal 304, 201-208.

Wang, Z., Xu, B., Lin, Y.L., Hu, C.Y., Tian, F.X., Zhang, T.Y. and Gao, N.Y., 2014. A comparison of iodinated trihalomethane formation from iodide and iopamidol in the presence of organic precursors during monochloramination. Chemical Engineering Journal 257, 292-298.

Weast, R.C., Astle, M.J. and Beyer, W.H., 1986. CRC Handbook of Chemistry and Physics,66th ed.; CRC press: Boca Raton, FL.

Wei, X., Chen, X., Wang, X., Zheng, W., Zhang, D., Tian, D., Jiang, S., Ong, C.N., He, G. and Qu, W., 2013. Occurrence of Regulated and Emerging Iodinated DBPs in the Shanghai Drinking Water. PLoS ONE 8(3).

Wolfrum, E.J., Ollis, D.F., Lim, P.K. and Fox, M.A., 1994. The UVH2O2 process: quantitative EPR determination of radical concentrations. Journal of Photochemistry and Photobiology, A: Chemistry 78(3), 259-265.

Wols, B.A. and Hofman-Caris, C.H.M., 2012. Review of photochemical reaction constants of organic micropollutants required for UV advanced oxidation processes in water. Water Research 46(9), 2815-2827.

Wu, C., Shemer, H. and Linden, K.G., 2007a. Photodegradation of metolachlor applying UV and UV/H_2O_2. Journal of Agricultural and Food Chemistry 55(10), 4059-4065.

Wu, D., Liu, M., Dong, D. and Zhou, X., 2007b. Effects of some factors during electrochemical degradation of phenol by hydroxyl radicals. Microchemical Journal 85(2), 250-256.

Xie, Y.F., 2004. Disinfection byproducts in drinking water: formation, analysis, and control. Lewis Publisher.

Xu, B., Chen, Z., Qi, F., Ma, J. and Wu, F., 2009. Rapid degradation of new disinfection by-products in drinking water by UV irradiation: N-Nitrosopyrrolidine and N-nitrosopiperidine. Separation and Purification Technology 69(1), 126-133.

Yang, S., Wang, P., Yang, X., Shan, L., Zhang, W., Shao, X. and Niu, R., 2010. Degradation efficiencies of azo dye Acid Orange 7 by the interaction of heat, UV and anions with common oxidants: Persulfate, peroxymonosulfate and hydrogen peroxide. Journal of Hazardous Materials 179(1-3), 552-558.

Yang, X., Zhan, M.J., Kong, L.R. and Wang, L.S., 2004. Determination of hydroxyl radicals with salicylic acid in aqueous nitrate and nitrite solutions. Journal of Environmental Sciences 16(4), 687-689.

Yang, Y., Pignatello, J.J., Ma, J. and Mitch, W.A., 2014. Comparison of halide impacts on the efficiency of contaminant degradation by sulfate and hydroxyl radical-based advanced oxidation processes (AOPs). Environmental Science and Technology 48(4), 2344-2351.

Ye, T., Xu, B., Lin, Y.L., Hu, C.Y., Lin, L., Zhang, T.Y. and Gao, N.Y., 2013. Formation of iodinated disinfection by-products during oxidation of iodide-containing waters with chlorine dioxide. Water Research 47(9), 3006-3014.

Yuan, R., Wang, Z., Hu, Y., Wang, B. and Gao, S., 2014. Probing the radical chemistry in UV/persulfate-based saline wastewater treatment: Kinetics modeling and byproducts identification. Chemosphere 109, 106-112.

Zhang, B.T., Zhang, Y., Teng, Y. and Fan, M., 2015a. Sulfate radical and its application in decontamination technologies. Critical Reviews in Environmental Science and Technology 45(16), 1756-1800.

Zhang, J.Y., Boyd, I.W. and Esrom, H., 1997. UV intensity measurement for a novel 222 nm excimer lamp using chemical actinometer. Applied Surface Science 109-110, 482-486.

Zhang, J.Y., Esrom, H. and Boyd, I.W., 1999. UV intensity measurement of 308 nm excimer lamp using chemical actinometer. Applied Surface Science 138-139(1-4), 315-319.

Zhang, T., Chen, Y., Wang, Y., Le Roux, J., Yang, Y. and Croué, J.P., 2014. Efficient peroxydisulfate activation process not relying on sulfate radical generation for water pollutant degradation. Environmental Science and Technology 48(10), 5868-5875.

Zhang, T.Y., Xu, B., Hu, C.Y., Lin, Y.L., Lin, L., Ye, T. and Tian, F.X., 2015b. A comparison of iodinated trihalomethane formation from chlorine, chlorine dioxide and potassium permanganate oxidation processes. Water Research 68, 394-403.

Zhang, X. and Minear, R.A., 2002. Decomposition of trihaloacetic acids and formation of the corresponding trihalomethanes in drinking water. Water Research 36(14), 3665-3673.

Zhang, Y., Zhang, J., Xiao, Y., Chang, V.W.C. and Lim, T.T., 2016. Kinetic and mechanistic investigation of azathioprine degradation in water by UV, UV/H_2O_2 and UV/persulfate. Chemical Engineering Journal 302, 526-534.

Zou, P., Shu, J., Sears, T.J., Hall, G.E. and North, S.W., 2004. Photodissociation of bromoform at 248 nm: Single and multiphoton processes. Journal of Physical Chemistry A 108(9), 1482-1488.

Zuo, Z., Cai, Z., Katsumura, Y., Chitose, N. and Muroya, Y., 1999. Reinvestigation of the acid-base equilibrium of the (bi)carbonate radical and ph dependence of its reactivity with inorganic reactants. Radiation Physics and Chemistry 55(1), 15-23.